FACULTEIT
BIO-INGENIEURSWETENSCHAPPEN

ILVO

A CHANGING NORTH SEA: THE POTENTIAL EFFECTS OF MARINE HEATWAVES ON SHRIMP ABUNDANCES IN THE BELGIAN PART OF THE NORTH SEA

Bartel Vertongen
Student number: 01905620

Promotors: Dr. Ilias Semmouri, Prof. dr. ir. Jana Asselman

Tutor: Dr. Bart Vanelslander

Master's Dissertation submitted to Ghent University in partial fulfilment of the requirements for the degree of Master of Science in Bioscience Engineering: Environmental Technology

Academic year: 2023-2024

UNIVERSITEIT
GENT

Ghent, August 23, 2024

The promotors,

Prof. Dr. ir. Jana Asselman

Dr. Ilias Semmouri

The author,

Bartel Vertongen

ACKNOWLEDGEMENTS

I want to start this dissertation in a very traditional way. This master thesis was not possible with all the people that supported me along this journey. It is a cliché, but I think it can be rightfully said. All of the following people helped to shape this master thesis and without them, it would not be what it is today.

First and foremost, I genuinely want to thank my promotor dr. Ilias Semmouri. From the first moment we met, Ilias assured me he would do his best to guide me and to help me as much as possible throughout the whole thesis trajectory, which he did. I could always send Ilias an email, a Teams message or go by in person if I had questions or when I needed some advice. Nothing was too much, even on Sun- or holidays, my questions were answered. During the feedback sessions, I always received very good and honest feedback, which I not only used to improve my thesis, but also my way of working. It was an absolutely pleasure to work with somebody who possesses such a deep passion and knowledge about the marine environment. Additionally, I would like to thank Ilias for his flexibility to firstly consider, and later approve that I could go on Erasmus while working on my thesis. This Erasmus exchange was a unique experience and would not be possible without Ilias, so again, thank you Ilias!

Next, I would like to thank my tutor dr. Bart Vanelslander from ILVO who always provided me with feedback and came up with suggestions and advice during the first months of my thesis. Additionally, I also would like to thank Prof. dr. ir. Jana Asselman for giving me the chance to work on this topic, and to provide me with clear and constructive feedback.

In particular, I also want to thank Noa. We spent a lot of time together working on our theses (and complaining about it). She was also always ready to answer my R-related questions and to hear my complaints about the lab work or other problems. Her presence, especially during the last weeks, made everything a little more bearable.

Next, I also want to thank Thomas Lanssens, Tim, Jade, Laure, Bennie and Koenraad from ILVO for the enjoyable (when the weather was good) and educational experiences during the DYFS-campaign aboard the RV Simon Stevin. I learned a lot about the different marine organisms in the North Sea and how to identify them. Also, I would like to thank Edwig and his father, who made time for us to share their stories about and experiences in the shrimp fishery.

I also would like to thank to Dries and Marie, who introduced me to Qgis and helped me produce several maps.

Finally, I would like to give a special thanks to my parents. Despite sometimes feeling more stress than I did, they always supported me, gave advice were possible and assisted me by reading my first versions over and over.

TABLE OF CONTENTS

TABLE OF ABBREVIATIONS

AMO	Atlantic Multidecadal Oscillation
B&D	Bligh and Dyer extraction
BPI	Bathymetric Position Index
BPNS	Belgian Part of the North Sea
BSA	Bovine Serum Albumin
CRS	Coordinate Reference System
CTD	Conductivity, Temperature and Depth
DEM	Digital Elevation Model
DTM	Digital Terrain Model
DYFS	Demersal Young Fish Survey
EAP	East Atlantic Pattern
EMODNet	European Marine Observation and Data Network
ENSO	El Niño Southern Oscillation
ESFRI	European Strategy Forum on Research Infrastructure
FV	Fishing Vessel
GAM	Generative Additive Model
GMT	Greenwich Mean Time
ICOS	Integrated Carbon Observation Centre
ILVO	Flanders Research Institute for Agriculture, Fisheries and Food
IPCC	Intergovernmental Panel on Climate Change
IQR	Interquartile Range
LW	LifeWatch
MCS	Marine Cold Spell
MHW	Marine Heat Wave
MIDAS	Marine Information and Data Acquisition System
NAO	North Atlantic Oscillation
NOAA	National Oceanic and Atmospheric Administration
ppm	Parts per million
ppt	Parts per trillion
RCP	Representative Concentration Pathway
RV	Research Vessel
SST	Sea Surface Temperature
VLIZ	Flanders Marine Institute
WNAO	Winter North Atlantic Oscillation
SRV	Spearman Rho Value

SUMMARY

The European brown shrimp (*Crangon crangon*) is deeply embedded in the Belgian culture. Since the Middle Ages, people have fished this coastal dweller to consume or to sell as food source. Despite a diminishing fishing fleet, the brown shrimp fishery remains a vital economic sector along the Belgian coast. However, in recent years, the availability of shrimp was subjected to some severe fluctuations. Years with large commercial landings were altered by years of markedly low catches. For instance, in 2023, reduced commercial landings led to a substantial increase in shrimp prices, resulting in economic challenges for fishermen and vendors. To date, neither fishermen nor scientists have been able to identify the cause(s) of these fluctuations.

This dissertation aims to identify the major influences on the recruitment process of *Crangon crangon* and to correlate recent fluctuations of shrimp abundance with prevailing environmental conditions. Initially, the occurrence of marine heatwaves (MHWs) in the Belgian Part of the North Sea (BPNS) was hypothesized to be one of the main drivers behind the variating abundances. Marine heatwaves are events during which water temperature exceeds a certain threshold value over a certain time period, resulting in anomalously high water temperatures. The majority of these MHWs have an anthropogenic origin as they are associated with climate change. Globally, MHWs are occurring with increasing frequency, thereby impacting marine life and associated ecosystem services. In the BPNS , it was observed that in years marked by intense MHWs (e.g. 2018, 2022), an increased number of commercial landings was noted. Therefore, the correlation between (elevated) water temperatures and shrimp abundances was initially investigated. However, as *Crangon crangon* stocks do not solely depend on water temperature, several other environmental parameters such as food availability or predator abundance were also included.

Since the recruitment of *Crangon crangon* is poorly studied in the BPNS, only a limited number of comprehensive data series were available. The Flanders Research Institute for Agriculture, Fisheries and Food (ILVO) provided data on shrimp abundances in the BPNS based on their annual Demersal Young Fish Survey (DYFS) conducted in September. This data series was subsequently combined with data from the LifeWatch framework, which is operated by the Flanders Marine Institute (VLIZ). Consequently, a general dataset was created which contained both information about the *Crangon crangon* abundances and several environmental parameters such as water temperature, nutrient concentrations or zooplankton densities. Using this dataset, several scatterplots were generated to investigate the direct correlations between environmental parameters and the *Crangon crangon* abundances. Additionally, Generative Additive Models (GAMs) were constructed to explore non-linear correlations.

The scatterplots and GAMs indicated that the recruitment process of *Crangon crangon* is influenced by multiple environmental factors beyond water temperature. Positive correlations were found for nutrient concentrations, the chlorophyll *a* concentration and the winter and summer North Atlantic Oscillation (NAO) index. Conversely, negative correlations were found for water temperature, salinity level, zooplankton density, whiting abundance, depth and fishery activities. Each of these parameters exerts influence on the recruitment process within specific temporal windows, underscoring the complexity of the influences on the recruitment process of *Crangon crangon* in the BPNS.

Alongside the data analysis, a brief nutritional assessment of brown shrimp in the BPNS was conducted. Several samples were collected during offshore campaigns in September and November 2023 and were used in protein (Bradford method) and lipid (Bligh & Dyer method) extractions. The aim of these extractions was to compare the protein and lipid content across a near-offshore and east-west gradient, as well as between the autumn and winter seasons. Despite the limited number of sampled shrimp, some significant differences in nutritional content were noticed. Especially the difference between the near- and offshore areas, where nearshore areas exhibited a significant higher protein and lipid content, showed promising results.

In conclusion, this dissertation is one of the first studies that attempts to explain the fluctuating behaviour of *Crangon crangon* in the BPNS. Several environmental parameters were identified exerting a significant influence on the recruitment. However, due to the limited availability of data and lacking literature, this study remains exploratory, merely proposing potential influencing mechanisms on *Crangon crangon* recruitment. Nonetheless, this study provides a valuable foundation for future research, which could provide a more comprehensive understanding of the recruitment processes and the drivers *Crangon crangon* fluctuations.

NEDERLANDSE SAMENVATTING

De Europese grijze garnaal (*Crangon crangon*) is diep verankerd in de Belgische cultuur. Sinds de Middeleeuwen al wordt deze kustbewoner bevist om te consumeren of te verkopen als voedselbron. Ondanks een afnemende vissersvloot blijft de garnaalvisserij nog steeds een belangrijke economische sector langs de Belgische kust. In de afgelopen jaren hebben zich echter aanzienlijke schommelingen voorgedaan in de garnaalvangst. Jaren met grote commerciële aanlandingen werden afgewisseld met jaren van opvallend lage vangsten. In 2023 bijvoorbeeld leidde een teleurstellende vangst tot een substantiële stijging van de garnaalprijzen, wat resulteerde in economisch uitdagende tijden voor zowel vissers als verkopers. Tot op heden zijn noch vissers noch wetenschappers erin geslaagd de oorzaak of oorzaken van deze schommelingen te achterhalen.

Deze masterthesis heeft als doel de voornaamste invloeden op het rekruteringsproces van *Crangon crangon* te identificeren en recente schommelingen van de garnaalpopulaties in het Belgische deel van de Noordzee (BPNS) te linken met heersende omgevingsomstandigheden. Aanvankelijk werd verondersteld dat het voorkomen van mariene hittegolven (MHWs) een significante invloed had op de garnaalpopulatie in BPNS. Mariene hittegolven zijn gebeurtenissen waarbij de watertemperatuur gedurende een bepaalde periode een bepaalde drempelwaarde overschrijdt, wat resulteert in sterk verhoogde watertemperaturen. Het merendeel van deze MHWs heeft een antropogene oorsprong, gezien hun link met klimaatverandering. Wereldwijd komen MHWs steeds vaker voor, waardoor het marine leven en bijhorende ecosysteemdiensten een steeds groter wordende druk ervaren. Echter, in jaren waarin intense MHWs werden waargenomen, zoals in 2018 of 2022, bleek het aantal commerciële aanlandingen gestegen te zijn. Daarom werd ook aanvankelijk de correlatie tussen (verhoogde) watertemperaturen en garnalenpopulaties onderzocht. Maar aangezien *Crangon crangon* bestanden niet uitsluitend afhankelijk zijn van de watertemperatuur, werden ook verschillende andere omgevingsparameters, zoals voedselbeschikbaarheid of de aanwezigheid van predatoren, onderzocht.

Aangezien de rekrutering van *Crangon crangon* in het BPNS beperkt bestudeerd is, was slechts een beperkt aantal uitgebreide dataseries beschikbaar. Het Vlaams Instituut voor Landbouw-, Visserij- en Voedingsonderzoek (ILVO) leverde gegevens over garnalenpopulaties in het BPNS, gebaseerd op hun Demersal Young Fish Survey (DYFS) die jaarlijks in september plaatsvindt. Deze dataserie werd vervolgens gecombineerd met gegevens uit het LifeWatch-framework dat beheerd wordt door het Vlaams Instituut voor de Zee (VLIZ). Zo werd een algemene dataset gecreëerd die zowel informatie bevat over de *Crangon crangon* populaties als verschillende omgevingsparameters zoals watertemperatuur, nutriëntenconcentraties of zoöplanktondensiteit. Met behulp van deze dataset werden diverse spreidingsdiagrammen gegenereerd om de directe correlaties tussen deze omgevingsparameters en de *Crangon crangon* populaties te onderzoeken. Daarnaast werden Generatieve Additieve Modellen (GAMs) geconstrueerd om niet-lineaire correlaties te bestuderen.

De spreidingsdiagrammen en GAMs gaven aan dat het rekruteringsproces van *Crangon crangon* wordt beïnvloed door meerdere omgevingsfactoren, naast de watertemperatuur. Positieve correlaties werden gevonden voor nutriëntconcentraties, de chlorofyl a concentratie en de winter- en zomerindex van de Noord-Atlantische Oscillatie (NAO). Daarentegen werden negatieve correlaties gevonden voor watertemperatuur, zoutgehalte, zoöplanktondichtheid, wijting populaties, diepte en visserijactiviteiten. Elk van deze parameters heeft invloed op het rekruteringsproces binnen specifieke temporele vensters, wat de complexiteit van de invloeden op het rekruteringsproces van *Crangon crangon* in de BPNS onderstreept.

Naast de data-analyse werd de nutritionele content van grijze garnalen in het BPNS kort onderzocht. Verschillende monsters werden verzameld tijdens verschillende offshore-campagnes in september en november 2023. Deze werden vervolgens gebruikt voor eiwitextracties (Bradford-methode) en lipidenextracties (Bligh & Dyer-methode). Het doel van

deze extracties was om het eiwit- en lipidengehalte te vergelijken over een near-offshore en oost-west gradiënt, evenals tussen de herfst en winter populaties. Ondanks het beperkte aantal bemonsterde garnalen werden enkele significante verschillen opgemerkt. Vooral het verschil tussen de near- en offshore gebieden toonde een veelbelovend resultaat.

Samenvattend is deze masterthesis een van de eerste studies die probeert het fluctuerende gedrag van *Crangon crangon* in het BPNS te verklaren. Verschillende omgevingsparameters die een significante invloed uitoefenen op de rekrutering werden hierbij geïdentificeerd. Echter, door de beperkte beschikbaarheid van gegevens en ontbrekende literatuur blijft deze studie exploratief. Desalniettemin kan deze studie dienen als basis voor vervolgonderzoeken die gericht zijn op een dieper begrip van het rekruteringsproces van *Crangon crangon* en de achterliggende drijfveren en invloeden op dit proces.

FACULTEIT
BIO-INGENIEURSWETENSCHAPPEN

ILVO

"The ocean's power of regeneration is remarkable - if we just offer it the chance."

-Sir David Attenborough

UNIVERSITEIT
GENT

LITERATURE

1 CHANGING SEAS AND OCEANS

The world is changing. Droughts, floods, forest fires, melting glaciers… are all visible consequences of a warming Earth. While climate change has existed since the origin of planet Earth, the climate never changed at faster rates than today, primarily due to excessive anthropogenic emissions originating from for example fossil fuel burning, cement production or deforestation (Hoegh-Guldberg & Bruno, 2010; LaRiviere et al., 2012; Tripati et al., 2009). Unlike terrestrial impacts, such as droughts and forest fires, the impacts of global warming on marine ecosystems are not well understood due to its vast size and complexity (Rosenzweig et al., 2008).

1.1 The deadly trio

In recent years, the levels of atmospheric carbon dioxide (CO_2) reached levels they never did before in the past 15 million years (LaRiviere et al., 2012; Tripati et al., 2009). Three distinct effects, often referred to as the "deadly trio", are directly related to these elevated carbon levels and cause a (permanent) shift in ecosystem structure and functioning: temperature rise (Belkin, 2009; Intergovernmental Panel on Climate Change (IPCC), 2007; Rayner et al., 2003; P. C. Reid & Beaugrand, 2012; Sherman et al., 2009), ocean acidification (Caldeira, 2007; Caldeira & Wickett, 2003; Cao & Caldeira, 2008) and deoxygenation (Andrews et al., 2013).

Just like forests, oceans and seas act as a carbon sink. It is estimated that the oceans have taken up approximately one-third of all human carbon dioxide (CO_2) emissions (Hoegh-Guldberg & Bruno, 2010).However, the absorption of atmospheric CO_2 does not come without any consequences. By absorbing high levels of atmospheric CO2, the pH of the ocean alters, shifting towards lower levels. This leads to the dissolvement of CaCO3, the main component of coral or shells (Henry et al., n.d.) This phenomenon is called "acidification of the ocean".

Besides the problem of temperature rising and acidification, there is a third major concern: deoxygenation of oceans. Oxygen is a crucial element for aerobic marine life and nutrient recycling (Gruber, 2008; Keeling et al., 2010). Consequently, reduced oxygen levels could significantly impact marine life and its accompanying ecosystem services (Poloczanska et al., 2016).

In this dissertation however, the focus will be primarily on the temperature rise with a particular emphasis on marine heatwaves (MHWs). The other two effects, acidification and deoxygenation, are out of the scope of this dissertation and will therefore not be discussed.

1.2 Increasing sea surface temperatures and marine heatwaves

The oceans act as an energy sink, absorbing approximately 93% of all excessive energy associated with emitted greenhouse gasses (Poloczanska et al., 2016). This absorption leads to a steady increase in ocean temperatures, especially in the last decades. Consequently, over the past 150 years, the oceans temperature increased with 0.88°C (Intergovernmental Panel on Climate Change (IPCC), 2023). Additionally, periods with anomalously high water temperatures, known as marine heatwaves, occur more frequently and have a longer duration (Oliver et al., 2021).

1.2.1 Definition and quantification

A marine heatwave (MHW) is a relatively new term introduced by Pearce et al. (2011) and describes a discrete period of prolonged anomalously warm water at a particular location and has the potential to significantly affect marine ecosystems (Oliver et al., 2021). In literature, various quantitative definitions for MHWs exist. The most widely used method quantifies a MHW as an event where water temperature exceeds a fixed threshold value for a certain period of time. This fixed threshold value is often defined as the 90th percentile of local climatology (Hobday et al., 2016). However, other studies, such as Frölicher et al. (2018), use a more severe threshold value, such as the 99th percentile, to identify more extreme events.
Additionally, researchers may use the upper thermal limits of a certain marine organism (e.g. coral) as the threshold value, as demonstrated by Liu et al. (2014). In this way, the impacts of the MHW on the highlighted marine organism can directly be studied (Smith et al., 2022).

Typically, with a fixed threshold value, only the MHWs in warm periods (e.g. August) are detected. If one wants to investigate the annual occurrence of MHWs in a certain region, a seasonal threshold value can be used, as demonstrated by Hobday et al. (2016). This threshold value is calculated, for example, on a daily basis over a period of 30 years and detects MHWs all year around. This approach helps to identify anomalously warm periods both during warm and cold periods, such as winter months (Hobday et al., 2016) .
Each quantification method has its own benefits and limitations, and therefore it is important to validate the chosen definition.

1.2.2 Mechanisms

To understand how MHWs are formed, it is essential to understand the variation in sea surface temperature (SST) and the underlying processes. The variation in SST is mathematically described by Moisan & Niiler (1998) (**Figure A- 1**) and is influenced by several physical processes such as air-sea heat flux, horizontal advection and lateral and/or vertical mixing (**Figure 1-1**).

A first important process that contributes to the formation of MHWs is the air-sea heat flux. This flux is the net result of the incoming shortwave(Q_{SW}) and longwave(Q_{LW}) radiation minus the outgoing shortwave ($Q_{SW(-b)}$), the latent heat (Q_{lat}) and the sensible heat (Q_{sens}) flux (Cronin et al., 2019). At the event of a marine heatwave, abnormally high incoming shortwave radiation, as a result of reduced cloud cover or an increased sensible heat flux due to a warm sea surface, are present (Oliver et al., 2021). These two situations often occur when a high-pressure region is present, which reduces the amount of wind, which also reduces the amount of vertical mixing. Additionally, because of the weak winds, less latent heat is carried away. These processes, independently or in combination, cause a rise of the seawater temperature which eventually results in an air-sea heat flux type MHW (Oliver et al., 2021).

In addition to the air-sea heat flux type MHW, there is also the advection type MHW. These are caused by anomalous ocean currents, or, in less extent, by anomalous temperature gradients (Oliver et al., 2017). Due to the friction between water and air, winds cause water to move in certain directions, creating significant flows such as the Ekman transport (Elias, 2021). These waterflows can flow across a temperature gradient, resulting in horizontal advection between the different surface layers. Additionally, these flows are often related to different up or downwelling processes, resulting in vertical advection. A change in wind patterns can thus cause anomalous waterflow which can bring additional heat, resulting in heatwaves. However, these changing currents can also inhibit MHW by the upwelling of cold water from the deep (Oliver et al., 2021) .

Other factors that contribute to the creation of a MHW include horizontal diffusion, vertical mixing due to vertical turbulent fluxes and entrainment of waters into the mixed layer due to temporal or spatial variation mixed-layer depths. However, these contributions are rather small and therefore often neglected (Oliver et al., 2021).

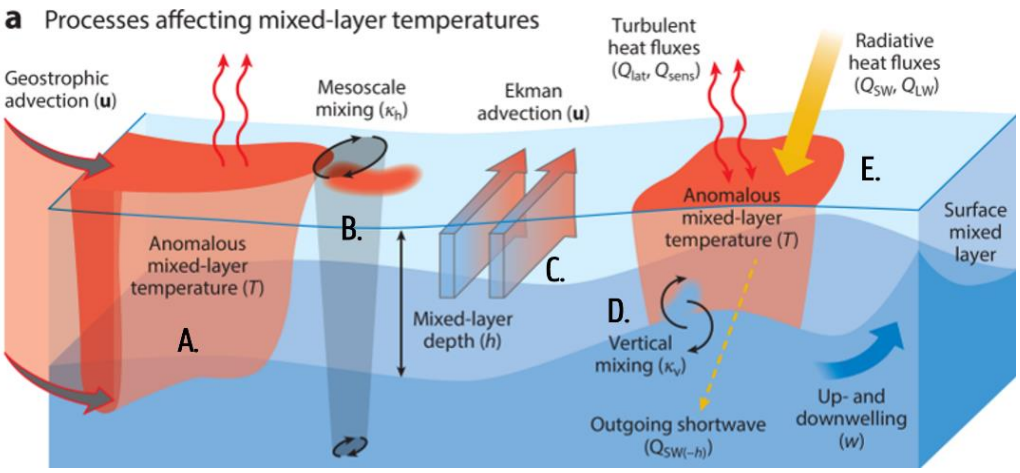

Figure 1-1 Physical processes which influence the temperature of the surface waters. [A] Entrainment of deeper water into a warm mixed layer [B]horizontal mixing [C] horizontal advection due to Ekman transport [D] Vertical mixing of two water layers [E] air-sea heat fluxes divided into: net incoming shortwave (Q_{SW}) and longwave radiation (Q_{LW}), outgoing shortwave radiation via the bottom of the mixed layer ($Q_{SW(-h)}$), net latent heat (Q_{lat}) and sensible heat (Q_{sens}). Figure derived from Oliver et al. (2021).

1.2.3 Global distribution

Typically, MHWs are more abundant in regions with a high variability in SST, such as the central and eastern Pacific Ocean. In the eastern tropical Pacific, a region dominated by the El Niño Southern Oscillation (ENSO) MHWs can last up to 60 days. In other tropical regions, MHWs typically last five to ten days. In extratropical regions, such as the northeast Atlantic, MHWs have a typical duration of around 10 to 15 days.

The most severe documented MHWs are those resulting from abnormally high air-sea heat fluxes, where the atmospheric state plays a central role in creation and maintenance. Notable examples of these types of heatwaves include the events in the Mediterranean Sea (MED) during 2003 (Olita et al., 2007) and 2006 (Bensoussan et al., 2010), in the northwest Atlantic (NWA) in 2012 (K. Chen et al., 2014, 2015), East China Sea (ECS) in 2016 (Tan & Cai, 2018), off coastal in Peru in 2017 (Echevin et al., 2018) and in the Tasman Sea (TAS) during 2017-2018 (Perkins-Kirkpatrick et al., 2019; Salinger et al., 2019) (**Figure 1-2**).

Other MHWs are related to anomalous heat transport through the ocean (e.g. horizontal advection). Examples include the event in the Angola Benguela upwelling system (BENG) in 2001 (Rouault et al., 2007) and off Western Australia (WA) in 2011 (Benthuysen et al., 2014; Feng et al., 2013). Some MHWs result however from a combination of multiple mechanisms, such as the MHW in the northeast Pacific (NEP) from 2014 to 2016. Additionally, some MHW are also associated with the retreat of Artic ice, such as the MHW in the Gulf of Alaska and the Bering Sea (AL) in 2016 (Oliver et al., 2018; Walsh et al., 2018) (**Figure 1-2**).

All of these mentioned heatwave events vary in duration and intensity, but uniformly negatively impact the present marine ecosystem leading for example to increased mortalities, the formation of harmful algal blooms (HABs) or reduced reproduction rates (Oliver et al., 2021; Smith et al., 2022).

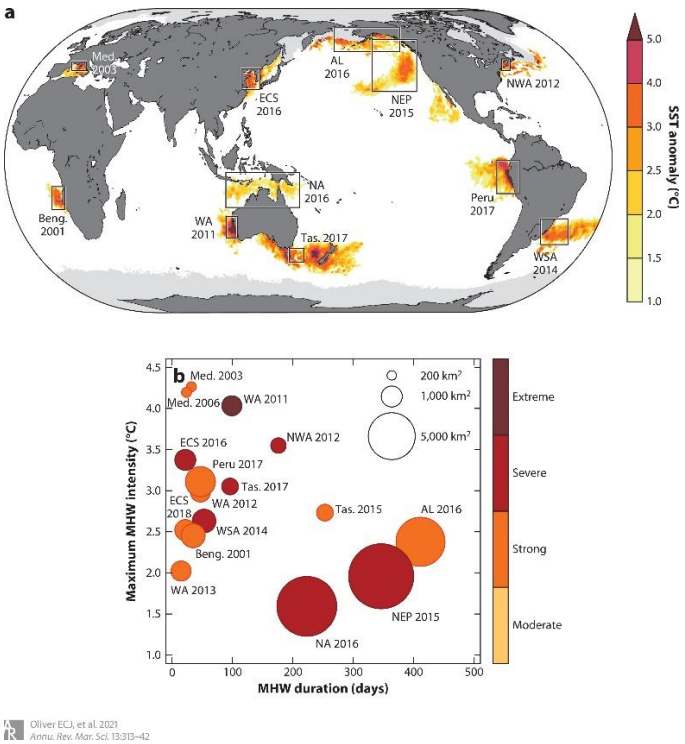

Figure 1-2 Global distribution of the most important historic marine heatwaves.(AL, Gulf of Alaska and Bering Sea; Beng., Benguela; ECS, East China Sea; Med., Mediterranean; NA, northern Australia; MHW, marine heatwave; NEP, northeast Pacific; NWA, northwest Atlantic; SST, sea surface temperature; Tas., Tasman Sea; WA, Western Australia; WSA, western South Atlantic.) (A) SST anomaly of the different heatwaves on the day of peak MHW intensity. (B) Properties for the MHW shown in figure A. Intensity, duration and colour code are determined based on spatially averaged time series. Figure taken from Oliver et al. (2021).

1.2.4 History and long-term trends

Despite being only defined in 2011, MHWs have been occurring already since preindustrial times. By using SST data of the period 1982-2016 and several Earth System Models (ESMs), Frölicher et al. (2018) tried to compare the probability of occurrence and the characteristics of MHWs of three distinct periods: a preindustrial period, the situation today and the future. They hereby identified a MHW as an event where SST exceeded the 99th percentile of local climatology, focussing on MHWs which occurred during summertime (see §1.2.1).
They found that MHWs occurred in the preindustrial period with an average duration of 11 days and with an estimated maximal intensity of 0.3°C-0.5°C.

Today, under a 1°C-global warming scenario, they estimated that MHWs had a nine times higher probability of occurrence, with an estimated average duration of 25 days and a maximal intensity of +0.8°C. Additionally, they estimated that the spatial extent over which a MHW could occur tripled in comparison with the preindustrial period. For the period of 1982-2016, satellite data of the SST was available, which made it possible to make very accurate estimations. From the data, they concluded that over these 35 years, the possibility of MHWs to occur increased with a factor of 1.29 and that the intensity increased with approximately 0.15°C.

For the future, different warming scenarios were tested, all leading to the same conclusion: MHWs will occur more frequently, last longer and will have a higher intensity. They observed in total two different Representative Concentration Pathways (RCP): RCP2.6 and RCP8.5. RCP2.6 corresponds with a low-emission scenario compatible with the Paris Agreement, while RCP8.5 corresponds with a high-emission scenario in which very few measures are taking to reduce climate change. The results of the modelling with both scenarios are shown in **Figure 1-3**.

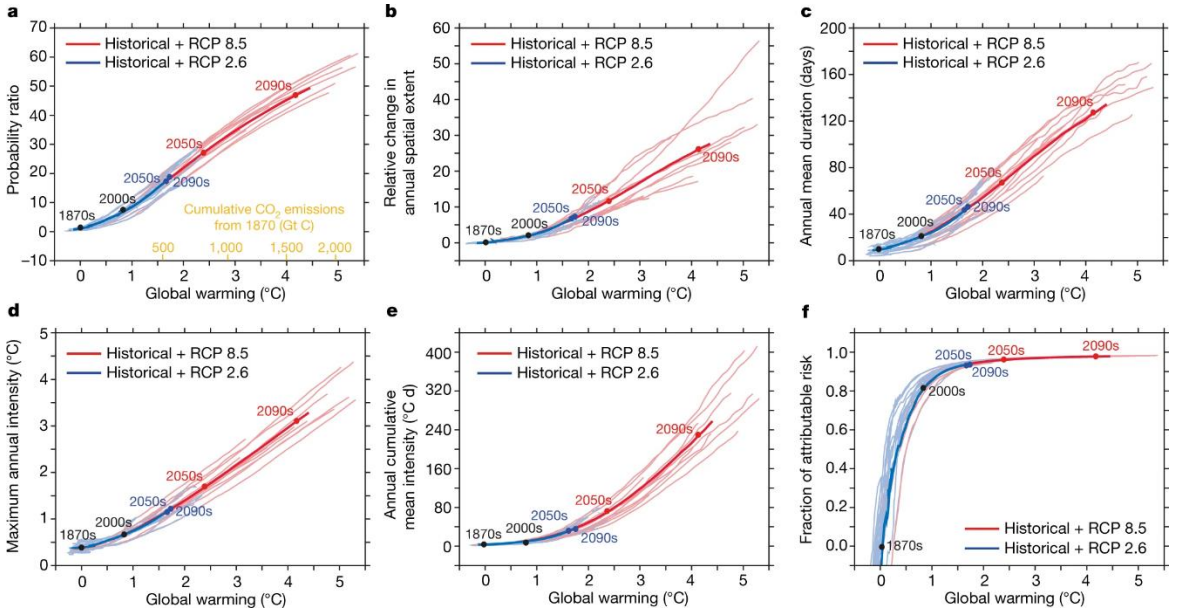

Figure 1-3 Simulations of changes of different MHW characteristics for two different emission scenarios (RCP 2.6 and RCP 8.5): [a] Annual mean probability ratio, [b] Ratio of the mean spatial extent of MHW in comparison to the extent under conditions at 1861-1880, [c] Duration of MHW, [d] Maximum intensity, [e] Cumulative mean intensity, [f] fraction of attributable risk of the MHW exceeding the 99th preindustrial temperature percentage. Thin lines represent the output of a single model. The thicker lines represent the multi-model averages. Figure taken from Frölicher et al. (2018).

Figure 1-3 illustrates the significant impact of global warming on MHWs. For instance, under a 3.5°C warming, the probability of occurrence would increase with a factor 41, with an estimated duration of around 112 days and a maximum intensity of 2.5°C. This would mean that an event which occurred every 100 days in preindustrial times, would take place every three days. The spatial extent of a MHW would also increase with a factor 21.

The simulations also show the importance of reducing climate change. In the RCP2.6 scenario, global warming will not exceed 2°C, resulting in an occurrence probability of "only" 20 times the preindustrial probability. If global warming would even stay below 1.5°C, the probability of occurrence would be only 40% of that under the 3.5°C warming scenario. Duration would then be 35% and maximum intensity 45% of those under the 3.5°C warming scenario (Frölicher et al., 2018).

But even the "small" increase in occurrence under the RCP2.6 scenario could have significant impacts on marine ecosystems. One of the first ever recorded impacts of MHWs was the Mediterranean Sea heatwave event of 2003, which caused a significant higher mortality rate among epibenthic communities (Garrabou et al., 2008). During the summer months, an anomaly of 2-3°C was observed, with an absolute seasonal maximum of 28.6°C on the August 26th (temperature in August 2002 and 2004 fluctuated between 24-25.5°C) (Sparnocchia et al., 2006). MHWs cause a shift in ecosystem structure and functioning and will eventually also affect human society and economies (Frölicher et al., 2018).

1.2.5 Anthropogenic role

In their study, Frölicher et al. (2018) also investigated the anthropogenic contribution to the increase in MHWs. Under the current global warming scenario, which is approximately +1°C compared to preindustrial times, 87% of all globally occurring MHWs can be attributed to global warming. Given that global warming is primarily driven by anthropogenic greenhouse gas emissions, it can be concluded that 87% of all MHWs today have an anthropogenic origin. When global warming would approach 2°C, this fraction would even further increase up to 97% (Frölicher et al., 2018).

1.2.6 Biological consequences of rising water temperatures

The effect of increased water temperatures on a marine organism depends on the thermal tolerance of the organisms. Stenotherm species for example have a narrow thermal niche and will therefore be more vulnerable to increased temperatures than eurytherms, which have a broader thermal range (Smith et al., 2022). Responses of marine species can range from introduction of nonnative species to reproductive failure or even mortality (Smith et al., 2022).

1.2.6.1 Increased mortality rates

Increased mortality rates induced by increased temperatures are often associated with harmful algal blooms, deoxygenation (see §1.1) and diseases (Smith et al., 2022). During a MHW event in the Red Sea in 2017 for instance, mass mortalities of over 40 coral fish species were reported due to thermal stress in combination with a bacterial infection (Genin et al., 2020).

1.2.6.2 Temperature induced migrations

As a result of increased water temperatures, many marine species are forced to leave their current habitats and seek for other places with more favourable conditions. By doing so, they disrupt balances in both the habitats they leave from and the habitats they newly enter (Poloczanska et al., 2016). Two distinct types of migrations are witnessed: polar and depth migrations.

First of all, species tend to flee the equatorial waters and to migrate towards more polars regions. In these equatorial regions, declines in recruitment and breeding successes are witnessed due to warming waters (Poloczanska et al., 2016). Additionally, due to the warming waters, marine species (e.g. shrimp) can migrate to deeper and cooler waters (Poloczanska et al., 2016).

1.2.6.3 Ecosystem service losses

Besides the marine ecosystem, MHWs also affects human interest by impacting several ecosystem services. The most impacted industries are hereby tourism and recreational fishing. For instance, a mass mortality and bleaching of coral in the Southeast Asian Sea, induced by MHWs, resulted in an estimated loss of US$49-47 million in tourist incomes (Smith et al., 2022).

2 THE BELGIAN PART OF THE NORTH SEA

2.1 Background

The Belgian part of the North Sea (BPNS) is located within the southern Bight of the North Sea, a well-mixed basin characterized by subtidal sandbanks which run parallel to the coast. It is a relatively shallow sea, with depths up to 40 m (Mortelmans et al., 2019; Semmouri et al., 2023). With a total surface of 3 454 km², the BPNS constitutes only 0.5% of the entire North Sea (**Figure 2-1**) (Health Belgium, 2020). Despite its small surface, the BPNS is an important area for various economic activities such as shipping, fishery or offshore wind parks. Consequently, the present ecosystem is significantly impacted by anthropogenic activities such as dredging, trawling or introduction of invasive species (Semmouri et al., 2023). Additionally, due to the discharge of several rivers (e.g. river Scheldt), the shallower waters of the BPNS form an eutrophicated system sensitive to harmful algal blooms (De Rijcke, 2017). The more offshore waters are in turn affected by the Atlantic Ocean which brings clear, warm and more saline water through the English Channel (Mortelmans et al., 2021). All the influences make the BPNS a hard and complex and challenging ecosystem to study, resulting in a scarce number of studies on for example *Crangon crangon*.

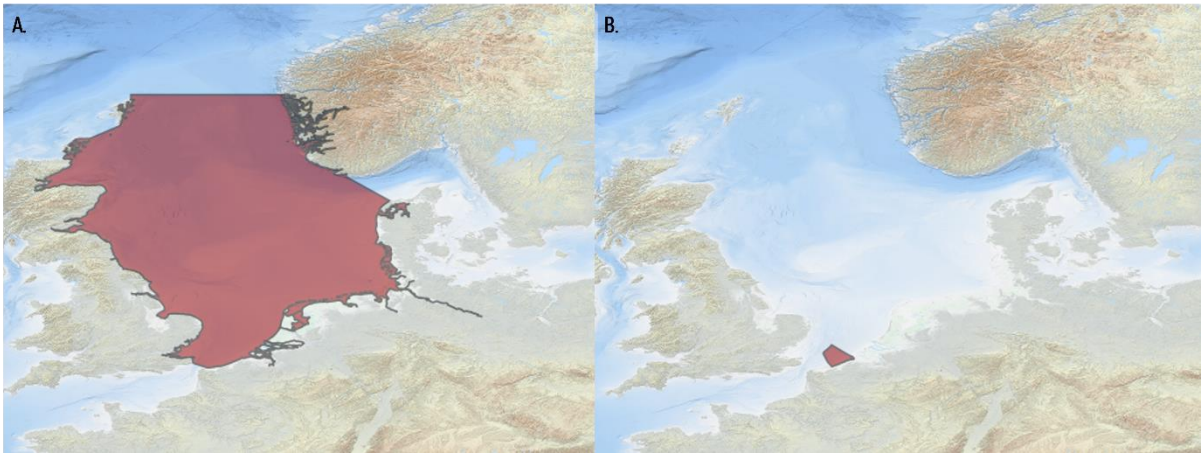

Figure 2-1 [A] Surface area of the North Sea. [B] Surface area of the Belgian part of the North Sea (BPNS). Figure A was derived from De Hauwere (2017), figure B from Oset Garcia (2016).

2.2 North-Atlantic climate indices

Weather and climate in the BPNS are defined by so-called "planetary-scale waves". These waves displace air in the north and south of planet Earth and are caused by atmospheric processes which are modulated by high mountains and land-sea boundaries (Stenseth et al., 2003). Changes in the behaviour of these waves due to for example varying heating patterns cause a variation in the present state of the climate which differs from the long-term mean state, which is computed over many years. These variations mostly occur on a seasonal or longer timescale and are referred to as "anomalies" (Hurrell & Deser, 2010; Stenseth et al., 2003). Typically, these variations also occur on a large geographical scale. One region on Earth could for example experience a cooler and drier period while another region thousand kilometres away could experience a warmer but wetter period. These simultaneous variations in climate on a global scale are called "teleconnections" (Hurrell & Deser, 2010; Stenseth et al., 2003). One of the best-known teleconnections is the North Atlantic Oscillation (NAO), which is discussed in §2.2.1 .
The climate anomalies -also called "modes" or "oscillations"- influence several climatological parameters (e.g. windspeed, air temperature) which, on their turn, also effect marine or terrestrial ecosystems (Drinkwater et al., 2003). They thus can influence the structure and functioning of ecosystem and accompanying ecosystem-services and therefore need to be predicted.

Scientists therefore developed several climate indices in order to study and understand the behaviour of different modes and to make climatological predictions on a seasonal scale (Wanner et al., 2001). In this section, different climate indices of the Northern-Atlantic region (NAO and AMO), to which the North Sea belongs, will be discussed (Hurrell et al., 2003; Knight et al., 2005; Mohamed et al., 2022; Scannell et al., 2016; Trenberth & Shea, 2006; van der Molen & Pätsch, 2022).

2.2.1 North Atlantic Oscillation

From all the climate indices used in the Northern-Atlantic region, the North Atlantic Oscillation index is the most studied one. It describes the behaviour of the NAO, a north-south alternation in atmospheric mass between the Artic and the tropical Atlantic. It is present during the whole year but is more prominent during the colder months (November-April) (Stenseth et al., 2003).
In essence, it involves the difference between two pressure areas: one low-pressure area near Iceland and one high-pressure area near the Azores. In case of a positive NAO index, there is an anomalously higher-pressure area in the Azore region and consequently a lower-than-normal pressure area around Iceland, resulting in a big pressure difference (Stenseth et al., 2003; Wanner et al., 2001). This results in a higher storm activity in the northern part of the Atlantic,

resulting in warmer but wetter winters in the North Sea (**Figure 2-2**, right). On the contrary, if the NAO index is negative, the pressure difference is smaller than usual, resulting in colder but drier winters. Note that the pressure distribution is not necessarily reversed, meaning that there is still a low-pressure area around Iceland and a high-pressure area around the Azores. A reversed situation, indicated with a very negative NAO index, occurs very rarely (Wanner et al., 2001).

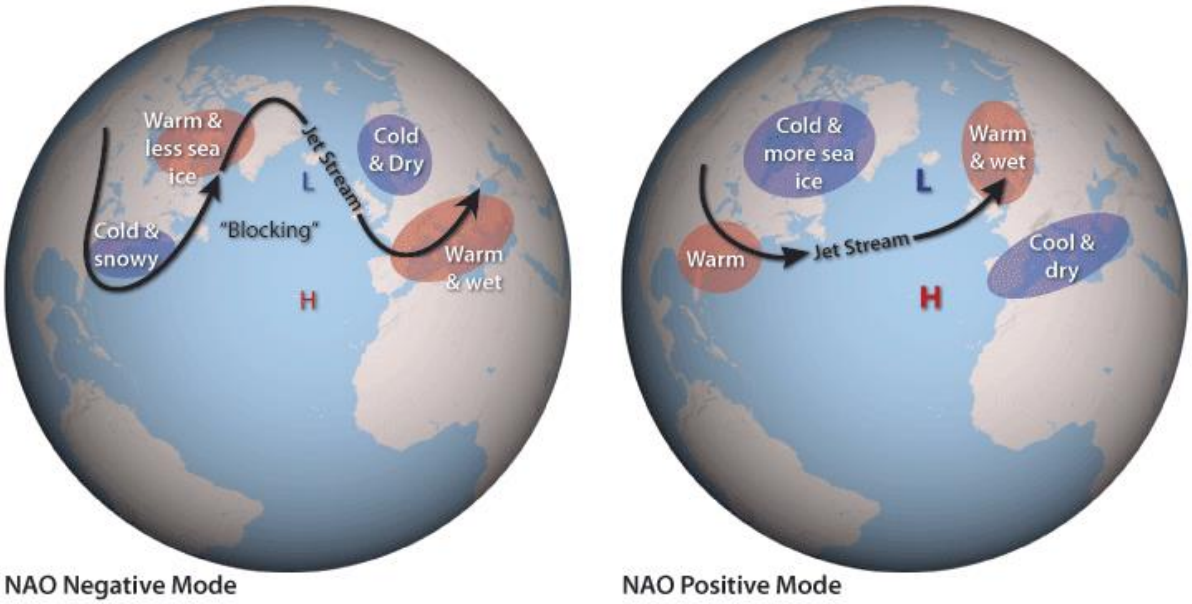

Figure 2-2 *The mechanisms behind the North Atlantic Oscillation and its climatological consequences. On the left side, the mechanism behind a negative NAO index is illustrated, which means that the difference in pressure area around Iceland and the Azores is small. As a result, Atlantic storms, carrying warm but wet winds are moving towards the Mediterranean region. This allows eastern winds, which are cold and dry, to flow to the northern Atlantic region. In northern Europe, reduced "storminess" and below-average precipitation and temperatures are noted. On the right, the exact opposite situation is illustrated during which a positive NAO index is present. Because of the high difference in pressure areas, Atlantic storms move towards the North-Atlantic region resulting in mild but wet winters. Figure taken from Lindsey & Dahlman (2009).*

2.2.2 Atlantic Multidecadal Oscillation

The Atlantic Multidecadal Oscillation or AMO is an oscillation of the sea surface temperature (SST) in the northern Atlantic Ocean over -as the name suggests- a multidecadal period. Anomalously warm SSTs are altered with cold ones, affecting the European summer climate, among other things (Knight et al., 2006). During its positive phase, warmer than normal SSTs can be observed in the northern Atlantic Ocean, whilst in the south colder temperatures are present (**Figure 2-3-B**). In its negative phase, this pattern is reversed (**Figure 2-3-A**) (Zhang, 2016). Currently, a positive AMO-phase is present.

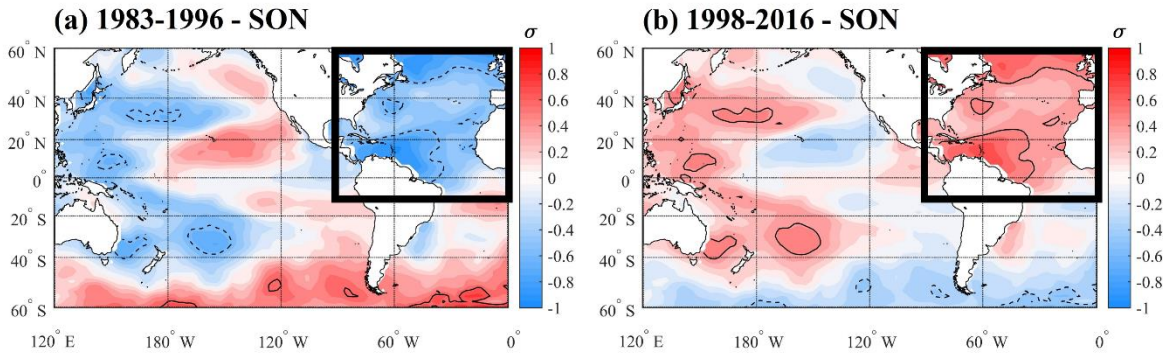

Figure 2-3 *Illustration of the [A] negative and [B] positive Atlantic Multidecadal Oscillation (AMO) phase. On both figures, the mean standardized SST anomalies in September-November (SON) are visualized. In the left graph, a negative AMO phase is illustrated, showing colder-than-usual SSTs in the northern Atlantic (top right of the figure, indicated with the black square). On the contrary, during the positive AMO phase, warmer-than-normal SSTs are observed. Figure taken from Loaiza Cerón et al. (2020).*

2.3 Heatwaves in the North Sea

2.3.1 Quantification

The quantification method of marine heatwaves (MHWs) and marine cold spells (MCSs) in the North Sea is described by Mohamed et al. (2023) and is based on the method of Hobday et al. (2016).
Marine heatwaves and marine cold spells are events where the SST respectively exceeds or stays under a seasonal threshold value for a period of at least five consecutive days. For MHWs, this threshold value corresponds with the 90th percentile of local climatology, with a baseline period of at least 30 years. For MCSs, this threshold value corresponds with the 10th percentile of local climatology (Mohamed et al., 2023).

For the southern North Sea, the climatological mean SST, which is calculated with data from the period 1982-2021, amounts 12.2°C, with a mean 90th anomaly of 13.6°C (+1.4°C compared to climatological mean). The 10th percentile anomaly is estimated on a value between 10.4°C and 11.6°C (-1.8 and -0.6°C, respectively) (Mohamed et al., 2023).

2.3.2 Spatiotemporal trends

In terms of marine heatwaves, the North Sea follows the global trend of an increase in frequency, duration and intensity. In the last four decades (1982-2021), a total of 71 MHWs occurred in the southern North Sea, of which 23 took place during summer (July, August, September) and 16 during winter (January, February, March) (**Table A- 1**) (Mohamed et al., 2023). High mean annual MHW days (more than 30) were observed in the region between the United Kingdom and Belgium, while the highest intensities were noted along the northern Dutch coast and the German Bight (see **Figure 2-4**) (Mohamed et al., 2023).

Over the observed period, a significant increase in annual MHW frequency and MHW days was witnessed with trends of +0.85±0.39 events (MHW) decade^{-1} and +14.36±8.16 days decade^{-1}. The highest increase of MHW days was observed in the region between Belgium, UK and The Netherlands, with an increasing trend of +22 days decade^{-1} (Mohamed et al., 2023).
Maximum intensity of a MHW also tends to increase with 0.12±0.08°C decade^{-1}. A peak frequency was witnessed in 2014 with 8 events, corresponding with 160 MHW days in one year, while peak intensities were observed in 2018 with anomalies up to 3-6°C during summer months (**Figure 2-5**) (W. Chen et al., 2022; Mohamed et al., 2023)

Figure 2-5 summarizes the number of heatwaves that occurred in the period between 1982 and 2021 in the southern North Sea. It is clearly noticeable that this amount only increases over these four decades, with a record-breaking amount of 31 MHWs during the last decade (2012-2021). Additionally, in the last two decades (2002-2021), only five years (2004, 2010, 2012, 2013 and 2015) had multiple MHWs below the climatological mean (1982-2021).

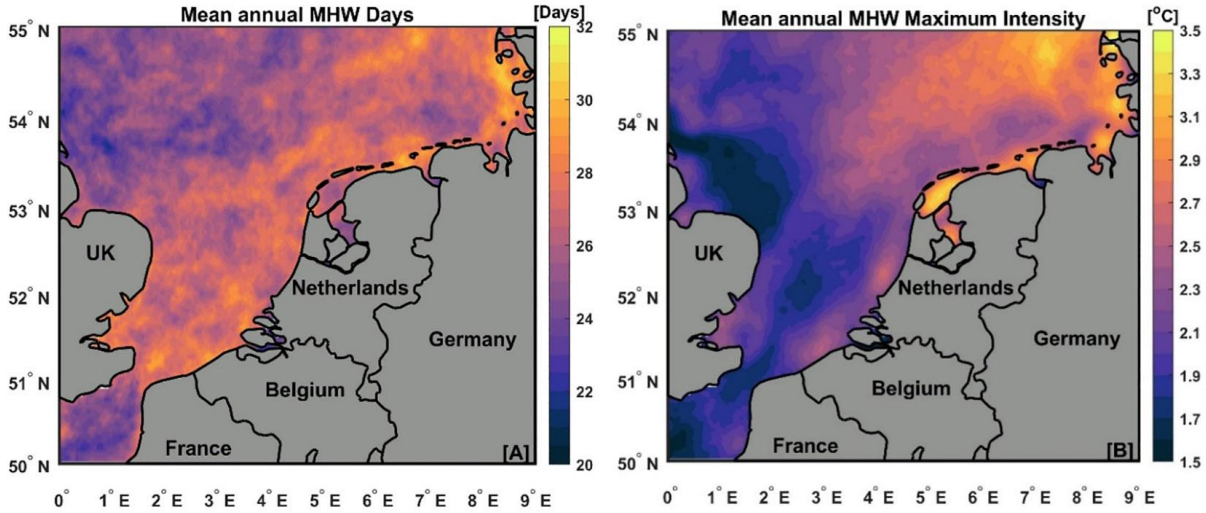

Figure 2-4 [Left] Spatial distribution of the mean annual MHW days (days) over the period 1982-2021. [Right] Spatial distribution of the mean annual maximum intensity recorded over the period of 1982-2021. Both figures are derived from Mohamed et al. (2023).

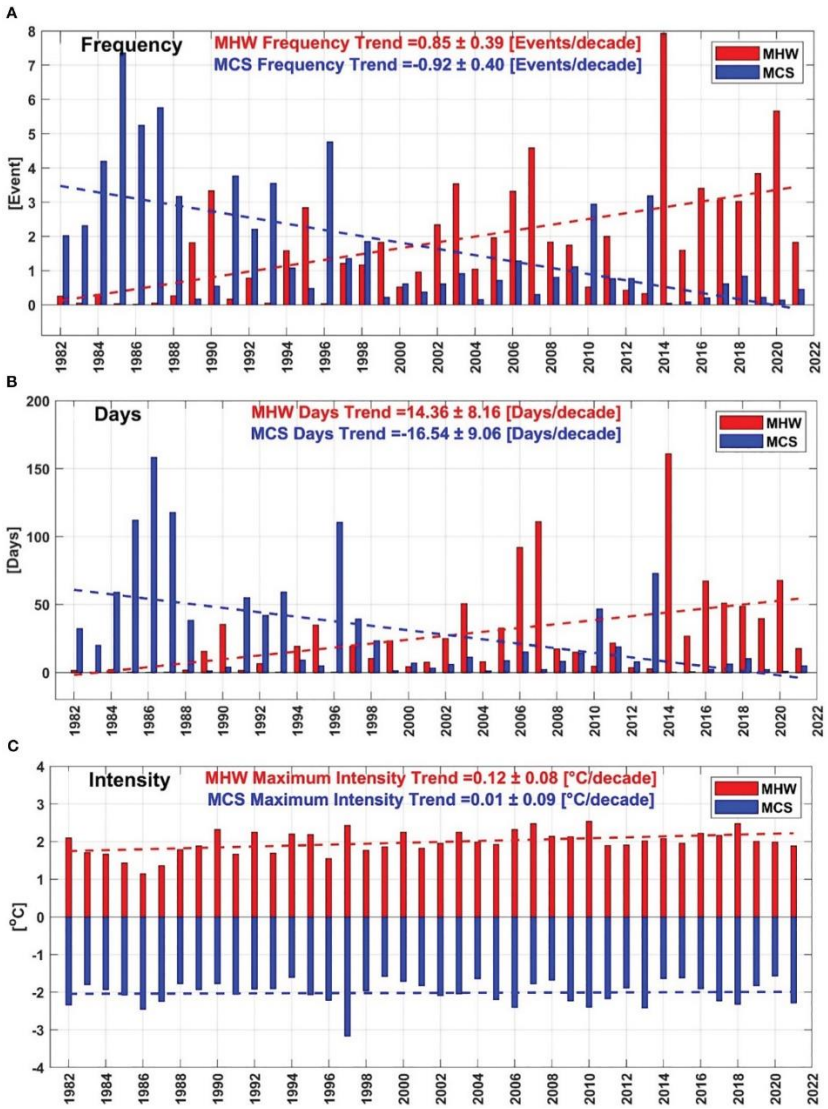

Figure 2-5 Graphs showing the annual (A) frequency, (B) days and (C) maximum intensity of the present MHWs and MCSs in the North Sea over the period 1982-2021. The general trends are indicated with the red (MHW) and blue (MCS) lines. The slope of the trend is shown in the upper part of each graph. Graphs taken from Mohamed et al. (2023).

2.3.3 Relation with climate modes (NAO, AMO)

Because of the link between atmospheric patterns and the origin and maintenance of MHWs, Mohamed et al. (2023) also investigated the link between the occurring MHWs in the North Sea and different climate modes, such as the NAO (see §1.2.2 and §2.2). They considered the NAO and AMO indices, which are also discussed in §2.2.

Firstly, the researchers looked into correlations between these climate modes and the SST. On an annual scale, they found significant correlations with the AMO index, but non for the (winter) NAO index. Additionally, the AMO index showed a significant correlation with the frequency and duration (days) of MHWs in the southern North Sea. The NAO is also significantly correlated with the frequency and duration of the MHWs, but only during wintertime. A complete summary of the found correlations can be found in **Table A- 2**.

3 ZOOPLANKTON-COPEPODS

3.1 Community composition

Zooplankton is collective name for aquatic organisms incapable of swimming against a current and grazing upon phytoplankton or preying on other zooplanktonic species. The zooplanktonic community contains a wide variety of species, ranging in size from microscopic protozoans to jellyfish of a couple of meters in length (Denne, 2018). Distinction in this community is made based on size and lifestyle. Species maintaining a complete planktonic lifestyle are considered holoplankton, while species who live a partial planktonic lifestyle like juvenile fish belong to the meroplankton. Additionally, based on size of the plankton, species can belong to micro-, meso-, or macroplankton if they are respectively smaller than 0.2 mm, between 0.2 and 2 mm or larger than 2 mm (Semmouri, 2022).
Within this vast group of organisms, copepods are typically the most abundant species, representing almost 80% of the total zooplankton biomass (Williams et al., 1994). In the BPNS, the zooplankton constitutes approximately 70% of calanoid and harpacticoid copepods, making them the most abundant zooplankton species (Mortelmans et al., 2021).

However, this is not always the case. The composition of a zooplankton community depends namely on water temperature and the connected nutrient mixing. Generally, two distinct situations can be identified.
When cold conditions are present, the top water layer will be colder than the underlying water layers. Since cold water is heavier than warmer water, the top layer will sink down, pushing the lower situated water layers upwards, creating a well-mixed and turbulent environment. In this environment, nutrients coming from the deeper waters are well mixed across the entire water column. These conditions are very favourable for the production of diatoms which will then dominate the phytoplankton community. Copepods graze primarily on these diatoms and will consequently flourish and dominate the zooplankton community. This short food web of diatoms and copepods is nutritionally rich, providing energy to various species spread across different trophic levels, such as fish, seabirds and marine mammals (Richardson, 2008).
However, when warmer conditions occur, the water column will be stratified, not allowing any mixing. Nutrients will only be present in deeper water, resulting in a depletion of the upper water layers. Nitrogen, a limiting nutrient for phytoplankton, is negatively correlated with water temperature and will thus be present at very low concentrations (Kamykowski & Zentara, 1986) . As a consequence, zooplankton is not dominated by copepods but by more gelatinous species such as salps (*Salpidae*), doliolids (*Doliolida*) and ctenophores (*Ctenophora*). In this food web, trophodynamics depend on nitrogen recycling, making it long and insufficient. Consequently, far less trophic levels are supported in comparison to the copepod food web. Nutrient enrichment, determined by water temperature, is thus a key factor for the present zooplankton community (Richardson, 2008) .

3.2 Copepods

3.2.1 Taxonomy and importance

Copepods, or scientifically *Copepoda*, are a class of the superclass *Multicrustacea*, which belongs to the subphylum of the *Crustacea*. The *Crustacea* are in turn part of the phylum of the *Arthropoda* (WoRMS, 2024). Approximately 14 000 species are identified that belong to this class, with slightly over 11 000 of them living in marine environments (situation in 2010) (J. W. Reid & Williamson, 2010).

The most common copepod species in the BPNS are the Calanoida, Canuelloida, Cyclopoida and Harpacticoida. In total, they represent approximately 70% of all present zooplankton in the BPNS. Calanoida, Canuelloida and Cyclopoida are merged into one group and represent 64% of the total zooplankton in the BPNS, good for a mean abundance of 1348 individuals m^{-3}. Maximum abundances of this group were noticed during the spring peak, reaching levels of 9876 individuals m^{-3} (Mortelmans et al., 2021). Harpacticoida on their turn represent 6%, averaging an abundance of 154 individuals m^{-3}, with maxima going up to 1522 individuals m^{-3} (Mortelmans et al., 2021).

Due to its high abundance in marine ecosystems, zooplankton fulfils several important functions. Firstly, they are a crucial link in the marine food web. By grazing on marine phytoplankton, zooplankton transfers energy from primary producers towards higher trophic levels such as fish or marine mammals (Mortelmans et al., 2021; Richardson, 2008). Secondly, they also play an important role in the energy recycling. Excretion products and carcasses of zooplankton, the so-called "marine snow", settles down to the seafloor at a slow but constant rate, providing not only the microbial and phytoplankton, but also the benthic community with nutrients such as carbon and nitrogen (Semmouri et al., 2023). Additionally, to nutrient recycling, this biological carbon pump has also the ability to shape and pace climate change by carbon sequestration. Much of the by zooplankton incorporated carbon stays in the sediment and will not be recycled back to the ecosystem, and thus is removed from the carbon cycle (Mortelmans et al., 2021; Richardson, 2008).

Additionally, zooplankton is considered as a good biological indicator of the presence of climate change within marine ecosystem (Richardson, 2008). They are poikilothermic, meaning that their physiological processes such as ingestion, respiration and reproductive development depend on temperature. A 10°C temperature rise could double or even triple these process rates (Mauchline, 1998). An increase or decrease of water temperature could thus directly affect the population size. Most zooplankton are also relatively short-lived, with a mean lifespan of less than one year. Consequently, population dynamics can be tightly coupled with variations in water temperatures, as demonstrated by Semmouri et al. (2023). By studying the population dynamics and trends, temperature anomalies can be discovered and understood.

3.2.2 Spatiotemporal trends in the BPNS

3.2.2.1 Seasonal patterns

Traditionally, the Calanoida+Canuelloida+Cyclopoida group follows a seasonal pattern which is characterized by two peaks . A first major peak is present in spring in June-July, followed by a second, smaller one in September (Mortelmans et al., 2021). Despite some small deviations, a similar pattern was noticed by Mortelmans et al. (2021) in the BPNS. They observed a slightly earlier spring peak (May-June) and an autumn peak that was absent in the near and midshore regions. Additionally, they observed in 2021 an additional, and never-before-documented peak of copepods in offshore regions in February-March. They attribute this to an early maturation of the copepods due to warmer waters, highlighting the importance of water temperature in the maturation process and life cycle of copepods.

3.2.2.2 Anomalies

Besides the usual seasonal patterns, Mortelmans et al. (2021) also noticed anomalies in copepod abundances in 2014, 2018 and 2019. Especially in 2018, the copepod abundance reached near-zero values in the nearshore regions. During the winters preceding these years, water temperature was colder than normal, probably affecting the intensity of the spring bloom. During spring and summer however, numerous MHWs occurred, resulting in warmer-than-normal water temperatures (see §1.2). Especially during July 2018 and August 2020, temperatures reached or even exceeded the thermophysical limit of the most present copepod species, *Temora longicornis* (22.5°C). A follow-up study of Semmouri et al. (2023) illustrates the impact of water temperature on copepod abundance and describe the direct impact of MHWs on the marine ecosystem of the BPNS (**Figure 3-1**). They state that this anomaly is a direct consequence of a gradually warming sea, induced by climate change.

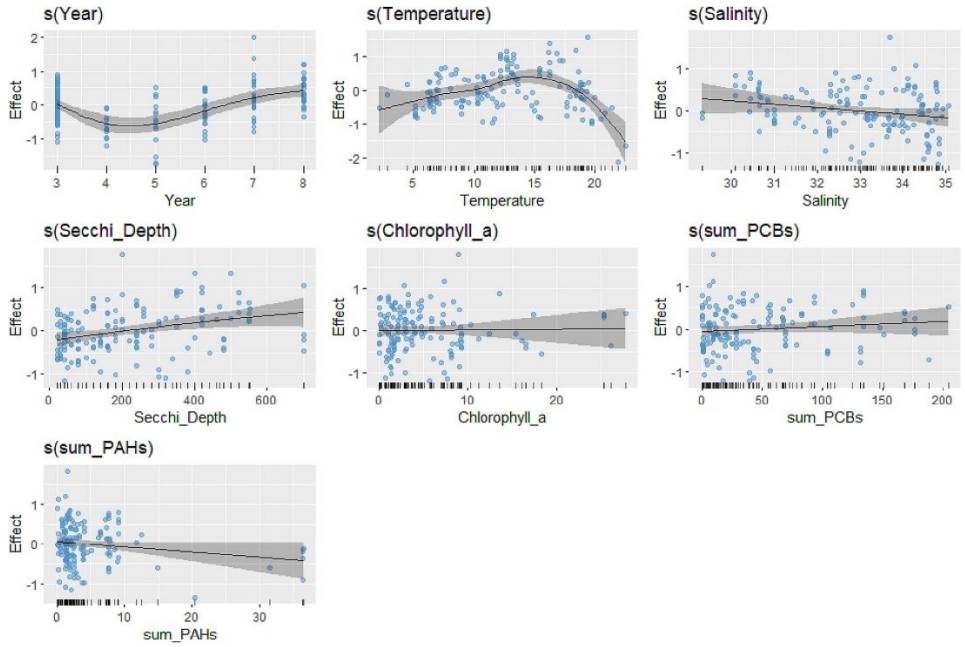

Figure 3-1 *Outputs of the Generative Additive Model (GAM) constructed by Semmouri et al. (2023), showing the influence of different variables such as water temperature or Secchi depth on the copepod abundance in the BPNS. One can see that temperature is positively correlated with abundance until a certain point. After this, the abundance shows a strong negative correlation with temperature, indicating that high water temperatures lead to a steep decline in copepod abundance. A detailed discussion is also provided by Semmouri et al. (2023).*

3.3 Correlation with NAO

Additional to temperature, zooplankton correlate with the previously discussed NAO index (see §2.2.1). Fromentin & Planque (1996) observed a negative correlation between the abundance of *Calanus finmarchicus* and the winter NAO index over the period 1958-1992 in the eastern North-Atlantic and North Sea (**Figure 3-2**). They attributed this correlation to the higher wind speeds present under higher NAO-indexes which cause a higher vertical mixing rate. This increases predator-prey contact, but also causes higher metabolic rates, which is also associated with higher water temperatures (Beaugrand et al., 2000). These high metabolic rates will, despite a higher predator-prey contact, result in a decline in zooplankton abundance (Beaugrand et al., 2000).

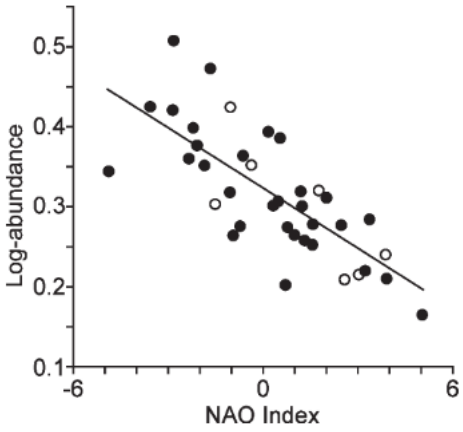

Figure 3-2 Correlation between the winter NAO index and the log abundance of Calanus finmarchicus in the Northeast Atlantic during the period 1958-1995. This graph was made by (Planque & Reid, 1998) and based on results from Fromentin & Planque (1996). Datapoints that were not reported by Fromentin & Planque (1996) are indicated in white. Figure taken from Drinkwater et al. (2003).

This trend is however not seen everywhere. In the Gulf of Biscay or Celtic Sea, no correlation between NAO index and zooplankton abundance was found. This is probably due to a reduced effect of the high winds associated with the high NAO index (Drinkwater et al., 2003). On the opposite site of the Atlantic, in the Gulf of Maine, a reversed pattern is observed. Here, a positive winter NAO index is correlated with an increase in zooplankton abundance (Conversi et al., 2001). In this region, zooplankton species are positively correlated with the water temperature at the bottom of the sea. Low temperatures thus result in low abundances (Greene, 2000). Low NAO-indices involve low bottom temperatures and consequently in low abundances (Drinkwater et al., 2003). One can thus say that zooplankton abundance is related with the present NAO-index, but that the type of correlation depends on the observed location.

4 THE EUROPEAN BROWN SHRIMP

4.1 The Belgian brown shrimp fishery

4.1.1 History

The brown shrimp fishery has a long and rich history at the Belgian coast. Since the late 16th century, shrimp are being fished and consumed by the local people, primarily farmers. For these generally poor people, shrimps were a welcome addition to their meagre diet. Typically, people dragged nets in the shallow parts of the sea, and those who could afford it even used horses (**Figure 4-1**). These "fisherman on horseback" became iconic for the Belgian coast, and in 2013, they were even added to the UNESCO world heritage list. Today, this profession is rather a touristic attraction or sport event, only appearing in certain cities along the Belgian coast, such as Oostduinkerke (Centrum Agrarische Geschiedenis (CAG), 2021a).

Figure 4-1 Then and now: fisherman on horseback in ±1900 (left) and in 2024 (right). Pictures taken from Centrum Agrarische Geschiedenis (CAG) (2021a)(left) and Histories (n.d.) (right).

Since the development of coastal tourism during the "Belle Epoque" in the late 19th century, there has been an increasing interest for the fishery community and its products. "Eating shrimp" became something one had to do when visiting the coast, resulting in a significant boom in the shrimp fishing industry. Due to the increasing demand, fish started to get fished more intensively. Especially after 1907, when the port of Zeebrugge was built, shrimp was fished more than ever. Wooden ships were replaced by diesel-powered ships, resulting in a fleet of around 150 ships by 1955. Today, only 16 of these ships remain, making Belgium a small player in the shrimp industry compared to other countries like the Netherlands or Germany (Centrum Agrarische Geschiedenis (CAG), 2021b). Nevertheless, Belgians are significant consumers of brown shrimp, accounting for consuming roughly half of all landed shrimp in Europe (situation in 2010)(Aviat et al., 2011; Centrum Agrarische Geschiedenis (CAG), 2021b). This underscores the deep cultural embedding of European brown shrimp in the Belgian culture.

4.1.2 Beam trawl fishing method

Whitin the Belgian brown shrimp fishing industry, the beam trawl method is the most widely used fishing technique (**Figure 4-2-A**). This technique, which originates from the 18th century, involves dragging two beam trawls over the seafloor, catching all benthic species on its path. A beam trawl consists of a metal beam supported by two sledge-shaped beam heads, allowing the beam trawl to slide on the seafloor (Montgomerie, 2022) . Additionally, depending on the present sediment type, tickler chains, chain mats or bobbins are also attached to the beam trawl. These structures disrupt the seabed, causing the benthic fish and shrimp to rise and get caught by the net (**Figure 4-2-B**).

Despite being used since the 1960s by Belgian fisherman, the beam trawl method has several disadvantages. Firstly, the beam trawl and tickler chains create distinctive trenches in the seafloor, hereby not only disrupting the sediment but also entire ecosystems, such as gravel beds (FOD Volksgezondheid, 2023). Secondly, beam trawling is not a highly selective fishing method, resulting in high bycatch rates. Bycatch refers to unwanted (fish) species which are discarded after being caught (e.g. *Merlangius merlangus*). Finally, beam trawl fishing also involves a high fuel consumption (Vermeersch, 2023).

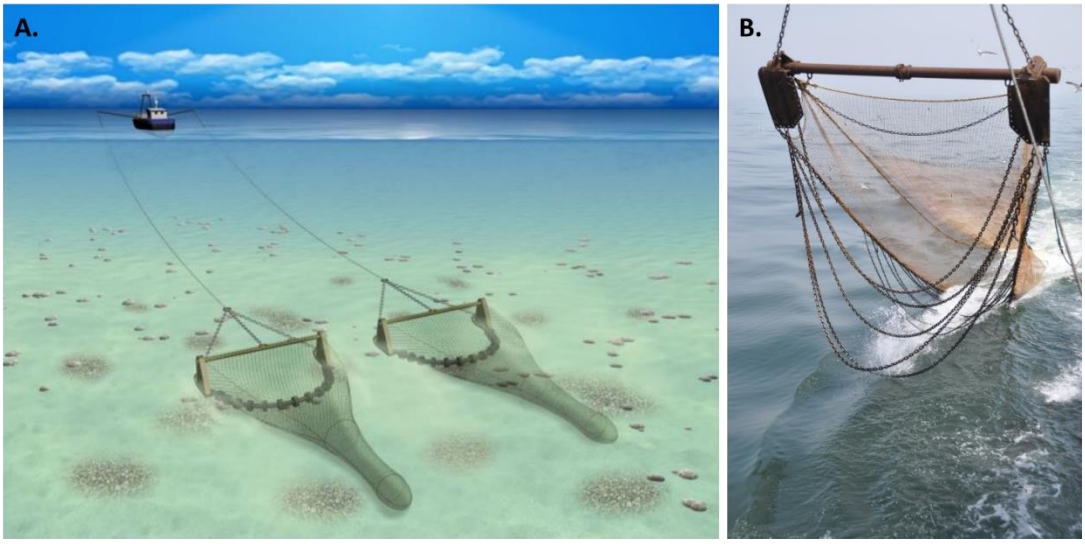

Figure 4-2 [A] Illustration of the beam trawl method as used by (Belgian) shrimp fisherman. [B] Detailed picture of a commercial beam trawl with tickler chains. Pictures taken from [A] Montgomerie (2022) and [B] Depestele et al. (2015).

4.2 Taxonomy and morphology

The European Brown Shrimp or *Crangon crangon* (Linnaeus, 1758) -in text referred to as *C. crangon*- belongs to the phylum of the *Arthropoda*, more specifically to the subphylum *Crustacea.* With a total of 60 000 known species, this subphylum exhibits a great diversity with species living in marine, freshwater and terrestrial environments. They are distinguished from the *Arthropoda* subphylum (insects) by the presence of a (thin) chitin exoskeleton (Mejía-Ortíz, 2019). Within the *Crustacea*, *C. crangon* belongs to the class of *Malacostraca* and the order of *Decapoda*. This order is, as the name suggests, characterized by the presence of five pairs of walking legs or pereiopods (**Figure 4-3**). Additionally, head and thorax are fused together into a cephalothorax. The abdomen is segmented in different pleons, on which paired pleopods are attached. These pleopods act as swimming legs and able the species to manoeuvre over, and on the sea floor sediment. The rear end of *Decapoda* is characterized by a fan-shaped tail which consists of a telson and uropods (**Figure 4-3**) (Vermeersch, 2023).

Within the order of *Decapoda*, several modifications to the pereiopods are present adapted to the different lifestyles. In the family of *Cragonidae* for example, to whom *C. crangon* belongs, the first pair of pereiopods is sub-chelated, meaning that this family does not have proper claws. Additionally, they are characterized by a short rostrum, which is also displayed in **Figure 4-3**. Within this family, 24 genera are present, including also the *Crangon* genus. This genus consists of 20 (sub)species, of which *C. crangon* is the type species (Moreira et al., 2012). A full taxonomic overview is provided in **Table A- 3.**

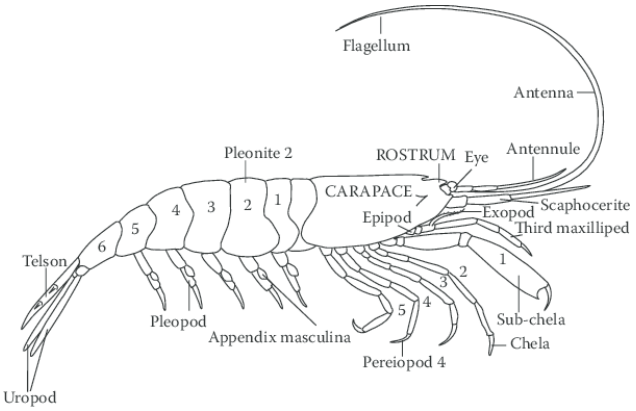

Figure 4-3 Morphology of the European brown shrimp (Crangon crangon). Picture taken from Campos & Van Der Veer (2008).

4.3 Abundance

C. crangon predominantly inhabits shallow coastal waters, typically found at depths ranging from 0 to 20 meters, with peaks up to 120 meters . In terms of substrate, sand or muddy sand is more favoured. Hence, *C. crangon* is a common and omnipresent resident of the shallow coastal shelf region in the northern-eastern Atlantic, which stretches from the White Sea, the Baltic Sea and Iceland to the Atlantic coast of Morocco, the Mediterranean Sea and the Black Sea. Especially in the North Sea, the brown shrimp is ubiquitous (Figure 4-4) (FAO, n.d.; Kuipers & Dapper, 1984). However, the presence of *C. crangon* in for example the North Sea is subject to some fluctuations, caused by the seasonality of its own life cycle and migration patterns (see §4.7.1). Juvenile shrimp are for example highly abundant in shallow waters in spring/summer, whilst adult shrimp peak on fishing grounds in autumn (Campos et al., 2010; Moreira et al., 2012). Additionally, cold winters often cause a decrease in shrimp abundance in the following year, just like drought years. Consequently, mild winters and pre-drought years favour shrimp abundances. During these cold winters, *C. crangon* are likely to migrate to deeper offshore waters, delaying the arrival of new generations in more shallow waters (Campos et al., 2010; Moreira et al., 2012).

Figure 4-4 Distribution of C. crangon in the North Atlantic region. Abundance of C. crangon is indicated in red . Figure taken from FAO (n.d.).

4.4 Nutritional content

Besides being an economic interesting and important product (see §4.8), shrimp are valued for their high nutritional value. They are rich in protein and poor in saturated fats, making them a healthy dietary choice. Water forms the most abundant component in the edible part of *C. crangon* (e.g. tail), with a concentration of approximately 80 grams per 100 grams of edible shrimp meat. Proteins are the second most abundant component, with concentrations of around 18 grams per 100 grams. Additionally, shrimp meat contains around one gram of lipids per 100 grams (**Table 4-1**) (Turan et al., 2011). Turan et al. (2011) stress however concentrations are influenced by e.g. the present season or water temperature and are therefore just a rough indication.

Table 4-1 Average concentrations (n = 70) of the different nutrient components of 100 grams C. crangon tissue ± the standard error. This table is based on Turan et al. (2011), who also describe the methods that were used to obtain these concentrations.

Component	Amount
Water (g)	79.21 ± 0.01
Protein (g)	18.47 ± 0.09
Lipid (g)	0.95 ± 0.05
Ash (g)	1.39 ± 0.01

Additionally, to the high protein levels, shrimp meat also contains a high amount of omega-3 fatty acids. These fatty acids reduce the cholesterol levels and therefore contribute to the high nutritional value of shrimp meat (Turan et al., 2011).

4.5 Life cycle

Four different life stages can be distinguished during the life cycle of *C. crangon*: an egg, juvenile, larvae and adult stage. After insemination, eggs are carried by females until they hatch. After hatching, planktonic larval shrimp go through five stages, after which they settle on the seafloor as juveniles. These juveniles then migrate to shallow nursery grounds where they mature into adults. Adult shrimp then return to deeper water to reproduce again (Campos & Van Der Veer, 2008).
A schematic overview of the entire lifecycle and different stages is provided in **Figure 4-5** (Campos & Van Der Veer, 2008).

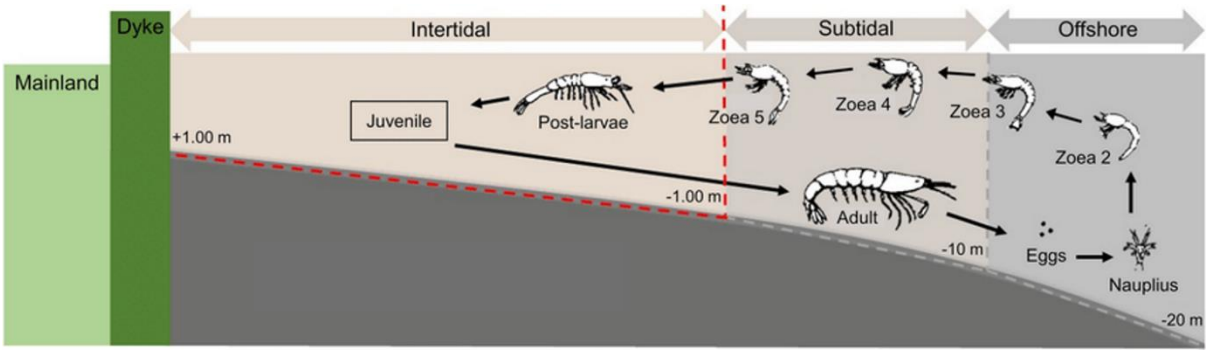

Figure 4-5 Overview of the lifecycle of C. crangon. After hatching, C. crangon goes through 5 larval stages, zoea 1-5, and is part of the pelagic plankton. After the larval life stage, C. crangon has its distinct look and will become a benthic organism. After approximately one year, C. crangon is mature and ready for reproduction . Figure taken from Penning et al. (2021).

4.5.1 Egg stage

Reproduction of *C. crangon* typically occurs in offshore waters at a depth between 10-20 metres. Typically, these waters have also a higher salinity level than more shallow waters and a sandy or muddy underground (Campos & Van Der Veer, 2008; Tulp et al., 2012). Females are internally inseminated and store the sperm and carry the eggs on their pleopods until they hatch. Female shrimp have a high fecundity, carrying up to 1500 eggs during one reproduction period (Moreira et al., 2012). Per year, two reproduction periods are present, one during wintertime (December-February) and one in summertime (July-August) (Tulp et al., 2012)
Eggs of *C. crangon* are not free floating in the plankton but are carried by female adults. The incubation period of the eggs depends on the present water temperature. Only the eggs incubated between 6-21°C are viable, and these will also experience different development rates, negatively correlated with the water temperature (Wear, 1974). Although different relations are described in literature (**Figure 4-6**; **Table A- 4**), it is generally assumed that egg development lasts around 2-3 weeks when exposed to temperatures around 20°C, and more than three months when incubation happens

at a temperature of 6°C (Campos & Van Der Veer, 2008). Besides temperature, salinity also plays a role in the egg development. Especially at low salinity levels (< 15 ppt), eggs tend to be less viable and are likely to be lost by the females. Egg size depends on the size of the female, with maximum diameter ranging up to 0.60 mm (Campos & Van Der Veer, 2008).

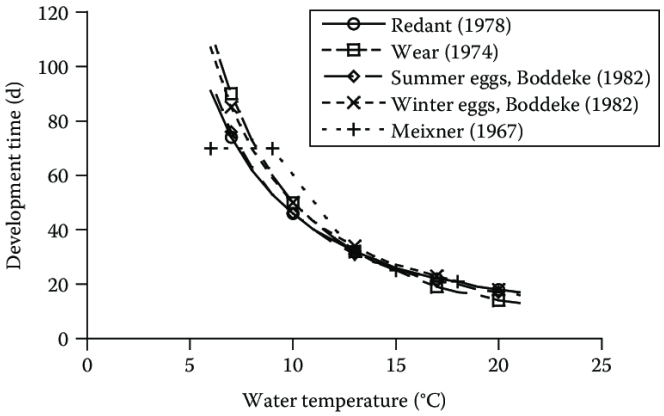

Figure 4-6 Visualization of different relations between duration of egg development in days (d) and water temperature (°C) as described in literature. In general, a negative correlation between the duration of the egg development and water temperature can be noticed. The equations of these different curves can be found in Table A- 4 in the appendices. Figure taken from Campos & Van Der Veer (2008).

4.5.2 Larval stage

After hatching, larval shrimp undergo five to six planktonic larval stages and an additional post-larval stage before turning into juveniles. During these several pelagic larval stages -also called "zoea"- *C. crangon* moults several times, increasing their length from 2 mm after hatching to 5-8 mm at the end of their last larval stage (Vermeersch, 2023). Additionally, after zoea-5, the larval shrimp undergo a metamorphosis, giving them their distinctive "shrimp-look". Once the metamorphosis is complete, the post-larval shrimp will settle down in more shallow waters and will maintain a benthic lifestyle, both as predator and prey. The settlement occurs 2-5 months after hatching when the shrimp have an average length of around 4.7 mm but is again dependent on the present water temperature (Campos & Van Der Veer, 2008; Vermeersch, 2023).

Development ideally takes place at temperatures between 9-18°C, with a duration ranging from 3-7 weeks when exposed to a water temperature of 18°C or 9°C respectively. The relation between the development duration and the water temperature is visualized in **Figure 4-7**, with the equations given in **Table A- 4**. Regarding the salinity, larval development will be ideally around a level of 32 ppt. If the salinity level is too low, development will take place at a slower rate (≈ 25 ppt) or even mortality occurs (< 16 ppt) (Campos & Van Der Veer, 2008).

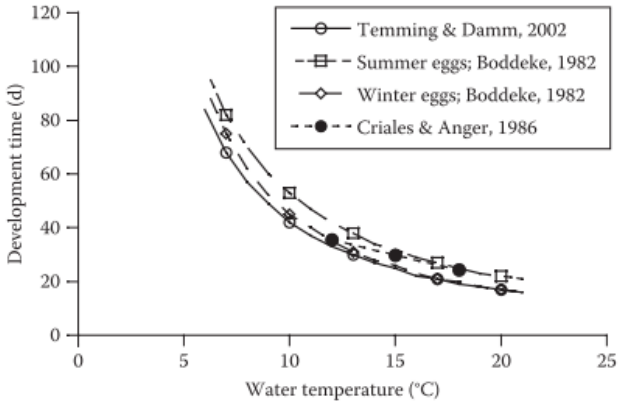

Figure 4-7 Visualization of different relations between duration of larval development in days (d) and water temperature (°C) as described in literature. In general, a negative correlation between the duration of the larval development and water temperature can be noticed. The equations of these different curves can be found in Table A- 4 in the appendices. Figure taken from Campos & Van Der Veer (2008).

4.5.3 Juvenile stage

After the post-larval settlement and before the development of sexual characteristics, shrimp experience the juvenile life stage. The abundance of juvenile shrimps follows a seasonal pattern similar to reproductive periods and larvae abundance, and peaks usually during spring. These juveniles use more shallow, low-salinity grounds to feed and mature. In this life stage, an ambush strategy is used, and juvenile shrimp rarely search actively for their prey. Again, development is temperature dependent, with a temperature range between 5°C and 25 °C (Campos & Van Der Veer, 2008; Moreira et al., 2012).

4.5.4 Adult stage

In order to determine whether or not shrimp are mature, one needs to search for the sexual characteristics of adult shrimp. For females, these are easily recognizable: sexually mature female shrimp carry eggs. For male shrimp however, these characteristics are not externally visible, and therefore their maturity only can be estimated. Campos et al. (2013) found that the maturation rate of juvenile shrimp is not a fixed process, but rather subjected to gender and temperature. Female shrimp for example will experience a higher growth rate than male adults.
In general, it's assumed that male adult shrimp have a length between 22-43 mm, whilst adult female shrimp measure between 30-55 mm. Feeding growth and maturation of adult shrimp takes place in the temperature range of 5-30°C with a positive correlation between increasing temperature and growth rate (**Figure 4-8**). Adult shrimp have an optimal growth rate of around 23°C, with maximum tolerable temperatures up to 30°C (Campos & Van Der Veer, 2008; Freitas et al., 2007). Salinity preferences are temperature- , age- and sex-dependent. At temperatures of 20-22°C, adult shrimp favour 28-29 ppt and 15-20 ppt when they are two and one year old, respectively. At lower temperatures (3-5°C), shrimp favour a salinity of 33 ppt. This thus means that when temperatures are higher, *C. crangon* favours less saline waters (Campos & Van Der Veer, 2008). Often, at temperatures higher than 15°C, males have a higher optimal salinity level compared to females. (Campos & Van Der Veer, 2008).
During (late) autumn, when temperature begins to drop, juvenile and adult shrimp migrate back to more offshore and deeper water to start reproduction again (Luttikhuizen et al., 2008).

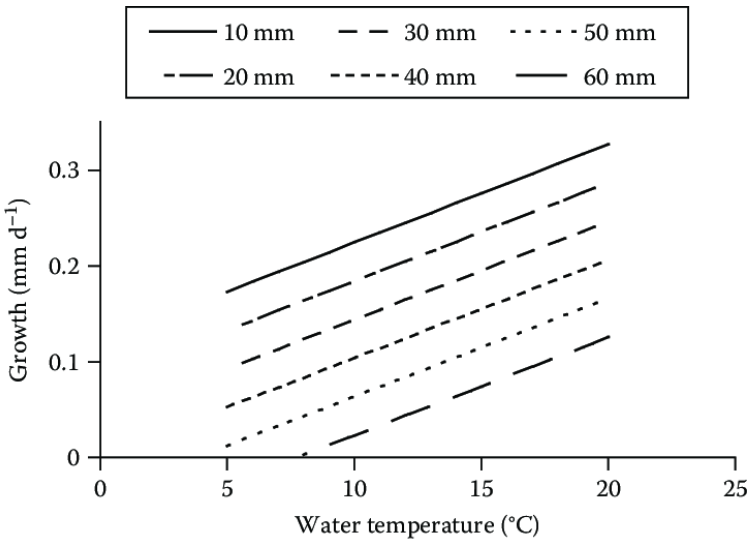

Figure 4-8 Growth rates of juvenile and adult shrimp in relation to water temperature. The growth rates are obtained under laboratory conditions with an optimal food availability. Graph derived from Campos & Van Der Veer (2008).

4.6 Role(s) in marine food web

Due to its high abundance in the southern North Sea, *C. crangon* fulfils a central role in the marine food web, both acting as an important predator and prey. They form an important link in the marine food chain by carrying energy from lower trophic levels to top predators such as whiting (*Merlangius merlangus)* (Hufnagl et al., 2010). *C. crangon* is also considered to have a very diverse diet, being described as trophic generalist (Evans, 1984; Pihl & Rosenberg, 1984), omnivorous (Kuhl, 1972; Lloyd & Yonge, 1947; Muus, 1967; Tiews, 1970) or carnivorous (Pihl & Rosenberg, 1984).

4.6.1 Role as predator

C. crangon is considered as an ecologically important benthic predator with a highly varied diet, which mainly consists of three groups: infaunal organisms (polychaetes, oligochaetes, bivalves, nemerteans, echiurans, sipunculids, burrowing amphipods and isopods), epifaunal organisms (corals, sponges, barnacles, Decapoda) and demersal organisms (mysids and fishes) (Campos & Van Der Veer, 2008). The latter one, and then more specifically juvenile plaice (*Pleuronectes platessa*), is considered as the main food source for large shrimp (>20 mm). For larval *C. crangon*, zooplankton and larger phytoplankton form the main food source (Hünerlage et al., 2019)
C. crangon is an ambush-type hunter. It will not search actively for prey but will wait in the sediment until prey is passing by. They therefore favour darker and/or turbid conditions over light habitats (Campos & Van Der Veer, 2008; Vertongen, 2024) .

4.6.2 Role as prey

Besides acting as a predator, *C. crangon* forms also an important prey species for several (juvenile) fish, such as cod (*Gadus morhua*), whiting (*Merlangius merlangus*), sand goby (*Pomatoschistus minutus*), herring (*Clupea harengus*) and several flatfish (*Pleuronectiforms*)(Campos et al., 2010; Temming & Hufnagl, 2015; Welleman & Daan, 2001). In some years, mass occurrence of juvenile whiting resulted in severe extinctions of brown shrimp, for example in 2016 (Hünerlage et al., 2019).
Additionally, to these (juvenile) fish, swimming crabs of the genus *Liocarcinus* also form an important benthic predator of juvenile *Crangon* who just settled (Hünerlage et al., 2019). Additionally, Hünerlage et al. (2019) also report that in some years (e.g. 2016) jellyfish (*Scyphomedusae*) form an important predator for pelagic *C. crangon.*

Besides preyed by other organisms, *C. crangon* is also preyed on by its own. Cannibalism is very common among *C. crangon*, which can even compromise 20% of their diet (Evans, 1984). Newly settled juvenile shrimp (< 6 mm) has the highest chance of being preyed on by adult shrimp (>30 mm) (Delbare et al., 2015).

4.7 Recruitment

Recruitment of fish, or in this case brown shrimp, refers to the process of young, juvenile fish evolving into older, adult individuals that can be fished. It is the most important process to regulate fish populations, but because of many variables (predation, food availability, water temperature, light intensity…), it is often complicated to fully comprehend (Camp et al., 2020; Tulp et al., 2012). *C. crangon* forms hereby no exception. Shrimp are considered "fishable" -also referred to as "commercial shrimp"- if they are larger than 50 mm in length (Campos et al., 2010; Luttikhuizen et al., 2008).

4.7.1 Seasonal migrations

As seen in §4.5, temperature plays an important role in the life cycle of *C. crangon*. This also forms the main driver of the seasonal migration patterns of *C. crangon* in, for instance, the North Sea. A first major migration can be observed during (late) autumn/winter when shrimp migrate back to deeper and more saline offshore waters, fleeing the colder nearshore waters (Luttikhuizen et al., 2008). They return to more shallow and brackish waters during spring/summer in their search for warmer waters. However, in peak summer, if water temperatures are too high, *C. crangon* can migrate again to deeper and colder waters, only to return in September and October when temperatures are again feasible (Campos & Van Der Veer, 2008). The optimal temperature depends on the life stage of the *C. crangon*, but for adults it is estimated that the optimal temperature is situated around 23°C, with a limit of 30°C (Freitas et al., 2007; Tulp et al., 2012).
Another driver for this secondary migration could be reproduction which typically occurs at depths of 10-20m (see §4.5.1) (Campos & Van Der Veer, 2008).

4.7.2 Autumn recruitment

4.7.2.1 Observed trends

As seen in §4.5.1, *C. crangon* produces eggs twice a year, once during winter (November-January), and once in summer (July-August). Commercial landings in autumn are however consistently larger than the landings in spring, and several hypotheses exist to explain this pattern. Boddeke (1976, 1982) suggested for instance that the fishery in autumn is correlated with maximum egg densities and that the summer generation has the major contribution to the autumn peak. He also stated that growth rates of summer brood are so large that maturation (i.e. reaching commercial size) is reached within 3-4 months, which could coincide with the autumn peak (**Figure 4-9-1**). On the other hand, Kuipers & Dapper (1981, 1984) suggest that the autumn peak is not caused by summer brood, but by the previous winter generation. This population settles in mass in spring and need approximately nine months to grow to commercial sizes. Additionally, they state that the summer population is subjected to a heavy predation pressure by e.g. gobies, resulting in only a small contribution to the autumn peak (**Figure 4-9-2**).
Campos et al. (2009) investigated these two hypotheses and came to the conclusion that the growth rate of *C. crangon* depends on the sex of the individual. Males need 1.5 years from settlement as juvenile to reach commercial sizes, while females only need one year. This would imply that the autumn peak, which mainly consists of adult females, would originate from juveniles who settled in the summer of the previous year. These juveniles evolved on their turn from the winter brood of that year. This would suggest that possible influences on the eggs and/or juveniles would have a lagged effect of one year on the commercial autumn peak (**Figure 4-9-3**).
Hünerlage et al. (2019) failed however to find a significant (positive) correlation between larvae in spring and the *Crangon* stock in autumn. They also could not find a correlation between the present stock size in autumn and the

offspring of next year. They state that the life cycle of *C. crangon* is influenced by several (a)biotic parameters and that lack of information about e.g. mortality rates form an obstacle to correctly predict stock sizes. Predation of juveniles and/or adults plays, according to Hünerlage et al. (2019), a key role in determining the standing *Crangon* stocks. Additionally, Tulp et al. (2012) found that *C. crangon* recruitment is also correlated with food availability, water temperature, light intensity and dissolved oxygen. These influences will also be discussed in §4.7.2.2and §4.7.3.2.

The summary of the above literature shows that the recruitment process behind *C. crangon* is yet to be understood, and that several hypotheses seem assumable.

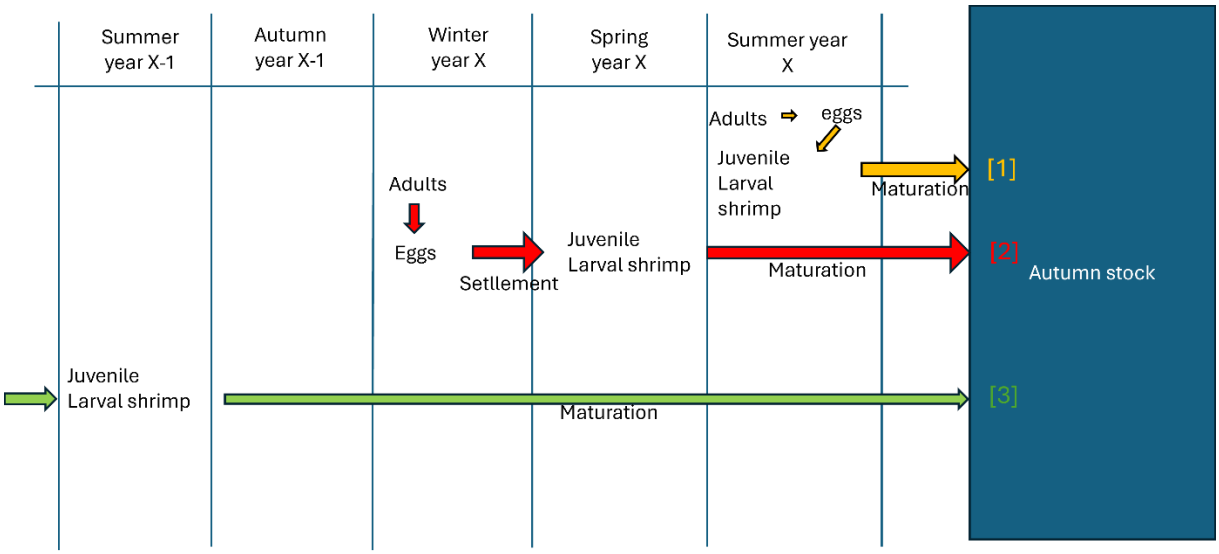

Figure 4-9 *Schematic overview of the different recruitment hypothesis found in literature. [1] The autumn stock is directly originating from the summer brood of the same year. Larvae and juveniles reach commercial sizes within 3-4 months (Boddeke, 1976, 1982). [2] The autumn stock is originating from the winter brood. Juveniles and Larvae peak in spring and will reach commercial sizes ±9 months after hatching (Kuipers & Dapper, 1981, 1984). [3] The autumn stock originates from the juveniles and larvae from the previous summer since they need ±1 year from settlement to reaching commercial sizes (Campos et al., 2009).*

4.7.2.2 Environmental influences on recruitment

Campos et al. (2010) found that predation pressure is the most important factor which determines the size of the autumn stock. The most important predator groups include Scorpaeniforms, Pleuronectiforms and Decapods and all showed a negative correlation with *Crangon* abundance. Influences of Pleuronectiforms and Decapods showed however a 1- and 2-year lag, respectively. On the contrary, Clupeioforms and Perciforms showed a positive correlation, indicating that they share the same environmental resources, but they don't predate on with *C. crangon*.

Besides this predator pressure, some abiotic parameters, such as water temperature or food availability, have a significant influence on autumn stock. The autumn stock is found to be negatively correlated with the winter water temperature. Colder winters will delay the larval development, resulting in a late peak spawning in May or June. These late hatching larvae will only reach commercial sizes (>50 mm) around autumn. Additionally, shrimp stocks in autumn are positively correlated with the winter NAO-index (Campos et al., 2010; Hünerlage et al., 2019).
Food availability also plays a key role in the recruitment. Larval survival depends on food availability, and thus, in the case of *C. crangon*, the presence of zoo- and phytoplankton. This means that shrimp stock in autumn is also positively correlated with the run-off of nutrients into the ocean. These amplify namely the bloom of phytoplankton, and thus results in a large food availability for larval *C. crangon* (Hünerlage et al., 2019). However, changing impacts on the autumn stock regarding food availability or run-off of nutrients have a lag of approximately one year. Additionally, Hünerlage et al. (2019) conclude that food limitation is the most important factor which hampers growth performance.

A summary of the recruitment and the accompanying influences is illustrated by **Figure 4-10**.

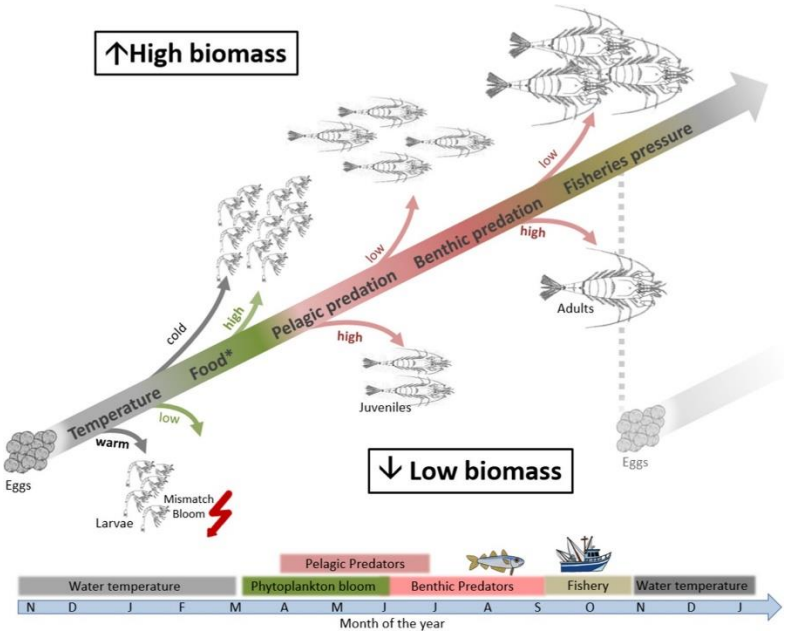

Figure 4-10 Schematic overview of the recruitment of C. crangon into the autumn fish stock, and their accompanying major influences. In the first life stages, winter temperature forms the major influence. This is respectively followed by food availability, pelagic and benthic predation and ultimately fishery. Figure taken from Hünerlage et al. (2019).

4.7.3 Spring recruitment

4.7.3.1 Observed trends

Spring recruitment is traditionally much smaller than autumn recruitment. This stock mainly consists of survivors of the previous winter which return to the nursery grounds (Campos et al., 2010). Campos et al. (2010) state that the abundance of this spring stock is positively correlated with the *Crangon* stock present in autumn of the previous year. However, no correlation was found between the present spring stock and the spring stock of the previous year (Campos et al., 2010).

4.7.3.2 Environmental influences on recruitment

Contrary to the autumn stock, the *Crangon* spring peak is positively correlated with the winter temperature. During severe winters with a low water temperature, shrimp migrate to deeper and more offshore water than normal and will therefore arrive later than normal on the fishing grounds. Additionally, during sever winters, the mortality rate increases and therefore fewer adult shrimp will be part of the spring stock (Campos et al., 2010; Hünerlage et al., 2019).

4.8 Trends in commercial landings in the BPNS

As seen in §4.5 and §4.7, the lifecycle and recruitment of *C. crangon* are subjected to various influences, which consequently also affect the annual landings by Belgian and European shrimp fishers. In **Figure 4-11**, the annual trend of commercial landings by Belgian and foreign fishermen in the BPNS are shown. This graph illustrates the annual landings to heavily fluctuate from year to year, with years of high landings (e.g. 2014, 2016, 2018) altering years with low landings (e.g. 2015, 2017). The years 2021 and 2022 were exceptional years in terms of shrimp landings, with an annual landing of 1554 and 2689 tonnes, respectively (Verlé et al., 2023). However, in the following year (2023) the landings of shrimp declined rapidly and caused an (unexplainable) deficit. This resulted in a significant increase in price. This trend continued in the first months of 2024, but was broken around May 2024, when the supply of shrimp again increased (Belga, 2024; Heylen, 2024). A similar trend was also observed during the period 2017-2018. In 2017, a reduced supply of shrimp led to

increased prices that persisted until the second half of 2018, when large amounts of shrimp were landed (again) (De Redactie, 2017; Tijs Mauroo, 2018). An unambiguous explanation for these trends is not (yet) found, but one suspects a combination of the presence of predators (e.g. whiting), unfavourable environmental conditions during the reproduction periods and bad weather during the fishing seasons (Belga, 2024; Heylen, 2024; Tijs Mauroo, 2018).

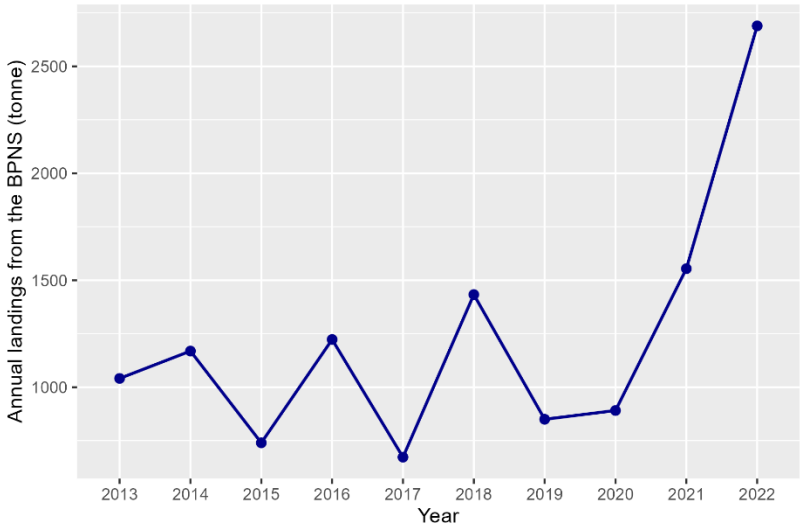

Figure 4-11 Representation of the annual commercial landings of C. crangon in the BPNS (all fishing vessels) (tonne). Data for the years 2023-2024 is not (yet) available. Data is acquired from Verlé et al. (2023), graph is produced in R(v4.3.1.) and the ggplot2-package.

The European brown shrimp is one of the most fished and consumed species in the BPNS, making it an important Belgian industry. The price of the landed shrimp depends on two main factors: the demand and the availability. The price itself is determined on auctions where the daily landings are sold to buyers and retailers. From 2018 until 2022, the average shrimp price was 4.6 € kg^{-1}, with the lower prices in the period August-October (2-5 € kg^{-1}), and higher prices obtained in spring/early summer (Verlé et al., 2023). However, as stated earlier, these prices are also depended on the offer. In January 2024 for example, the offer of brown shrimp in Belgium was seven times lower compared to normal landings, resulting in very high prices, sometimes reaching 18-20 € kg^{-1} (unpeeled shrimp) and 80 € kg^{-1} (peeled shrimp) (Belga, 2024; Heylen, 2024). These fluctuating prices consequently result in changing commercial revenues, as illustrated in **Figure 4-12**. In years of poor landings, such as 2019, this results in reduced revenues, leading to economic challenges for fishermen, vendors, and other stakeholders in the industry.

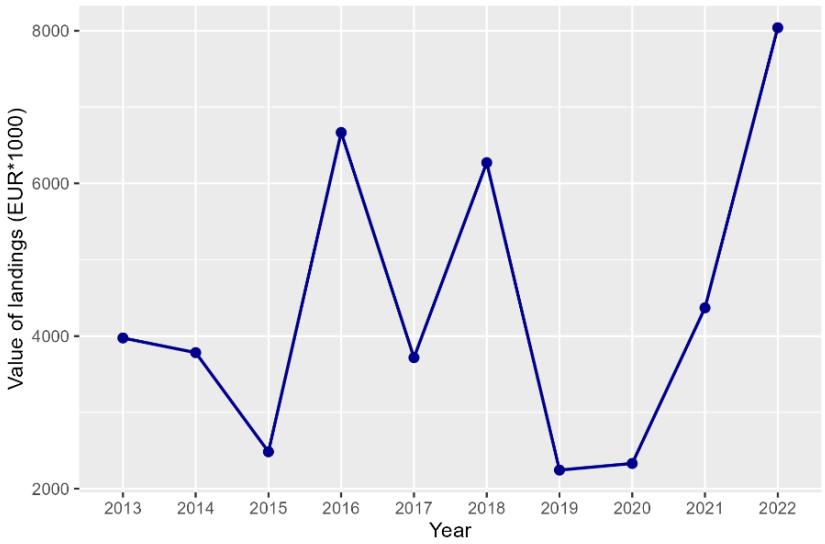

Figure 4-12 Fluctuation of the value of the annual landings caught in the BPNS, all countries combined. This is the result of a fluctuating price and number of landings. Data is acquired via (Verlé et al., 2023), graph was produced using R (v4.4.0) and the ggplot2-package. .

RESEARCH OBJECTIVES

The European brown shrimp (*Crangon crangon*) is strongly imbedded in the Belgian culture, which is illustrated by the number of annual consumed shrimp. Consequently, the shrimp fishery industry is still an important economic sector at the Belgian coast despite a strongly reduced fleet. However, in recent years, shrimp abundance in the BPNS has experienced some notable fluctuations, with periods of substantial commercial landings altering with years of poor yields. These fluctuations resulted in a variable shrimp price, sometimes resulting in economic challenges for (local) vendors and fishermen .

Therefore, it is important to develop a better understanding of the distribution, recruitment and stock sizes of *Crangon crangon*, and how climate change could impact these. This dissertation aims to understand the fluctuations in *Crangon crangon* abundances and to identify its main drivers. Additionally, the potential impact of climate change -in the form of marine heatwaves- will also be explored. To achieve this, data on various environmental variables, such as water temperature or pigment concentrations, will be compiled into a comprehensive dataset. This dataset will be utilized to generate scatter plots and Generalized Additive Models (GAMs) in order to identify correlations with *Crangon crangon* abundances in September. This study will focus on addressing the following central questions:

- What are the main influences on the *Crangon crangon* recruitment?
- Which environmental variables have a significant contribution to the variability of the *Crangon crangon* stock, and how are they related to the observed spatiotemporal trends?
- What is the influence of occurring marine heatwaves on the (present) *Crangon crangon* stock and its recruitment processes in the BPNS?

Additionally to the data analysis, a (brief) nutritional content assessment will be conducted. Samples collected during multiple offshore campaigns will be utilized in protein and lipid extractions. Results of these extractions will be compared based on the region of sampling. The main research question during this assessment is:

- Is there a significant difference in protein and/or lipid content across a near-offshore and/or east-west gradient, as well as between seasonal periods?

MATERIAL AND METHODS

5 DATA SERIES

In this dissertation, datasets from various sources are merged and compared. The observed period spans from **2014** to **2023** and will be applied to all utilized data series.

5.1 *Crangon crangon* abundance data

Shrimp abundance data is acquired from the online DATRAS Trawl Survey Database of the Flanders Research Institute for Agriculture, Fisheries and Food (ILVO). This database contains data of various pelagic (*Merlangius merlangus, Limanda limanda, Pleuronectes platessa)* and benthic (*Crangon crangon*) commercially interesting species. This data is collected during an annual Demersal Young Fish Survey (DYFS) in the BPNS.

5.1.1 DYFS-campaign

5.1.1.1 Offshore sampling

Every year in September, ILVO organizes a "Demersal Young Fish Survey" (DYFS) in the BPNS . According to the sample protocol described by Raat (2023), 33 monitoring stations are sampled during a multi-day campaign (**Figure 5-1**; **Table B- 1**). The goal is to obtain fishery-independent abundance and size estimates of several commercial fish or epibenthos species, such as dab (*Limanda limanda*), plaice (*Pleuronectes platessa*) or brown shrimp (*Crangon crangon*). In addition, the quantity and species composition of epibenthos is also determined.

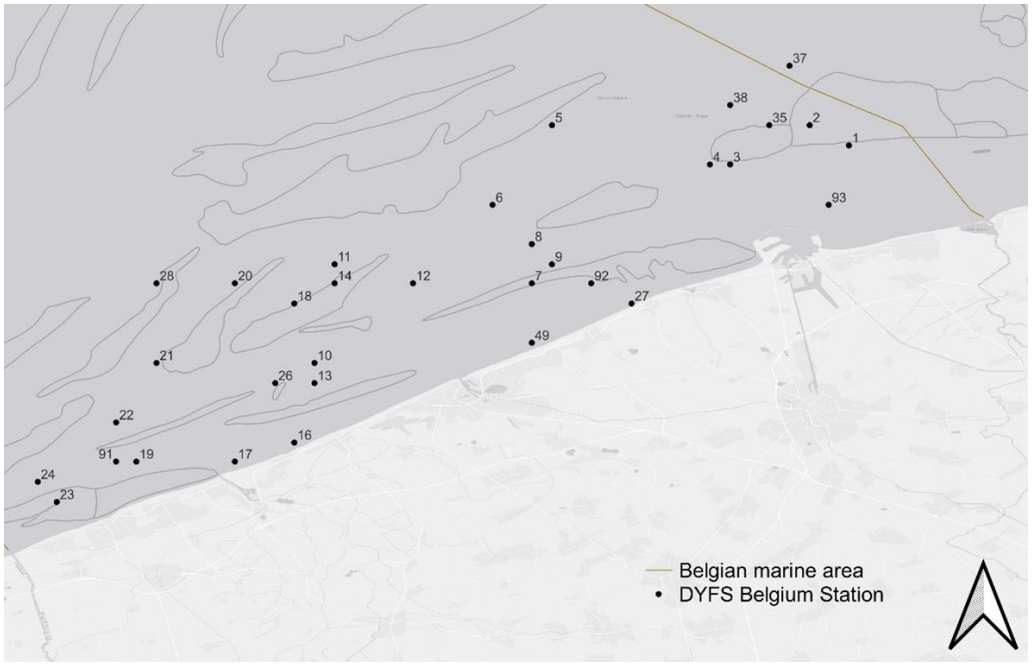

Figure 5-1 *Locations of the different sampling station of the 2023-DYFS-campaign of ILVO. All stations were sampled during this campaign, except station 91 which is part of the sea farm of Colruyt since 2022. Figure taken from Raat (2023).*

The samples are obtained with the beam trawl fishing method, using a six meter beam trawl and a fishing net with a mesh size of 22x22 mm (**Figure 5-2-B**). Each haul involves towing the beam trawl over the sea bottom for 15 minutes, starting from the moment the net touches the seafloor, with a speed of 3.5 knots (6.5 km h^{-1}) against the tidal direction

(**Figure 5-2-A**). The DYFS campaign is annually organized in September, during which hauls are only conducted between 08h00 and 17h00 (GMT+1). RV Simon Stevin was used to conduct the sampling. In 2023, the DYFS campaign started 11/09/2023 and ended 20/09/2023.

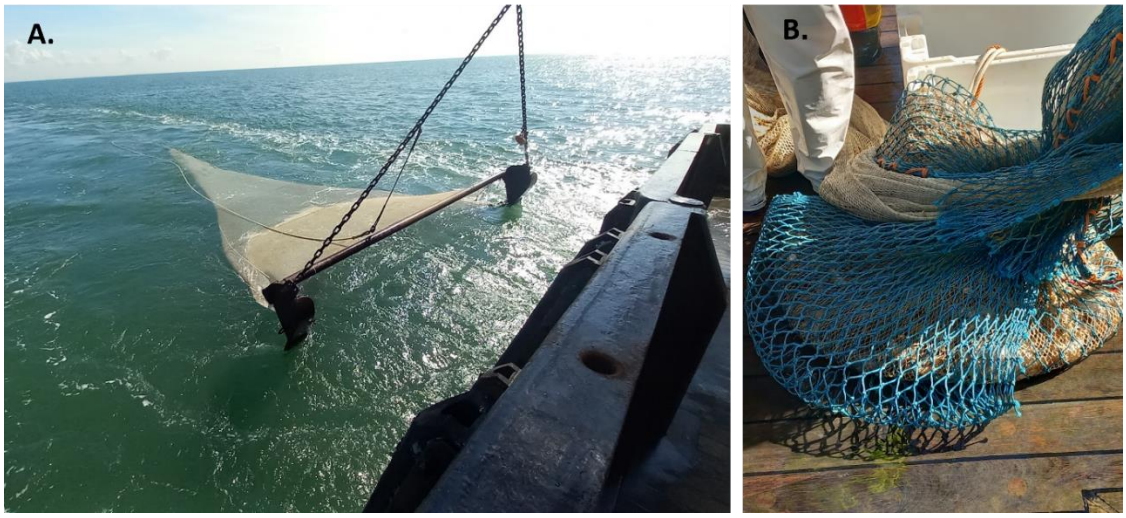

Figure 5-2 *[A] The beam trawl which was used during the 2023 DYFS-campaign. The beam trawl has just been put in the water and is ready to be submersed. Picture taken on 14/09/2023 from the stern of RV Simon Stevin. [B] Detailed picture of the pit of the beam trawl. The pit is still filled with the catch of the haul and is ready to be opened. Picture taken on 13/09/2023.*

After each haul, the catch is divided into three fractions by a coil sorter (**Figure 5-3**). This sorter comprises three sieves, each responsible for a different fraction. A first sieve is part of the inner drum, has sieve openings of 15 mm and separates the large fish species from smaller fish and epibenthos. The latter fall through the openings onto the outer drum. The remaining fish fraction in the inner drum is washed out and collected as the **EPI-L** fraction. The outer drum, with sieve openings of 6.3 mm, separates undersized from commercial-sized shrimp. Undersized shrimp and small epibenthos species fall through, forming the **EPI-S** fraction. At last, a crab sieve separates commercial-sized shrimp (>50 mm) from crabs. The shrimp fall through the openings of the sieve and are collected as the **EPI-M** fraction. Crabs remain on the sieve surface and are transported to the **EPI-L** fraction. Fractions and sieve dimensions are summarized in **Table 5-1**.

Table 5-1 *Summary of the most frequent occurring species and sieve dimensions of the EPI-L, EPI-M and EPI-S fraction. Table based on Raat (2023).*

Fraction	Species	Sieve Dimension (mm)
EPI-S	Brittle star (*Ophiuroidea*) Small shrimp	0 - 6.3
EPI-M	Commercial-sized brown shrimp (*Crangon crangon*) Juvenile fish (*Limanda limanda*, *Pleuronectes platessa*) Juvenile crabs	6.3 - 12
EPI-L	Adult fish (*Merlangius merlangus*) Crabs	> 12

Figure 5-3 Flush sorting machine on board RV Simon Stevin. The collected catch from the pit (1) is emptied into the cistern (2), after which it is divided into three fractions: EPI-S (3), EPI-M(4) and EPI-L(5). These fractions are collected in mutually different baskets. The EPI-S fraction ends up in the blue basket with red handles, the EPI-M fraction in the blue baskets and the EPI-L fraction in the orange baskets. Picture taken on 14/09/2023.

5.1.1.2 Onshore length measurements

After sampling, the shrimp are brought back ashore and are stored overnight in the fridge (-20°C) at the D1 building of ILVO in Ostend. The following day, length measurements are conducted with the "SmartShrimp" software, an algorithm developed in-house at ILVO by Yann Collignon ILVO in 2015, using the .Net framework 4.5. The SmarthShrimp algorithm performs length measurement based on light contrast with an accuracy of 1-2mm. Image processing is conducted with the Halcon® framework. The measurement protocol is described by Raat (2023) and can be found in Appendix B: Methods.

5.1.2 DATRAS Data

Data from the DYFS campaigns is accessible via the online DATRAS Trawl Survey Database (Millar et al., 2023). Haul data of the DYFS-campaign is acquired over the period 2014-2023, containing abiotic parameters and biological abundances of *Crangon crangon* and (juvenile) *Merlangius merlangus.* The DATRAS database can be accessed in R with the commando *"getDATRAS"* from the *icesDatras* R-package (see also §6.1.1). A summary of the selected parameters for data processing can be found in **Table 5-2**.

Table 5-2: Summary of the used parameters from the DATRAS database of ILVO in R.

Parameter name	Parameter description	Unit
StNo	Station which is sampled	-
Year	Year of sampling	-
Month	Month of sampling	-
Day	Day of sampling	-
HaulDur	Haul duration	Min
Depth	Depth of the sampled station	m
Distance	Distance covered from the start to the end of the sampling	m
SurTemp	Surface temperature present at the sampled station	°C
BotSal	Salinity level present at the sampled station	ppt
TotalNo	Total number of caught brown shrimp during the sampling	#individuals

The parameters "TotalNo" and "Distance" were subsequently used to calculate the shrimp abundance per surface of sample area according **Equation 5-1**;

Equation 5-1 Calculation of Crangon crangon abundance per sampled surface area

$$Shrimp\ abundance\ \left(\frac{\#IND}{m^2}\right) = \frac{TotalNo}{Width\ beam * Distance}$$

The width of the used beam, as seen in §5.1.1, is six meters. This equation was applied to every sample station and each year of the observed period. In the results this parameter will be called "Abundance" and will show the amount of shrimp present per sampled squared meter (#IND m^{-2}).

5.2 (A)biotic data

5.2.1 Campaigns

The LifeWatch (LW) framework is established as part of the European Strategy Forum on Research Infrastructure (ESFRI). The framework offers several facilities (e.g. models) and datasets (e.g. abundances, environmental parameters). It can be seen as a virtual laboratory for conducting research on biodiversity or ecosystem functions.
As described by Mortelmans et al. (2019) the Flanders Marine Institute (VLIZ) contributes to the Belgium LifeWatch infrastructure by sampling a grid of 17 stations since 2012. Nine of these stations, illustrated in **Figure 5-4**, are sampled during 1-day survey trips with a monthly frequency (Station 700/710/780/130/230/330/120/215/ZG02, encircled **Figure 5-4**. Other stations are sampled seasonally and will therefore not be considered for statistical analysis in this dissertation. Locations of the LW stations are chosen based on available historic data and complementary with other existing water-quality measuring stations of other marine institutes. Sampling is carried out aboard the RV Simon Stevin.

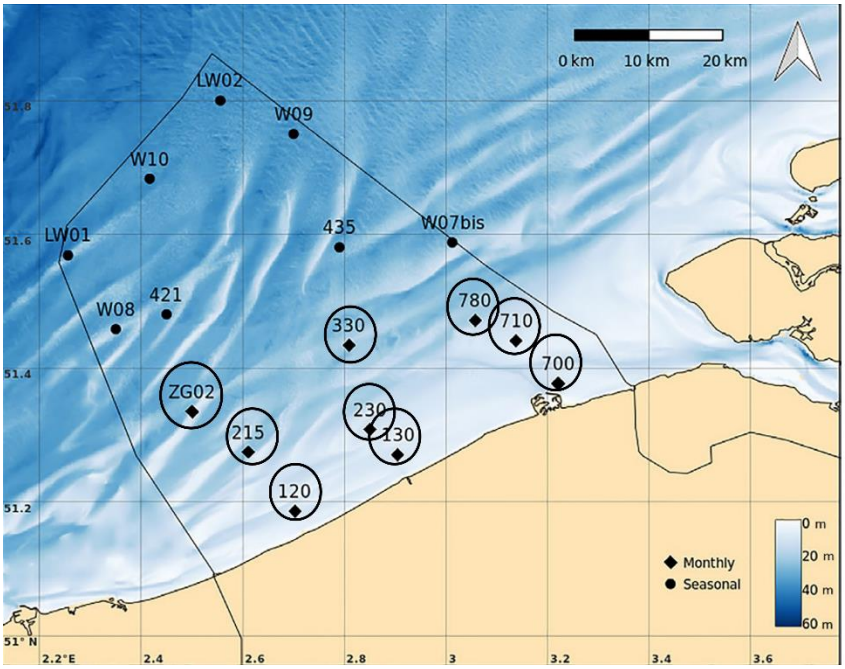

Figure 5-4 Locations of the different stations sampled during the LifeWatch campaigns. Stations 120, 130, 700, 710,230, 215, 780, 330 and ZG02 are sampled on a monthly basis (black circles). The other stations are sampled seasonally and are therefore not considered during the data processing. Figure derived from Mortelmans et al. (2019).

5.2.2 (A)biotic data collection

All of the sampled data aboard RV Simon Stevin is stored by the Marine Information and Data Acquisition System (MIDAS), containing navigation, meteorologic and oceanographic data. This data is then automatically uploaded to the VLIZ ICT network within 24 hours (Mortelmans, Deneudt, et al., 2019). Through the online LifeWatch Data Explorer portal (https://rshiny.lifewatch.be/station-data/)(LifeWatch Belgium, 2023) or via the *lwdataexplorer* R-package (Hernandez et al., 2021), these data series can be freely obtained.

Available LifeWatch abiotic data can be divided into two subsections: underway data (Flanders Marine Institute (VLIZ), 2017) and monitoring station data (Flanders Marine Institute (VLIZ), 2020). For this dissertation, only monitoring station data will be utilized. This dataset contains measurements of various abiotic parameters (e.g. salinity, nutrients) of the 17 monitoring stations which were discussed in the previous section (see §5.2.1). Abiotic measurements are conducted at a depth of 3 meters using a CTD-carousel (Conductivity, Temperature, Depth). A complete sampling protocol including the different sampling methods is provided by Mortelmans, Deneudt, et al. (2019) and will not be further discussed. Monitoring data is accessible through the LifeWatch Data Explorer portal (LifeWatch Belgium, 2023) or via the *lwdataexplorer* R-package (Hernandez et al., 2021).

Biotic data (e.g. copepods abundance) is obtained in a similar way via the earlier mentioned LifeWatch portal.

Used parameters include salinity, conductivity, Secchi depth, pigment concentrations, pigment concentrations and copepod densities. A full summary is provided in **Table B- 2**.

5.2.3 Buoy data

Additionally to the abiotic data measured with the RV Simon Stevin , LifeWatch also provides data collected by the ICOS-buoy located on the Thornton bank in the BPNS (**Figure B- 2**, yellow dot). ICOS, which stands for Integrated Carbon Observation Centre, is a European research centre that provides long term observations for better understanding of the (marine) carbon cycle and greenhouse gas emissions. The ICOS-buoy, operational since 2015 and managed by VLIZ, not only measures carbon dioxide but also other abiotic parameters such as water temperature of chlorophyll levels . Hourly

measurements of several parameters can be accessed through the LifeWatch Data Explorer portal (Flanders Marine Institute (VLIZ), 2015) or via the *lwdataexplorer* R-package (Hernandez et al., 2021). However, due to mechanical issues to the sensors and the buoy itself, there is a data gap between 06/08/2015-08/02/2018.

5.3 Geographic data series

Geographical data is derived from the European Marine Observation and Data Network (EMODNet) and processed in Qgis (see §6.1.2). EMODNet is a network of organizations that facilitate the availability of marine data. Before its foundation, marine data was fragmented and difficult to access because data collection was carried out by various organizations and researchers with their own purposes. EMODNet resolved this by centralizing and standardizing all data in one central database, freely available for all kinds of research purposes. In this dissertation, EMODNet is consulted with the aim to create a bathymetric and sediment profile of the seafloor of the BPNS. Several data series, which are discussed below, are obtained through the online EMODNet Map Viewer (https://EMODNet.ec.europa.eu/geoviewer/#!/).
In this thesis, bathymetric data is extracted from EMODNet to create a bathymetric and sediment profile of the seafloor of the BPNS. Data is obtained according to the "EPSG:4326" projection and the "Decimal 22.5°" coordinate format.

5.3.1 Bathymetric data

Bathymetric data of the BPNS is extracted from the dataset "*Digital bathymetry (DTM 2022)*" and can be found in the "depth" subdivision of the Bathymetric division of EMODNet (EMODNet Bathymetry Consortium, 2022). This dataset was published on 31/01/2022 and contains observations ranging from 01/01/1816 to 11/07/2022. Data is accumulated in a gridded layer with grid dimensions of 1/16 * 1/16 arc minute of longitude and latitude (ca 115 * 115 meters) Each grid provides water depth of the different North Atlantic seas or regions (e.g. North Sea, Bay of Biscay, Baltic Sea).
The used Digital Terrain Model or DTM comprises on the one hand of 21 937 bathymetric survey data sets, and on the other hand a collection of DTMs provided by 64 organizations spread over 28 countries adjacent to European seas. In addition, bathymetric products from the "Landsat 8" and "Sentinel" satellites are also included. Missing areas were completed by integrating the "GEBCO 2022" and "IBCAO" datasets (EMODNet Bathymetry Consortium, 2022).

5.3.2 Substrate data

Whitin the EMODNet-Geology project, sea substrate data is compiled from external partners, resulting in a general dataset comprising five substrate classes. Four of these classes ("mud to sandy mud", "sand", "coarse sediment", "mixed sediment") are based on the Folk triangle (Folk, 1954), and one additional class ("rock and boulders") was added by the EMODNet-Geology project team. If more detailed information of the region is available, extra classifications are added. In this way, datasets with 5, 7 or 16 classifications are available (Multiscale-Folk5, Multiscale-Folk7, Multiscale-Folk16 respectively). In this dissertation, the substrate dataset with seven classifications, Multiscale-Folk7, is preferred. Classifications are: "Mud", "Sandy Mud", "Muddy Sand", "Sand", "Coarse Sediment", "Mixed Sediment" and "Rock & Boulders". The Multisclale-Folk7 dataset is visualized in **Figure B- 3** (European Marine Observation and Data Network (EMODNet), 2023).

5.4 Sandbank data

Data about the seafloor profile is retrieved through the online BWZee tool (https://www.vliz.be/projects/bwzee/index.php), which offers information about several marine species and their habitat (Verfaillie et al., 2015). The position of sandbank crests, slopes, seafloor depressions and flat areas is summarized in the "*Bathymetric Position Index (structures) : small scale structures indicating slopes, crests and depressions on the Belgian continental shelf (UG_RCMG_BPI_s)"* layer. The Digital Elevation Model (DEM), using the Bathymetric Position Index (BPI), was used to create this layer by determining the location of these structures in the BPNS (Iampietro & Kvitek, 2002; Weiss,

2001). The DEM was assembled by the Renard Centre of Marine Geology with bathymetric single beam data from the Ministry of the Flemish Community (Department of Environment and Infrastructure, Waterways and Marine Affairs Administration, Division Coast, Hydrographic Office) along with data from the Hydrographic Office of the Netherlands and the United Kingdom. The obtained data is visualized with Qgis, resulting in **Figure B- 4**.

5.5 NAO data

NAO data is obtained via the National Oceanic and Atmospheric Administration (NOAA) (https://www.cpc.ncep.noaa.gov/products/precip/CWlink/pna/nao.shtml) (National Oceanic and Atmospheric Administration, 2023). The NOAA derives the NAO index by projecting NAO loading pattern onto the daily anomaly 500 millibar height field over 0-90°N. The complete NAO determination procedure is described by Barnston & Livezey (1987) The daily mean NAO index is available from 1950 to the present day. In this dissertation, NAO data is selected for the period 01/01/2014-31/12/2023.

6 DATA PROCESSING

6.1 Processing software

6.1.1 R and RStudio

Data merging, processing, visualization and analysis is performed with R Statistical Software, version 4.3.1. (2023-06-16 ucrt) in RStudio, version 2023.12.0.369 (Posit team, 2023; R Core Team, 2023). Various software packages are used for multiple purposes. *IcesDatras* (v1.4.1) is used to extract data from the DATRAS Trawl Survey Database (Millar et al., 2023). LifeWatch data (abiotic, biotic and buoy) is accessed via the *lwdataexplorer* package (v0.0.0.9000) (Hernandez et al., 2021). To install the latter, the *devtools* package (v2.4.5.) is required (Wickham et al., 2022). *Dplyr* (v1.1.4.), *tidyr* (v1.3.0.) and *tidyverse* (v2.0.0.) are used throughout all scripts for data cleaning, manipulation and integration (Wickham et al., 2019; Wickham, François, et al., 2023; Wickham, Vaughan, et al., 2023). Data visualization is conducted with *ggplot2* (v3.4.4) and *ggpubr* (v0.6.0.), with *RColorBrewer* (v1.1.3) providing the ColorBrewer color palette (Kassambara, 2023; Neuwirth, 2022; Wickham, 2016). The *regclass* package (v1.6) provides basic tools for regression modelling, which are used in correlation plots (Petrie, 2020). *Writexl* (v1.4.2.) is used for data exportation from RStudio to excel files (.xlsx) (Ooms, 2023). GAMs creation and visualisation is performed with the *mgcv* (v1.8.42.), *gratia* (v0.9.0.) and psych (v2.3.9.) packages (Revelle, 2023; Simpson, 2023; S. N. Wood, 2003, 2004, 2011a, 2017; S. N. Wood et al., 2016).

6.1.2 Qgis

Geographical data, derived from EMODNet, is visualized with Free and Open Source QGIS software, version 3.28.12-Firenze LTR (QGIS.org, 2023). Various coordinate reference systems (CRS) are employed across different projects. The project CRS of **Figure B- 3** is WGS84 (CRS84) (OGC:CRS84). **Figure B- 2** is created with WGS84/pseudo Mercator (EPSG 32631) as project CRS. **Figure B- 4** has WGS84/UTM zone 31 N (EPSG 32631) as project CRS.

The coordinates of the plotted ILVO and LifeWatch stations are summarized in **Table B- 2**. For plotting the ILVO stations, coordinates are extracted from the DATRAS Trawl Survey Database for the year 2021, which marks the last year all 33 stations were sampled (Millar et al., 2023). Since 2022, station 91 is part of the Colruyt sea farm and thus no longer available for sampling. The coordinates provided in the DATRAS database correspond with the locations where the beam trawl resurfaced after a haul. Coordinates of LifeWatch stations are derived from Mortelmans et al. (2019).

Data processing and manipulation of the geographic data, such as the slope calculation (see §5.4) is however conducted with RStudio.

6.2 Data integration

In order to facilitate spatial analysis and exploratory studies, LifeWatch- and ILVO data are merged in one general dataset. Merging criteria include the sampling month and year, and location in the BPNS. However, due to a limited amount of matching stations, the following approximation is made. The area in which the stations are located is divided into a grid with nine cells (**Figure 6-1**) determined by both a nearshore-offshore gradient(Nearshore/Midshore/Offshore) and an East-West gradient (East/Central/West). This configuration is an adaptation of the distribution used by Mortelmans et al. (2021). The grid allows the coupling of (a)biotic measurements, derived from LifeWatch, with shrimp abundances measured at ILVO stations. It is thus assumed that all ILVO stations in the same cell experience identical (a)biotic measurements recorded by the present LifeWatch station. This approximation needs to be taken into account when interpreting the results.

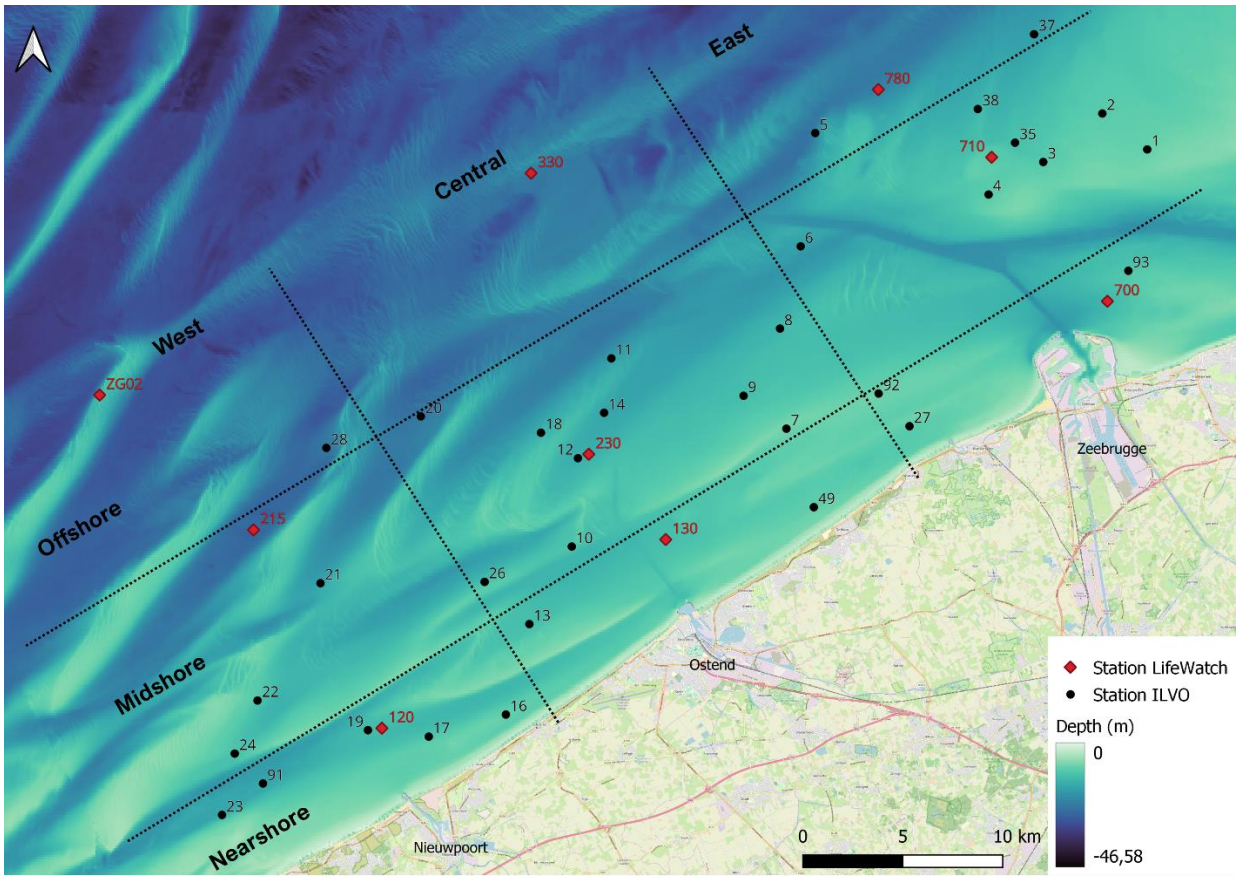

Figure 6-1 Bathymetric map with the locations of the ILVO and LifeWatch stations (indicated with the black dot and red diamond respectively). A grid is made based on a near-offshore and East-West gradient. In this way, LifeWatch measurement can be coupled with shrimp abundances measured at ILVO stations. The locations of the stations of ILVO are based on the coordinates of year 2021 since this is the last year all 33 stations were monitored. Coordinates are derived from the online DATRAS database (Millar et al., 2023). The coordinates from LW stations date from the year 2012 and are derived from Mortelmans et al. (2019). The cities Zeebrugge, Ostend and Nieuwpoort are also indicated as reference. Map made on 17/12/2023.

6.3 Data analysis

6.3.1 Statistical analysis: linear correlations

All statistical tests are conducted using RStudio (see also §6.1.1). Linear correlation plots require the *ggpubr* package (Kassambara A, 2023). The Spearman rank correlation is used to determine linear correlations between (a)biotic variables and *C. crangon* abundance. Correlations are considered significant if p-values are smaller than 0.05.

6.3.2 Generalized additive models (GAMs)

Besides linear correlation test, Generalized Additive Models (GAM) are also applied in order to identify non-linear correlations between *C. crangon* abundance and other (a)biotic parameters. GAMs are constructed with the *mgcv* package v1.9-1 (S. Wood, 2023) which is installed in R v4.4.0. Before the actual modelling, possible outliers which could (strongly) influence the model behaviour are filtered out based on the interquartile range (IQR) method. According to this method, outliers are defined according to **Equation 6-1**.

Equation 6-1 *Formula for outlier identification using the interquartile (IQR) method.*

$$Outlier = [25^{th} percentile] - 3 * IQR \ \vee [75^{th} percentile] + X * IQR$$

-

In total, outliers of three parameters are removed: chlorophyll *a* and *b*, and slope to maximum.

Each constructed GAM uses the general form shown in **Equation 6-2**.

Equation 6-2 *General form of a GAM, with y_i the dependent variable, x_{ji} the independent variable, $s_j()$ the spline function (**Equation 6-3**), β_0 the parametric term that represents the mean of the dependent variable and ε the error term.*

$$y_i = \beta_0 + \sum_j s_j(x_{ji}) + \varepsilon_i$$

The smooth or spline functions are constructed with basis functions of the form shown in **Equation 6-3**.

Equation 6-3 *Smooth or spline function of the independent variable., with bk a basis function and βk the chosen weight of the basis function.*

$$s(x) = \sum_{k=1}^{K} (\beta_k * b_k(x))$$

Consequently, in each model, the log10((abundance m^{-2})+1) acts as the dependent variable (y_i) while the different (a)biotic parameters represent the independent variables (x_{ji}). The chosen (a)biotic parameters for constructing the GAMs are listed in **Table 6-1**.

Table 6-1 Selected parameters to construct GAMs for the general dataset.

Parameter	unit
Salinity	ppt
Depth	m
Chlorophyll *a* concentration	µg L^{-1}
Average spring chlorophyll *a* concentration	µg L^{-1}
Chlorophyll *b* concentration	µg L^{-1}
Beta-carotene	µg L^{-1}
Average spring Beta-carotene concentration	µg L^{-1}
Ammonium concentration (NH4)	µmol.N-NH_4 L^{-1}
Nitrate concentration (NO3)	µmol.N-NO_3 L^{-1}
Nitrite concentration (NO2)	µmol.N-NO_2 L^{-1}
Phosphate concentration (PO4)	µmol.N-PO_4 L^{-1}
Water temperature	°C
NAO index	-
Winter NAO index	-
Summer NAO index	-
Days above 20°c	days
Slope to maximum in 750m	°
3-month average temperature (winter, spring, summer, autumn)	°C
6-month average temperature (winter, summer)	°C
Juvenile whiting abundance	#individuals m^{-2}
Water temperature	°C
Shrimp landings in the previous year	tonne
Average Calanoid density in spring	#individuals m^{-3}

Model diagnostic plots from the *gratia* package (v0.9.0) are used to control if the distribution of the GAMs corresponds with the data distribution (**Figure 6-2**). Normality is assumed if the QQplot shows a straight line of residuals and if the histogram of residuals showed a bell-shaped curve. If the observed and fitted values show a similar variability in the "response vs fitted values" plot, homogeneity is concluded (S. N. Wood, 2017; Zuur et al., 2009).

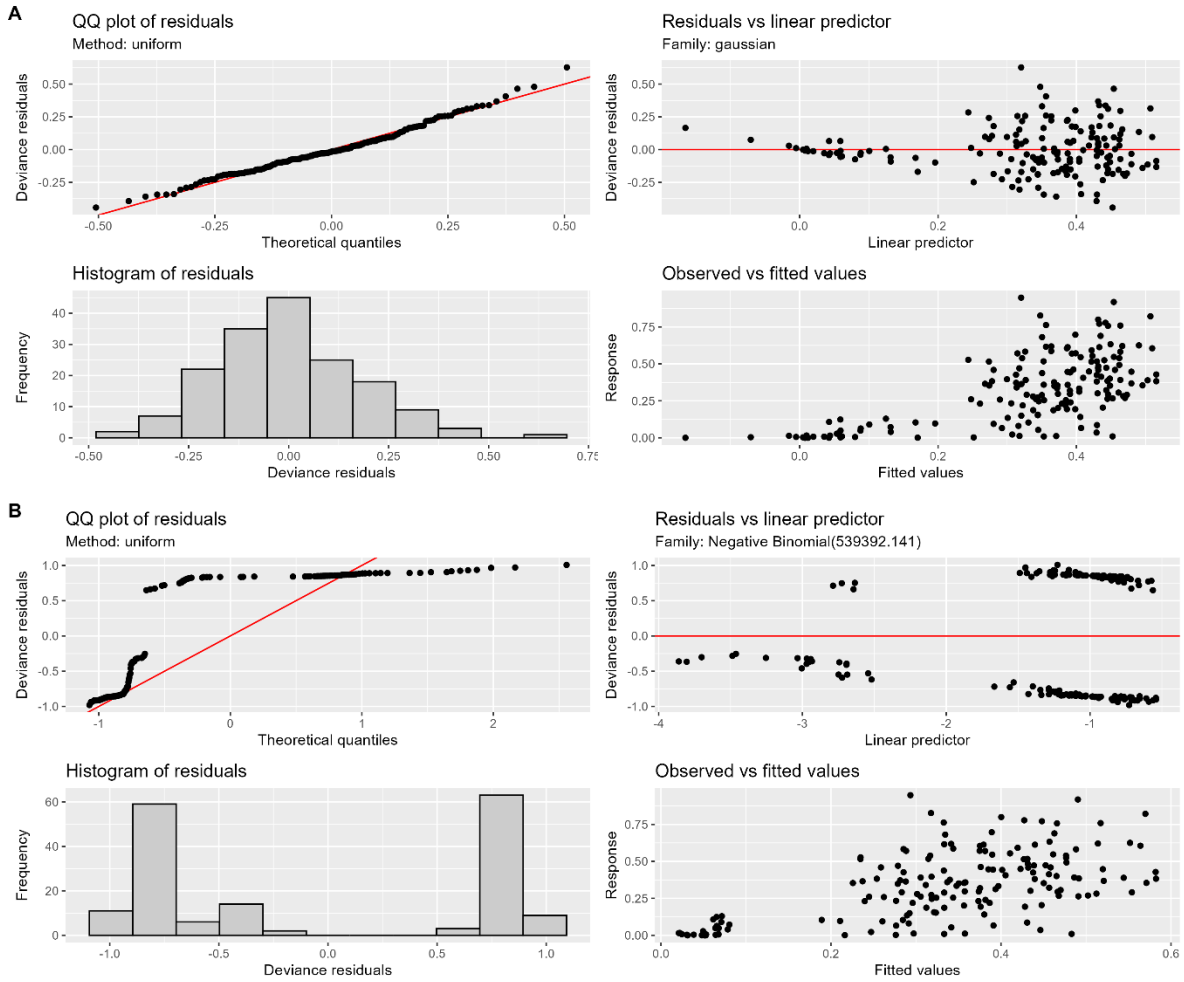

Figure 6-2 Two diagnostics plot of [A] a normal distributed model and [B] a negative binomial distributed model which both try to explain the normal distributed the log10-transferred C. crangon abundance. [A] According to this plot, the right distribution of the GAM was chosen. Data points are located on the diagonal in the QQ-plot, the histogram has no heavy tails and shows bell-shaped curve, the residual vs linear predictions plot shows no clear pattern and is evenly distributed around 0 ,and the response vs fitted values follows a clear diagonal pattern and does not fan out. [B] According to this plot, the wrong distribution of the GAM was chosen. Datapoints are not following the diagonal in the QQplot, the histogram has heavy tails and does have a bell-shaped curve, clear patterns are visible in the residual vs linear prediction plot, and the response vs fitted values plot fans out towards the end. Plots created in R (v4.3.1.) and the gratia-package.

The log-transformation of the brown shrimp abundance (IND m^{-2}) follows a normal distribution, and therefore GAMs following the gaussian distribution are used.

To avoid collinearity, variables with a concurvity > 0.7 are excluded from GAMs. If a variable's concurvity is too high, its smooth function can be explained by a combination of other smooths and therefore has no contribution in explaining the dependent variable y_i. No universal rules are present to define a proper boundary for concurvity, and therefore the value of 0.7 is based on a similar study conducted by Semmouri et al. (2023). The restricted maximum likelihood method (REML), described by S. N. Wood (2011b), is chosen to estimate the correct smooth parameters.
After constructing multiple GAMs, the Akaike's information criterion (AIC) is used to define the best fitted model: the lower the AIC score, the more data is explained by the model and thus the better fit (Cavanaugh & Neath, 2019).

7 NUTRITIONAL CONTENT

During the 2023-DYFS-campaign of ILVO, *Crangon crangon* samples were collected at 16 of the 33 stations. Additionally, four hauls were also conducted at Station 230 of LifeWatch in November. Detailed information of each haul is listed in **Table B- 3**. These samples are used for protein and lipid analysis, with sample preparation and extraction protocols based on the extraction protocols of protein, lipid and fatty acid concentration in *Mytilus edulis*, described by Deruytter (2018).

7.1 Station selection and sample collection

Before sample preparation, a selection of the sampled stations is made based on an east-west gradient and a near-offshore gradient, creating a grid similar to the one illustrated in **Figure 6-1**. From these stations, only shrimp of the EPI-M fraction will be used for nutritional analysis, since this is a commercial size (see §5.1.1.1). However, due to practical constraints during the DYFS campaign, not every cell of the grid was sampled. For instance, at station 17 or 38, a haul was conducted but no shrimp of the EPI-M fraction was caught. These are the only stations sampled in their respective cells (East-near shore; West-offshore, respectively), and therefore no information will be available for these cells. An overview of the selected stations for lipid and protein extraction can be found in **Figure 7-1**.

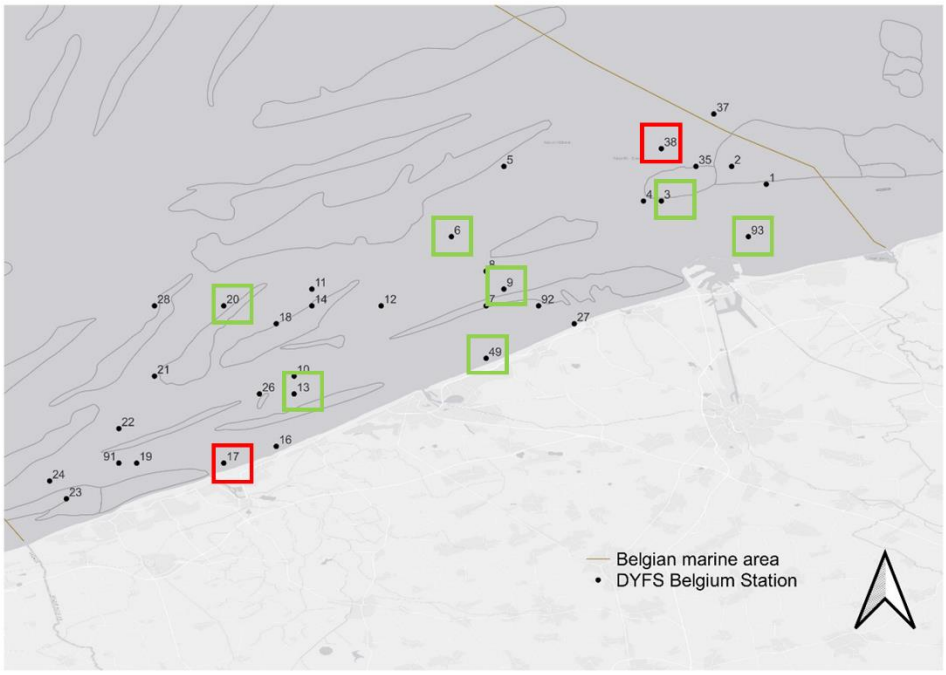

***Figure 7-1** Overview of the selected stations for protein and lipid analysis. Green squares indicate that samples are collected at this station, red squares indicate that hauls were conducted at this station, but no samples were taken (due to insufficient abundance). Detailed information of each haul is summarized in **Table B- 3**. Figure derived from Raat (2023).*

7.2 Sample preparation

In total, two different extractions will be conducted to retrieve protein, lipid and fatty acids of the caught shrimp. These extractions require a similar sample preparation, which is therefore generally discussed.

First of all, five shrimps are randomly selected for each of the stations in **Figure 7-1**. Full body length and weight is determined for each shrimp. Next, the last three segments of the body (segments 4, 5, 6 in **Figure 4-3**) are dissected from the body, including the telson. After pealing, 5 mg (wet weight) of shrimp tissue is weighted and placed in 1.5 or 2 ml

(lipid extraction) Eppendorf microcentrifuge tubes. This will be repeated two times since every extraction requires 5 mg of shrimp flesh. Samples are then stored in a freezer at -20°C.
Next, deionized water is added to the tubes and shrimp flesh is grinded with an autoclaved homogenizer with Teflon head. When the flesh is sufficiently homogenized, the samples are immediately frozen with liquid nitrogen and stored at -80°C.

7.3 Protein content (Bradford method)

Protein measurement is based on the Bradford analysis (Bradford, 1976): dye Brilliant Blue G (Bradford reagent, Sigma B6916) reacts with the present proteins and causes a colour shift from 465 to 595 nm (blue colour) which will be measured by a Thermo Labsystems Multiscan Ascent 354 Plate reader.

To start, deionized water is added to the tubes and shrimp flesh is grinded with an autoclaved homogenizer with Teflon head pestle. When the flesh is sufficiently homogenized, samples are placed on ice and 200µL Tris (pH 6.8; 0.6 mg Trizma base(Sigma T-1503) in 100ml deionized water) is added. Samples are homogenized by pipetting up and down and another 200 µL Tris is added while rinsing the Teflon head pestle. Next, samples are centrifuged at 7607 RCF at 4°C in an Eppendorf Centrifuge 5424R for 15 minutes. After these 15 minutes, a dilution of 1:50 is conducted by adding 4 µL of sample to 200 µL Tris. After vortex mixing the diluted sample for ± 15 seconds with a VWR® Collection REAX vortex mixer, 25 µL sample is put into a 96-multiwell plate. Three replicates of each sample are made. Next, 250 µL of Bradford reagent (Sigma B6916) is added **quickly** to each well with a multitip pipette because colorization takes place at a fast rate. After adding the Bradford reagent, the plate is incubated in the dark for 15 minutes at room temperature.
After incubation, the well is placed in a Thermo Labsystems Multiscan Ascent 354 Plate reader which shakes the plate for 5 seconds and then measures the optical density at 595 nm.

Bovine Serum Albumin or BSA (Sigma P5619) is used as protein standard. A stock solution of 0.4 mg ml^{-1} is made by adding 10.375 ml deionized water to 4.15 mg BSA in Erlenmeyer of 10 ml. From this stock solution, 200 µL is added to 1 ml Eppendorf tubes and stored at -20°C for further use. These standards have a lifespan of ± 6 months.
A standard concentration range of 0.4/0.2/0.1/0.05/0.025 mg ml^{-1} is made, followed by 3 blanks of deionized water. The 1:2 serial dilution is carried out in the 96-multiwell plate. In total, 3 set of standards and blanks are made. Simultaneously to the samples, Bradford reagent is also added to the standard series.

7.4 Lipid content (Bligh and Dyer method)

Lipid content is determined with the Bligh and Dyer method (Bligh & Dyer, 1959): Chloroform ($CHCl_3$) is used to dissolve present lipids. In combination with sulfuric acid (H_2SO_4), these lipids are burned at 200°C to create carbon what results in a black colour. The amount of present carbon will be measured at 340 nm by a Thermo Labsystems Multiscan Ascent 354 Plate reader.

While stored on ice, 100 µL of deionized water is added to the Eppendorf tubes. Next, the samples are homogenized with an autoclaved homogenizer with Teflon head, which is rinsed with another 100 µL deionized water. Next, samples are taken to the fume hood where 500 µL chloroform ($CHCl_3$, sigma c 2432), 500 µL methanol (CH_3OH, sigma Aldrich 34885) and 250µL deionized water is added. After vortex mixing with a VWR® Collection REAX vortex-mixer, the samples are centrifuged in an Eppendorf Centrifuge 5424R for 10 minutes at 845 RCF at 4°C. Next, 3 times 100 µL is taken from each sample and diluted with 300 µL chloroform in a 5 ml glass tube. These tubes are then heated at 60°C for 30 minutes in a VWR® VENTI-Line® drying oven. Finally, 500 µL of sulfuric acid (H_2SO_4, Prolabo 20692, recaptur 98%) is added to the tubes, which are vortexed gently. When stirred too fast, the sulfuric acid on the walls will incinerate and this will result in black flakes in the liquid.

Tripalmitin (fatty acid, C16:0, Sigma T5888) is used as standard. An amount of 62.5 mg of Tripalmitin is weighed of in a 10 ml volumetric flask and is dissolved with 10 ml of chloroform. Next, a 1:2 serial dilution is performed with chloroform in 5 ml glass tubes, starting with 2 ml of the latter solution. From the first tube, which has a concentration of 6.25 mg ml^{-1}, 1 ml is transferred into the next tube and diluted with 1 ml of chloroform. This process is repeated 6 times, resulting in a dilution series with the following concentrations: 6,25 mg ml^{-1}; 3.12 mg ml^{-1}; 1.56 mg ml^{-1}; 0.78 mg ml^{-1}; 0.39 mg ml^{-1}; 0.19 mg ml^{-1}; 0.09 mg ml^{-1}. One blank with 1 ml of chloroform is also added at the end of the series. Each tube is then vortexed. Next, 100µL from each tube is added to a new tube which is heated at 60°C for 30 minutes. When cooled down, 500 µL of sulfuric acid is added and gently vortexed.

After adding the sulfuric acid to both the samples and standard series, the glass tubes are heated at 200°C for 15 minutes in the VWR® VENTI-Line® drying oven. After these 15 minutes, the samples and standards are cooled down to room temperature for another 15 minutes. When cooled down, 250 µL from each sample is put into a well of a 96-multiwell plate, which is then put into a Thermo Labsystems Multiscan Ascent 354 Plate reader. The plate reader will shake the plate for 5 seconds and then measure the optical density at 340 nm.

8 CHAT GPT

In this dissertation, Chat GPT was solely used to rewrite certain paragraphs. However, no additional or new information was obtained through Chat GPT.

RESULTS

9 TRENDS IN POPULATION DENSITIES

9.1 Spatial distribution

To observe differences in spatial distribution of *C. crangon* in the BPNS, boxplots of the log-transformed (log_{10}) abundance (#IND m^{-2}) were made for each year and each station (**Figure 9-1**). Abundance data of September was used , and a pseudo count (all data point +1) was implemented to account for zero-values.

A Kruskal-Wallis test revealed that the relative abundance of *C. crangon* (#IND m^{-2}) significantly differs over the different stations and throughout the years ($\chi^2(32) = 82.174$, $p < 0.01$; $\chi^2(8) = 17.539$, $p < 0.05$, respectively). A post hoc Dunn test was used to identify mutual differences. No significant differences between two years were observed (Dunn test, BH adjusted, $p > 0.05$)

Additionally, no significant correlation was found between the *C. crangon* abundance and their position towards sandbanks in the BPNS, regardless of sampling time (**Figure C- 1**).

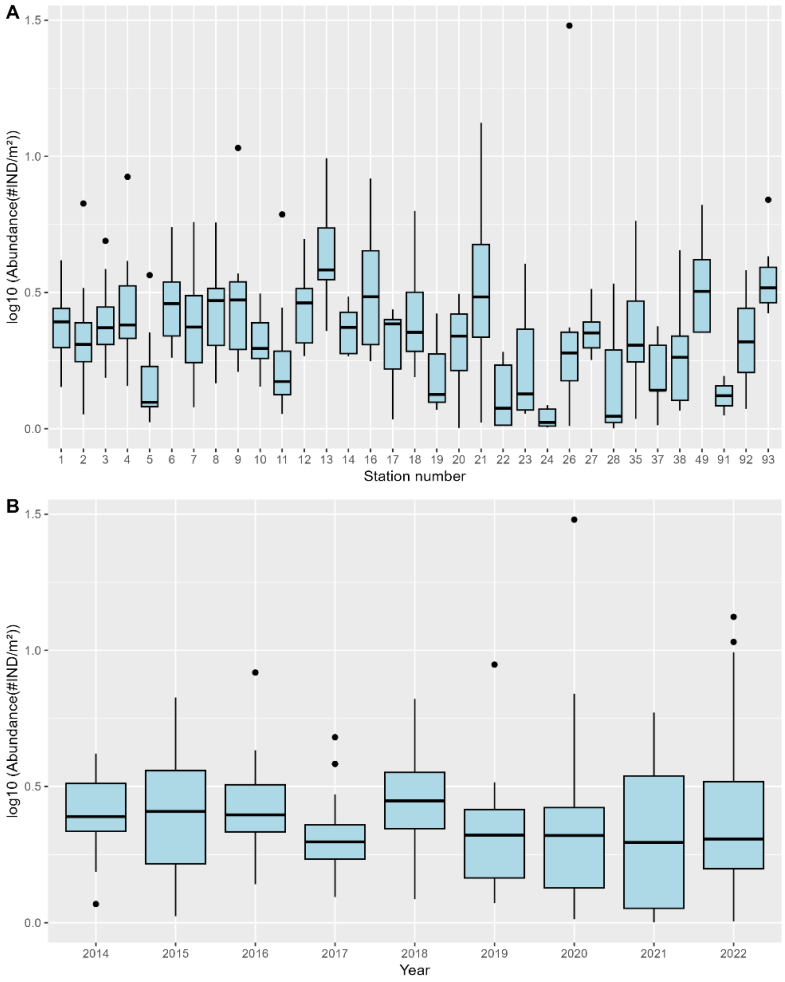

Figure 9-1 *Boxplots of the abundances, expressed as #IND m^{-2} of C. crangon in the BPNS per [A] station and [B] per year. Abundances were log10-transformed to account for outliers. Pseudo count (all data+1) was applied in order to take the logarithm of zero-values ($log_{10}(1) = 0$).*

9.2 Relation to abiotic parameters

9.2.1 Water Temperature

Throughout the observed period, water temperatures were at their highest in July, August and September. Consequently, in this dissertation, these months will be called the summer months. Conversely, January, February and March exhibited the coldest water temperatures and are therefore designated as the winter months (**Figure 9-2**). Hence, April, May and June are considered as the spring months, while October, November and December are classified as the autumn months. On a six-month scale, a similar assumption is made. October through March will be considered as the winter period, while April to September is seen as the summer period. Unless otherwise stated, these seasonal assumptions will be applied for all subsequent results.

During the observed period, highest maximum water temperatures occurred in August 2018 and August 2022, reaching 22.67°C and 22.04°C, respectively. July followed a similar trend, with highest maximum temperatures in 2018 (21.73°C) and 2022 (21.24°C). In September, the highest maximum temperatures were recorded in 2022 (21.76°C) and 2023 (21.56°C), followed by 2018 (20.35°C) (**Figure 9-2-A**).

Regarding the monthly mean water temperatures, similar trends were observed. Highest mean temperatures were reached in August 2018 and August 2022, with a mean temperature of 21.31°C and 21.20°C, respectively. In July, the highest mean temperatures were recorded in 2018 (19.85°C) and 2019 (19.61°C), followed by 2022 (19.52°C). In September, the highest mean temperatures were noted during 2023 and 2022, with 20.05°C and 19.94°C, respectively, followed by September 2018 which had a mean temperature of 19.28°C (**Figure 9-2-B**).

Furthermore, the LifeWatch buoy that was used for these results was located in more offshore waters than the observed LifeWatch and ILVO stations, indicating that the maximum and monthly water temperatures in more nearshore waters were even higher than those presented.

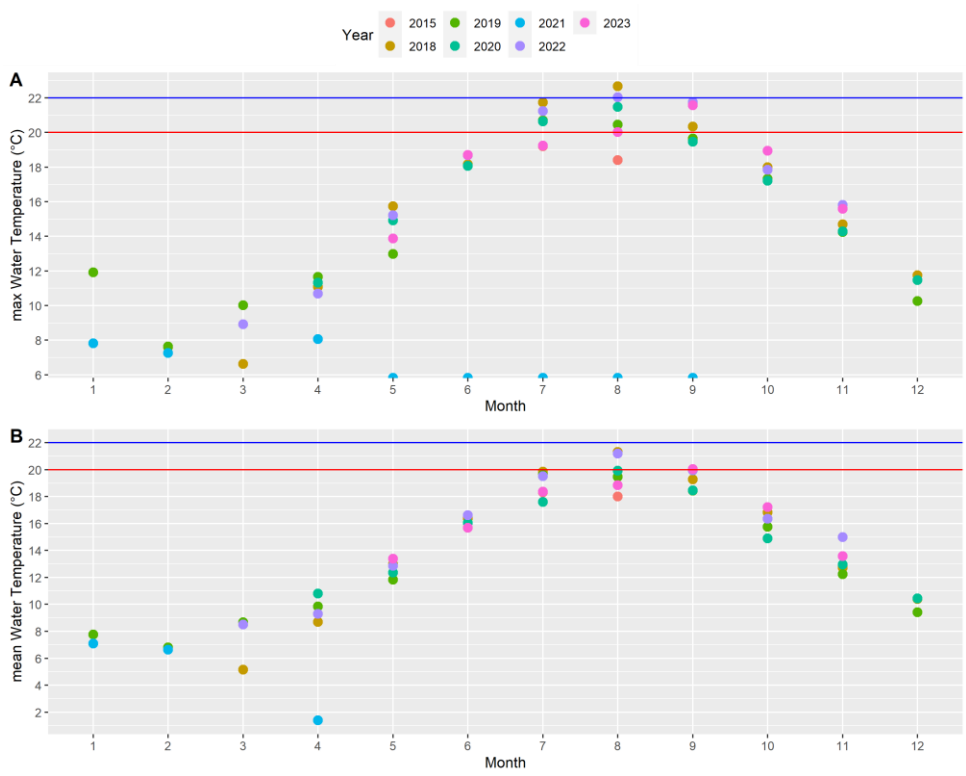

Figure 9-2 (A) Maximum temperature measured by ICOS-buoy of VLIZ at a depth of 3m in each month. Measurement period ranges from January 2014 to December 2023. (B) Average monthly temperatures for the period 2014-2023. Measurements are conducted with ICOS-buoy of VLIZ at a depth of 3m. Data for 2014, 2016 and 2017 is lacking because of technical issues relating to the buoy. Data of December 2023 was at the moment of creation not available. The red line indicates the 20°C threshold value, the blue line the 22°C threshold value. These values were chosen arbitrarily.

Additionally, for each year, the days above 20°C and 22°C were determined. In 2022, the highest number of days with water temperatures exceeding 20°C was recorded, totalling 62 days. In comparison, 2018 had 52 days with a water temperature above 20°C, of which 7 days exceeded 22°C. In contrast, during 2022, only 1 day recorded a temperature above 22°C (**Table C- 1**).

A positive correlation was found between the number of days with a water temperature above 20°C or 22°C and the abundance of *C. crangon* in September. Specifically, the Spearman Rho values (SRV) were 0.22 for days exceeding 20°C and 0.33 for days exceeding 22°C, respectively ($p < 0.01$) (**Figure C- 2**).

On a six month scale, a significant negative correlation was found between the mean winter temperature (October-March) and the *C. crangon* abundance, with a Spearman Rho of -0.35 ($p < 0.01$) (**Figure 9-3-C**). However, no correlation was found for the mean summer temperature (April – September) ($p > 0.05$) (**Figure 9-3-A**). Highest mean summer temperatures were recorded in 2017 and 2019, followed by 2022 and 2023. The mean summer temperatures of 2018 are relatively low in comparison to the latter years (**Figure 9-3-B**). Compared to other years, relatively low water temperatures were recorded during the winter periods of 2021 and 2018, while winter temperatures in 2022 were around the average (**Figure 9-3-D**)

Scatterplots for the mean water temperature on a 3- month scale were also constructed, but no significant correlations were observed ($p > 0.05$). During the winter months, water temperatures were the lowest in 2021 and 2018, whilst 2017 recorded the highest - a trend also evident in the spring period. In summer, relatively high mean water temperatures were recorded in 2022, 2020 and 2016, with 2018 exhibiting temperatures around the average. In autumn, relatively high mean water temperatures were recorded in 2022 (**Figure C- 3**).

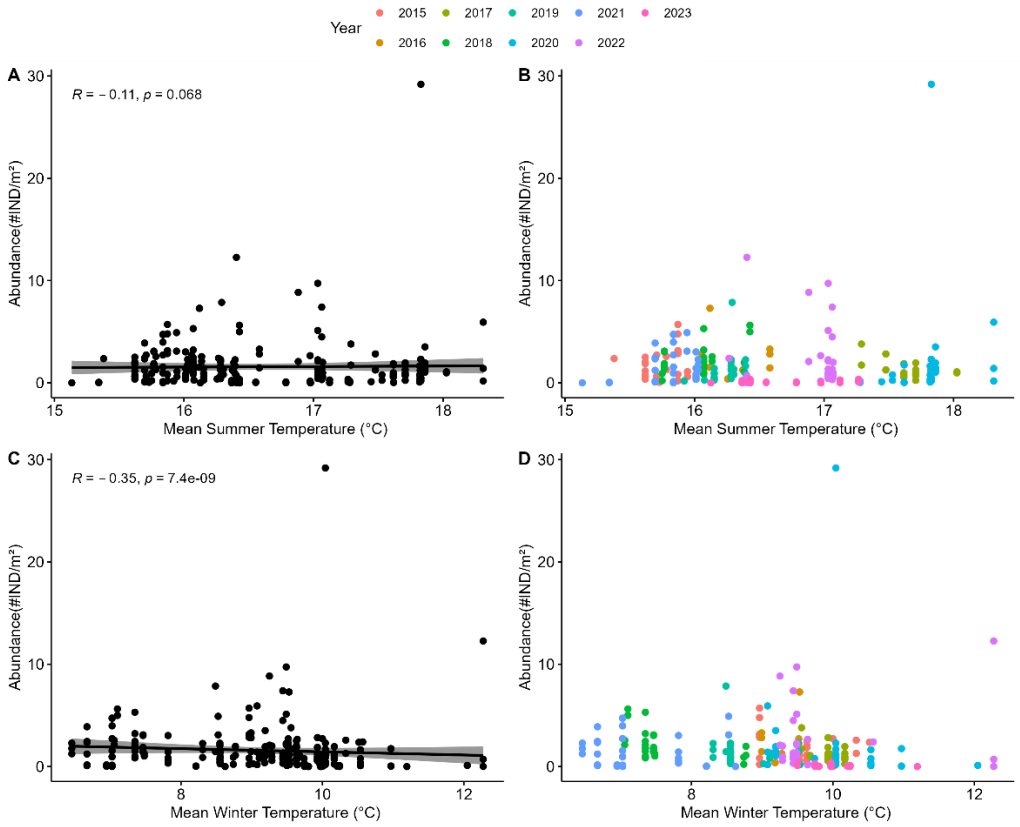

Figure 9-3 *Scatter plots of the mean water temperatures (°C) on a six-month scale in relation to the abundance of C. crangon in September (#IND m^{-2}) in the BPNS. Scatter plots [A] and [C] show the Spearman correlation, with the Spearman Rho value and p-value shown in the graph. Shaded areas represent the 95% confidence interval. Scatter plots [B] and [D] illustrate the same scatterplots as in [A] and [C] respectively but show a colour distinction based on the year of measurement. The summer period ranges from April to September, the winter period from October to March. The mean winter temperature of 2023 for example is thus calculated from October-December 2022 and January-March 2023.*

9.2.2 Salinity

The *C. crangon* abundance is negatively correlated with the bottom salinity, with a Spearman Rho of -0.23 ($p < 0.01$). Furthermore, datapoints with relatively high salinity levels (34-35 ppt) are generally situated at lower longitudes compared to those with lower salinity levels. The latter datapoints experience, due to their more northern location, a higher influence of the Scheldt estuary, which forms an influx of freshwater and nutrients to the North Sea (**Figure 9-4**).

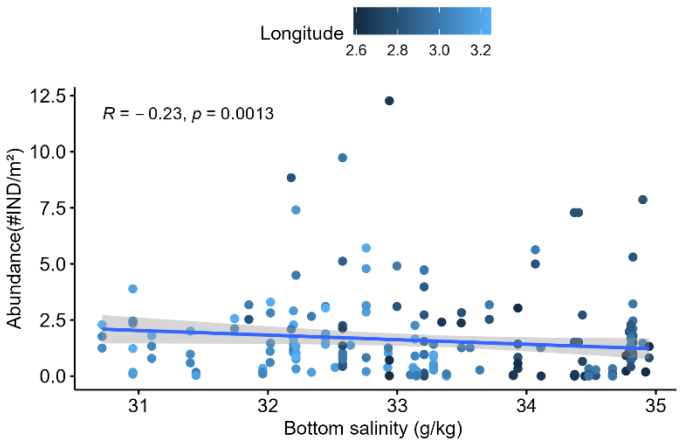

Figure 9-4 Relation between the bottom salinity (ppt), measured at the sampled stations, and the C. crangon abundance in September (#IND m^{-2}). Spearman Rho- and p-values are shown in the scatterplot, the shaded area represents the 95% confidence interval. The colour gradient represents the longitude of the data points.

9.2.3 Nutrients

To investigate the correlation with nutrient concentrations, scatterplots were constructed for four nutrients: ammonium (N-NH_4), Nitrate (N-NO_3), Nitrite (N-NO_2) and Phosphate (P-PO_4). Among these studied nutrients, only phosphate concentration (µmol P-PO_4 L^{-1}) exhibited a significant positive correlation with the abundance of *C. crangon* in the BPNS in September (SRV = 0.16, p < 0.05. No other significant correlations were observed (p > 0.05).) (**Figure 9-5**).

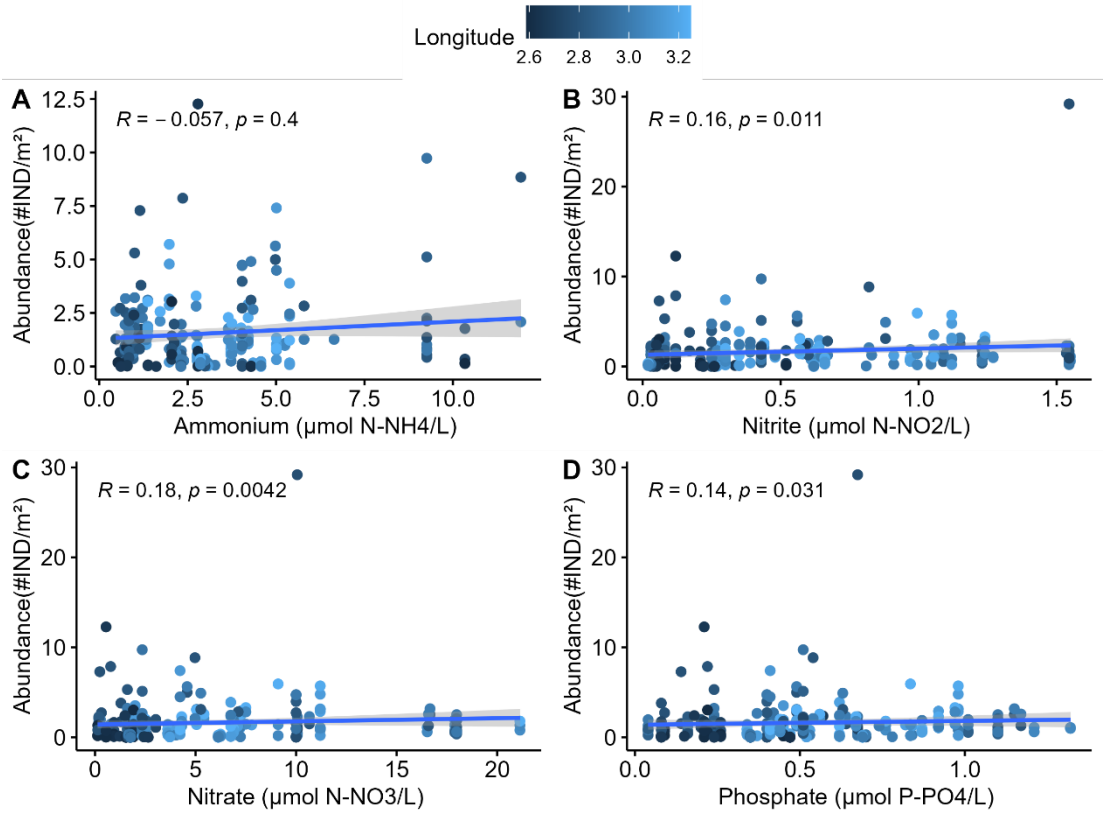

Figure 9-5 Relation of present nutrients in the water to the C. crangon abundance in September. Scatterplots are shown for [A] ammonium (µmol N-NH4 L^{-1}) [B] nitrite (µmol N-NO2 L^{-1}), [C] nitrate (µmol N-NO3 L^{-1}) and [D] phosphate (µmol P-PO4 L^{-1}) concentrations. Spearman Rho values and p-values are shown in the plots, shaded areas represent the 95% confidence interval. The colour gradient represents the longitude of the data points.

9.2.4 Pigments

Significant positive correlations are found between the *C. crangon* abundance (#IND m^{-2}) and the beta carotene (**Figure 9-6-A**), chlorophyll *a* (**Figure 9-6-B**) levels (µg L^{-1}) measured in September, with Spearman Rho values of 0.22 ($p < 0.01$) and 0.23 ($p < 0.01$) and 0.19 ($p < 0.05$), respectively. However, these scatterplots show a large confidence interval towards higher pigment concentrations, and therefore need to be interpreted with cause. These outliers are however not removed because of the biological value, but they should be carefully interpreted. No significant correlation was found for chlorophyll *b* ($p > 0.05$) (**Figure 9-6-C**)

Additionally, scatter plots were also made to illustrate the relation between the abundance of *C. crangon* in September and the mean beta carotene (**Figure 9-6-D**), chlorophyll *a* (**Figure 9-6-E**) and chlorophyll *b* (**Figure 9-6-F**) levels (µg L^{-1}) during the spring months of the same year. For these scatterplots, the spring period was extended with one month, ranging from March to June. Positive correlations were found for beta carotene and chlorophyll *a* concentration, with a respective Rho value of 0.29 and 0.25 ($p < 0.01$). In contrast, mean spring chlorophyll *b* concentrations did not exhibit a significant correlation ($p > 0.05$). For these scatterplots, outlier points do not to seem present and therefore also don't influence the shape of the curve.

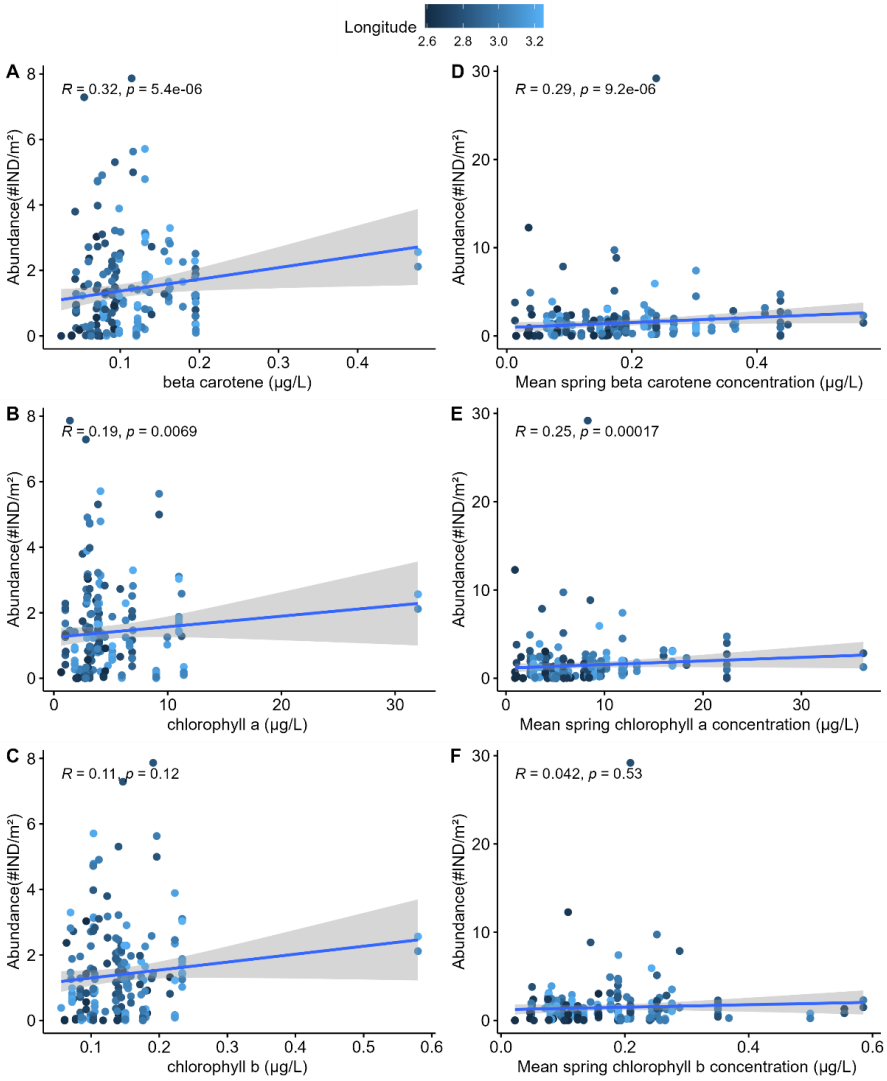

Figure 9-6 *Left column: Correlation between [A] beta carotene, [B] Chlorophyll a and [C] Chlorophyll a concentrations (µg L^{-1}) and the C. crangon abundance in September. Right Column: Correlation between mean [D] beta carotene, [B] Chlorophyll a and [C] Chlorophyll b concentrations (µg L^{-1}*

[1]) in spring (March -June) and the C. crangon abundance in September. Spearman Rho values and p-values are shown in the plots. The shaded areas represent the 95% confidence interval. Outliers are NOT removed because of the biological importance. The colour gradient represents the longitude of the data points.

9.3 Relation to biotic influences

9.3.1 Zooplankton – copepods

The abundance of *C. crangon* in September (#IND m^{-2}) is significantly negatively correlated with the mean calanoid copepod densities in spring(#IND m^{-3}), with a Spearman Rho of -0.18 ($p < 0.01$) (**Figure 9-7-A**). For these scatterplots, the spring period is defined as March through June. Harpacticoid densities in spring show no correlation ($p > 0.05$) (**Figure 9-7-B**). A large confidence interval suggests that more data needs to be accumulated in order to present a more reliable result.

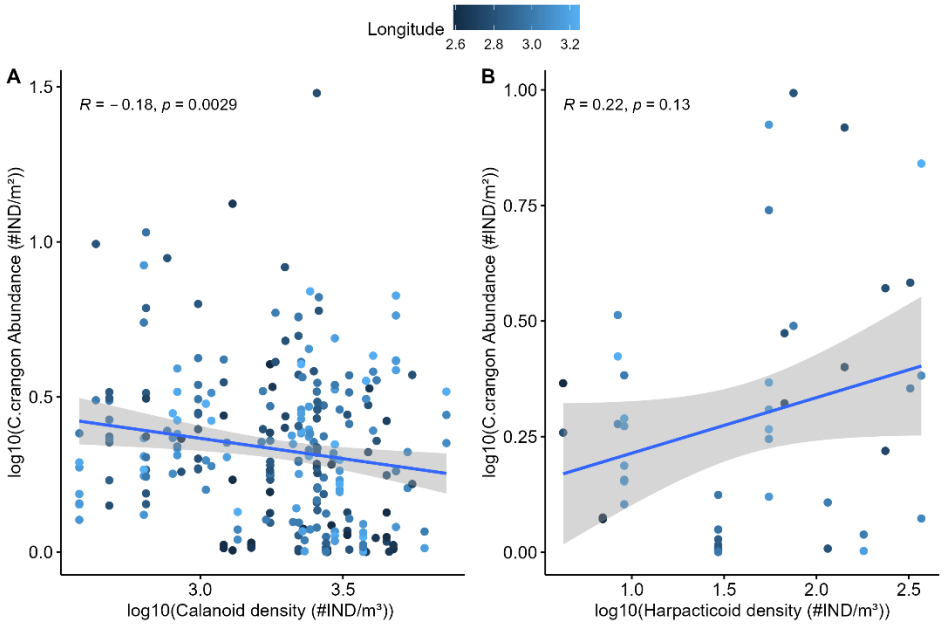

***Figure 9-7** Relation between the C. crangon abundance (#IND m^{-2}) and the average [A] Calanoid and [B] Harpacticoid densities (#IND m^{-3}) in spring (March-June). Abundances of C. crangon, Calanoid and Harpacticoid were log10-transformed, pseudo-count (all data+1) was implemented in order to account zero-values. Spearman Rho- and p-values are shown in the plots. Shaded areas represent the 95% confidence interval. The colour gradient represents the longitude of the data points.*

9.3.2 Juvenile whiting abundance

A peak of juvenile whiting in September was observed in 2023, with a relative abundance of ± 0.050 individuals m^{-2} (11850 sampled individuals), followed by 2018 during which a relative abundance of 0.016 individuals m^{-2} was noted (7801 individuals sampled). The lowest amount was observed in 2022, with only a relative abundance of 0.0014 individuals m^{-2} (276 individuals sampled) (**Figure C- 4**).

A significant, negative correlation was observed between log_{10}-transformed Whiting abundance and log_{10}-transformed *C. crangon* abundance, both measured in September, with a Spearman Rho value of -0.15 ($p < 0.05$) (**Figure C- 5**). The trend in this scatterplot is influenced by a few extreme datapoints which reflect the unusually high abundances in 2018 and 2023. These datapoints however can't be removed since they represent actual high abundance events.

9.4 Relation to North Atlantic Oscillation

The average seasonal NAO index was calculated for each year of the studied period (**Figure 9-8**). During summer, the highest NAO index was recorded in 2018, with a value of 1.677, followed by 2014 (0.037) and 2020 (-0.040). Lowest values were reached in 2015 (-1.530) and 2023 (-1.260). During spring, the highest NAO indices were recorded in consecutive 2018 (1.483), 2015 (0.268) and 2022 (0.075). Lowest values were noted in 2019 (-1.082), 2021 (-0.633) and 2014 (-0.529). During winter however, the highest NAO index was recorded in 2015 (1.520), followed by 2020 (1.204) and 2022 (1.176). During, 2021, the lowest value was reached (-0.08), followed by 2023 (0.355), 2018 (0.700) and 2019 (0.700). Trends per season are also illustrated in **Figure C- 6**.

The seasonal NAO index of 2018 exhibits an unusual pattern. Unlike other years, it remains positive throughout the whole year and follows a mirrored pattern compared to other years. Starting from the winter NAO index, the value increases until summer, after which the index decreases again, but does not drop below zero. In contrast, other years typically show a decrease to a negative value in spring and summer.

Another unusual pattern, although less pronounced, is observed in the NAO trend of 2022. During spring the NAO value decreases, but then remains relatively close to zero throughout summer and autumn without showing any significant increase.

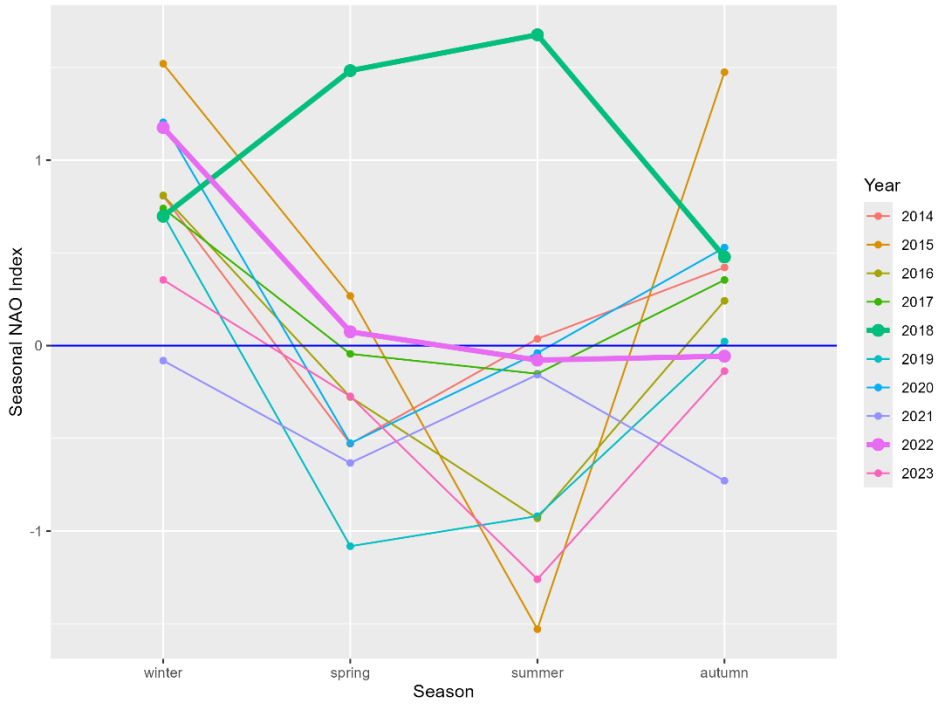

Figure 9-8 *Overview of the trend of the seasonal NAO indices per year. The trends of 2018 and 2022 are highlighted in bold because of their unusual pattern.*

C. crangon abundance shows a positive correlation to both the winter NAO index (WNAO, January-March) and the extended NAO index (WNAOex, December - March), with a Spearman Rho of 0.23 ($p < 0.01$) and 0.29 ($p < 0.01$) respectively (**Figure 9-9**). Additionally, a positive correlation was also observed between *Crangon* abundance and the average summer NAO index (SNAO), with a Spearman Rho of 0.23 and a p-value < 0.01 (**Figure 9-10**).

.

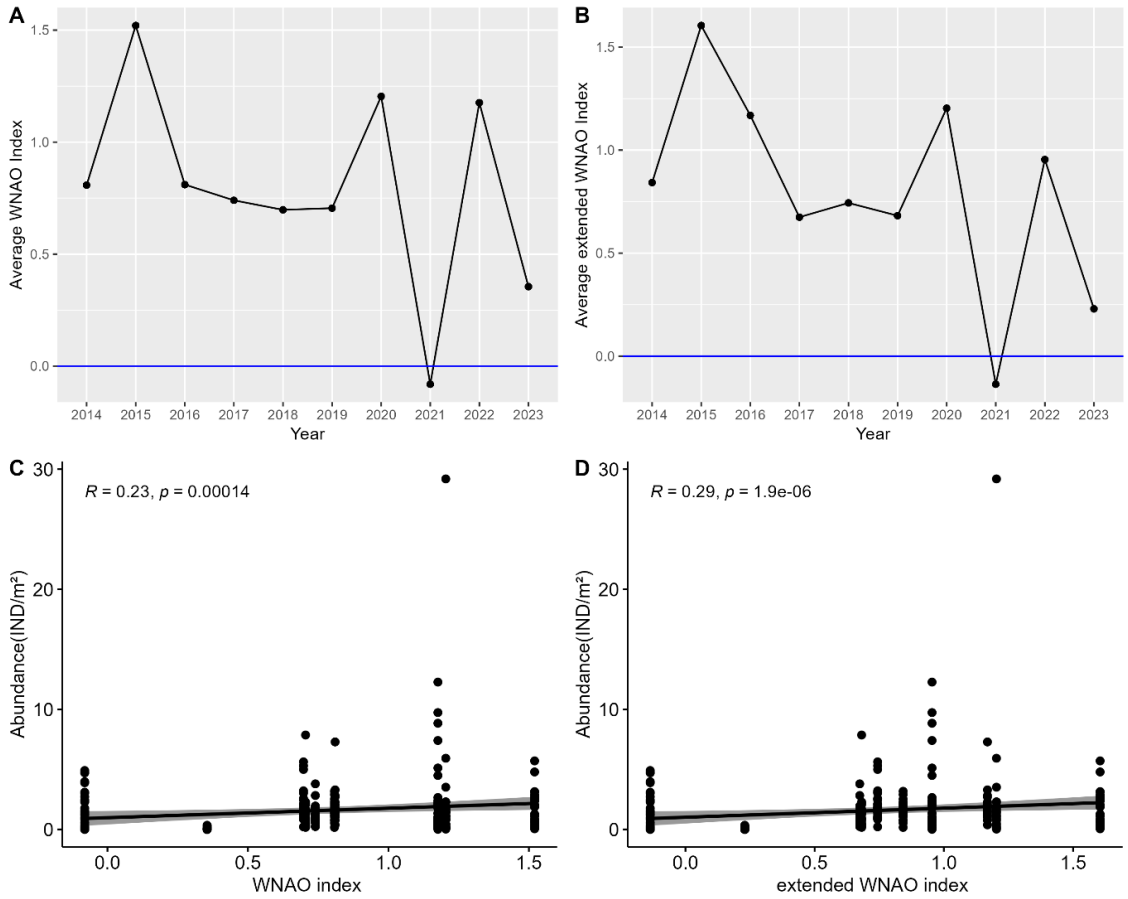

Figure 9-9 *[A] Trend of the average winter (January-March) NAO index (WNAO) over the studied period (2014-2023). [B] Trend of the average extended winter (December-March) NAO index (WNAOex) over the studied period (2014-2023). Graph [C] and [D] illustrate the relation of the WNAO and WNAOex respectively with the C. crangon abundance (#IND m^{-2}) in September. Both scatterplots show a positive correlation, with Spearman Rho- and p-values shown in the graphs. Shaded areas indicate the 95% confidence interval.*

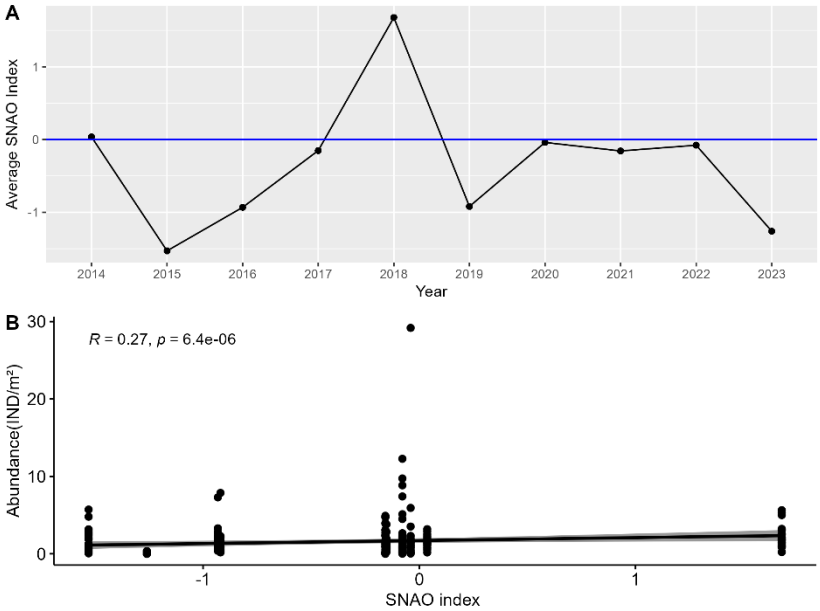

Figure 9-10 *[A] Annual trend of the summer NAO index (SNAO) in the studied period of 2014-2023. A peak is observed in 2018, and the lowest value in 2015. [B] Relation between the C. crangon abundance in September (#IND m^{-2}) and the SNAO. A positive correlation is observed, with a Spearman Rho value of 0.27 and a p-value < 0.01. Shaded areas represent the 95% confidence interval.*

9.5 Anthropogenic influences: fishery

In addition to abiotic and biotic influences, shrimp abundances can also be affected by anthropogenic influences such as fishing activities. As seen in literature (§4.8; (Verlé et al., 2023)), the Belgian part of the North Sea functions as an important fishing ground for *C. crangon,* making it essential to consider anthropogenic influences. Consequently, a negative correlation was observed between the abundance of *C. crangon* in September and the annual landed amount of shrimp in the BPNS in the previous year, with a Spearman Rho of -0.41 ($p < 0.01$) (**Figure 9-11**).

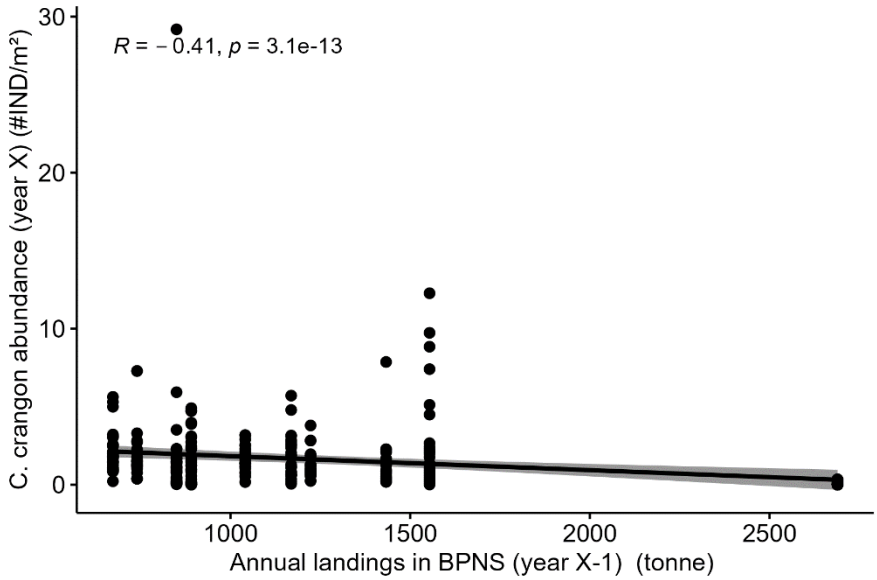

Figure 9-11 *Correlation between the C. crangon abundance (#IND m^{-2})(y-axis) and the annual landing of shrimp in the BPNS in the previous year (tonne) (x-axis). The Spearman Rho value (SRV) and the p-value are shown in the plot, shaded areas represent the 95% confidence interval.*

10 MODELS ON SHRIMP DENSITIES

To investigate non-linear correlations, several Generalized Additive Models (GAMs) were constructed. In model 1, the variables depth (m), the average summer water temperature (6-month scale) (°C), the present chlorophyll *a* concentration (µg L^{-1}), nitrate concentration (µmol N-NO_3 L^{-1}), juvenile Whiting abundance (#IND m^{-2}), *C. crangon* landings in the previous year (tonne) and the average spring Calanoid density (#IND m^{-3}) explained 41.6% of the deviance (**Figure 10-1**). Parameters with a significant contribution were depth ($p < 0.05$), the 6-month average water temperature ($p < 0.05$) and the landed shrimp in the previous year($p < 0.01$).

Model 2 compromises the depth (m), the average summer water temperature (3-month scale) (°C), the present chlorophyll *a* concentration (µg L^{-1}), present phosphate concentration (µmol P-PO_4 L^{-1}), juvenile Whiting abundance (#IND m^{-2}), *C. crangon* landings in the previous year (tonne), extended winter NAO index (December-March) and the average spring Calanoid density (#IND m^{-3}) as explanatory variables, and explains 42.2% of the deviance (**Figure 10-2**). Significant influences were observed for depth, *C. crangon* landing in the previous year and the winter NAO index, all with p-values < 0.01.

Model 3 compromises the present phosphate concentration (µmol P-PO4 L^{-1}), average spring (March-June) Calanoid density (#IND m^{-3}), water temperature in September, the extended winter (December – March) NAO index (WNAOex) and the average spring(March-June) chlorophyll *a* concentration (µg L^{-1}) and explains 26.7% of the deviance. Significant

influences were the measured water temperature ($p < 0.01$) and the mean chlorophyll *a* concentration in spring ($p < 0.01$).
(**Figure 10-3**). A summary is provided in **Table 10-1**. Diagnostic plots for the constructed models were provided in the appendices (**Figure C- 7**, **Figure C- 8**, **Figure C- 9**, respectively)

Table 10-1 *Summary of the selected GAMs. The parameters that were chosen to explain the log10-transformed abundance of C. crangon are shown in the "Model" column. Smooth terms with a significance < 0.05 are highlighted in bold. Scores according to the AIC are represented in the last column. Parameter are: depth (m), Average six-month summer temperature (Summer.6M; °C), chlorophyll-a concentration in September (chl A; µg L^{-1}), Nitrate concentration (Nitrate; µmol N-NO_3 L^{-1}), juvenile whiting abundance (juvWhiting, #Individuals m^{-2}), annual commercial landings in the preceding year (CatchPrevYear; tonne), average calanoid densities during spring (Calanoid_spring; #Individuals m^{-3}), Phosphate concentration (Phosphate; µmol P-PO_4 L^{-1}), Average three-month summer temperature (Summer.3M; °C), the extended winter NAO index (WNAOex; -), the average chlorophyll-a concentration during spring(chl A_spring; µmol L^{-1}) and the present water temperature (temp.LW; °C).*

Model ID	Model visualisation	Model	Deviance explained (%)	AIC	Diagnostics plot
1	**Figure 10-1**	**Depth** + **Summer.6M** + chl A+ Nitrate + juvWhiting + **CatchPrevYear** + Calanoid_spring	41.6	-86.502	**Figure C- 7**
2	**Figure 10-2**	**Depth** + Summer.3M + chl A + Phosphate + juvWhiting + **CatchPrevYear** + **WNAOex** + Calanoid_spring	42.2	-88.040	**Figure C- 8**
3	**Figure 10-3**	Phosphate + Calanoid_spring + **temp.LW** + WNAOex + **chl A_spring**	26.7	-20.259	**Figure C- 9**

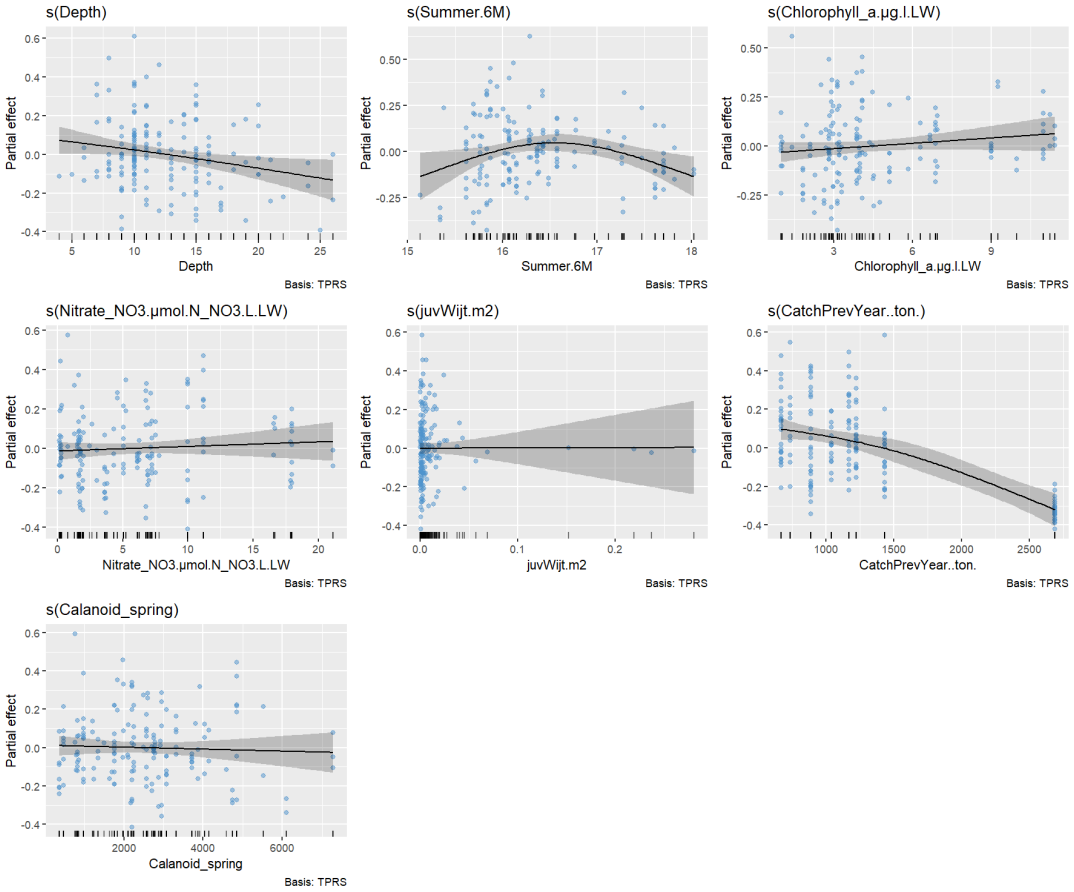

Figure 10-1 *Generalized Additive Model (GAM) plots showing the partial effects of the selected explanatory variables to the log10-transformed abundance of C. crangon in September in the BPNS. Variables are – from left to right- depth (m), the average summer water temperature (6-month scale) (°C), the present chlorophyll a concentration (µg L^{-1}), nitrate concentration (µmol N-NO_3 L^{-1}), juvenile Whiting abundance (#IND m^{-2}), C. crangon landings in the previous year (tonne) and the average spring Calanoid density (#IND m^{-3}). Ticks on the x-axis represent the observed datapoints. The y-axis represents the partial effect of the selected variable. Shaded areas represent the 95% confidence interval.*

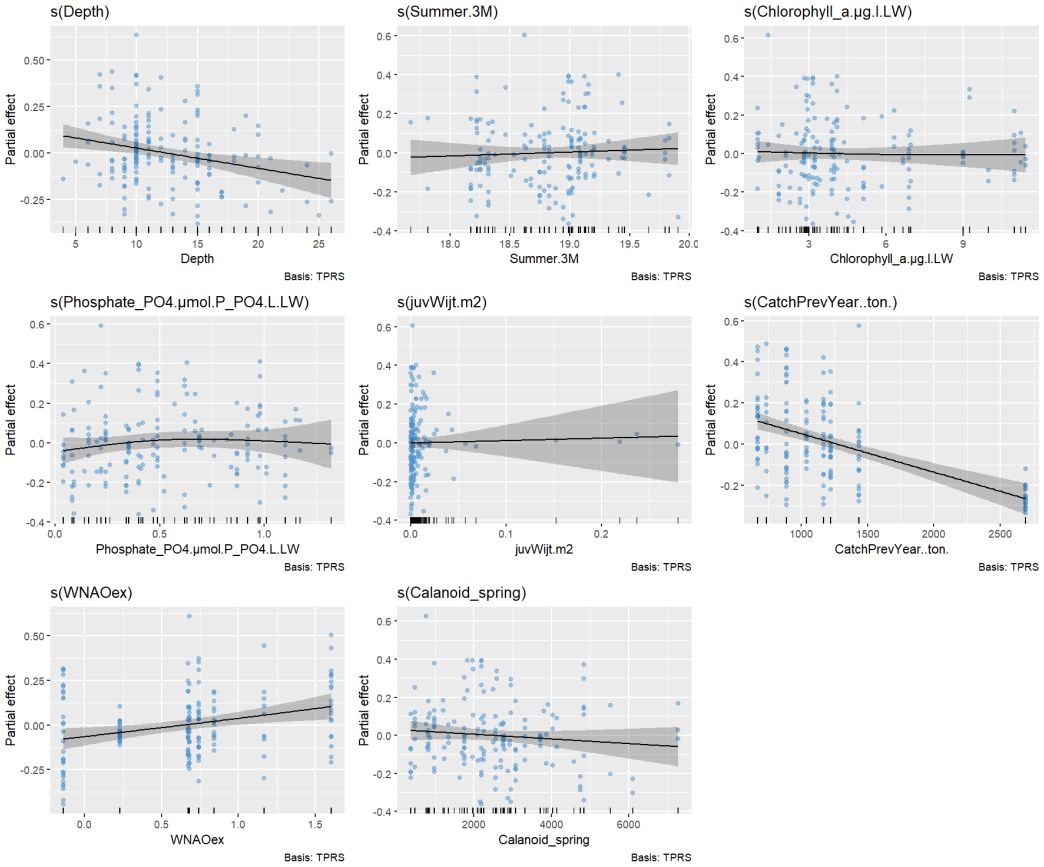

Figure 10-2 *Generalized Additive Model (GAM) plots showing the partial effects of the selected explanatory variables to the log10-transformed abundance of C. crangon in September in the BPNS. Variables are – from left to right- depth (m), the average summer water temperature (3-month scale) (°C), the present chlorophyll a concentration (µg L^{-1}), present phosphate concentration (µmol $P\text{-}PO_4$ L^{-1}), juvenile Whiting abundance (#IND m^{-2}), C. crangon landings in the previous year (tonne), extended winter NAO index (December-March) and the average spring Calanoid density (#IND m^{-3}). Ticks on the x-axis represent the observed datapoints. The y-axis represents the partial effect of the selected variable. Shaded areas represent the 95% confidence interval.*

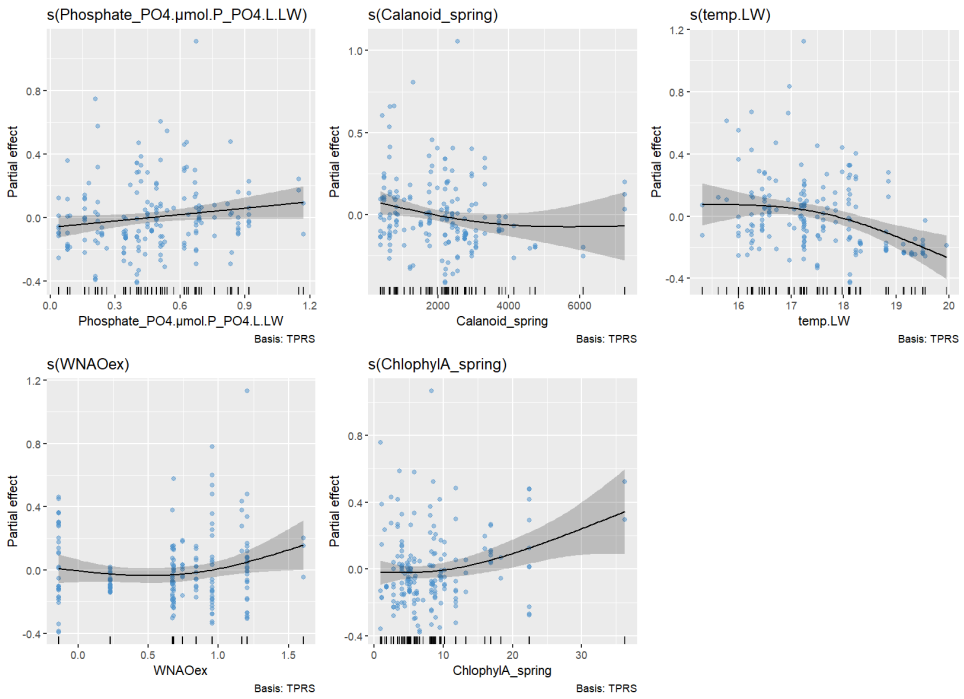

Figure 10-3 Generalized Additive Model (GAM) plots showing the partial effects of the selected explanatory variables to the log10-transformed abundance of C. crangon in September the BPNS. Variables are – from left to right- the present phosphate concentration (µmol P-PO4 L^{-1}), average spring (March-June) Calanoid density (#IND m^{-3}), water temperature in September, the extended winter (December – March) NAO index (WNAOex) and the average spring(March-June) chlorophyll a concentration (µg L-1). Ticks on the x-axis represent the observed datapoints. The y-axis represents the partial effect of the selected variable. Shaded areas represent the 95% confidence interval.

11 NUTRITIONAL CONTENT

Protein and lipid contents of 35 shrimp sampled in September 2023 and six shrimp sampled in November 2023 were determined and visualized based on their east-west and near-offshore location (**Figure 11-1**), and time of sampling (**Figure 11-2**). The average protein and lipid concentrations according to the region and season of sampling are summarised in **Table 11-1**. Individual results and the used regression curves are summarised in **Table C- 2** and **Table C- 3**, respectively.

Statistical analysis is performed using a non-parametric Kruskal-Wallis test, potentially followed by a post hoc Dunn-test in order to identify specific, significant differences. Differences are considered statistically significant if the adjusted p-value (Benjamini-Hochberg (BH) method) is smaller than 0.05.

11.1 Protein content

11.1.1 Spatial differences

A Kruskal-Wallis test indicated that there is a significant difference in protein content according a near-offshore gradient, where near shore areas exhibited a significant higher protein content than offshore areas ($\chi^2(2) = 7.451$, $p < 0.05$) (**Figure 11-1-A**). Regarding the east-west gradient, a significant difference was found between the west and central part of the BPNS, where the central regions showed a significant higher protein content than the west part ($\chi^2(2) = 12.126$, $p < 0.01$) (**Figure 11-1-B**). Other regions did not show any significant differences.

11.1.2 Seasonal differences

A significant difference in protein content was found between shrimp caught in autumn (September) and winter (November), with higher protein levels in autumn (Kruskal-Wallis, $\chi^2(1) = 6.533$, $p < 0.01$) (**Figure 11-2-A**).

11.2 Lipid content

11.2.1 Spatial differences

According to a Kruskal-Wallis test, there is a significant difference in lipid content over a near-offshore gradient, with a significant higher lipid content in nearshore waters compared to mid- and offshore waters ($\chi^2(2) = 14.535$, $p < 0.01$). No significant were found across an east-west gradient ($p > 0.05$)(**Figure 11-1-C, Figure 11-1-D**).).

11.2.2 Seasonal differences

A Kruskal-Wallis test showed a significant difference in lipid content between the shrimp sampled in autumn and winter, with higher lipid contents in winter compared to autumn ($\chi^2(1) = 7.1802$, $p < 0.01$) (**Figure 11-2-B**).

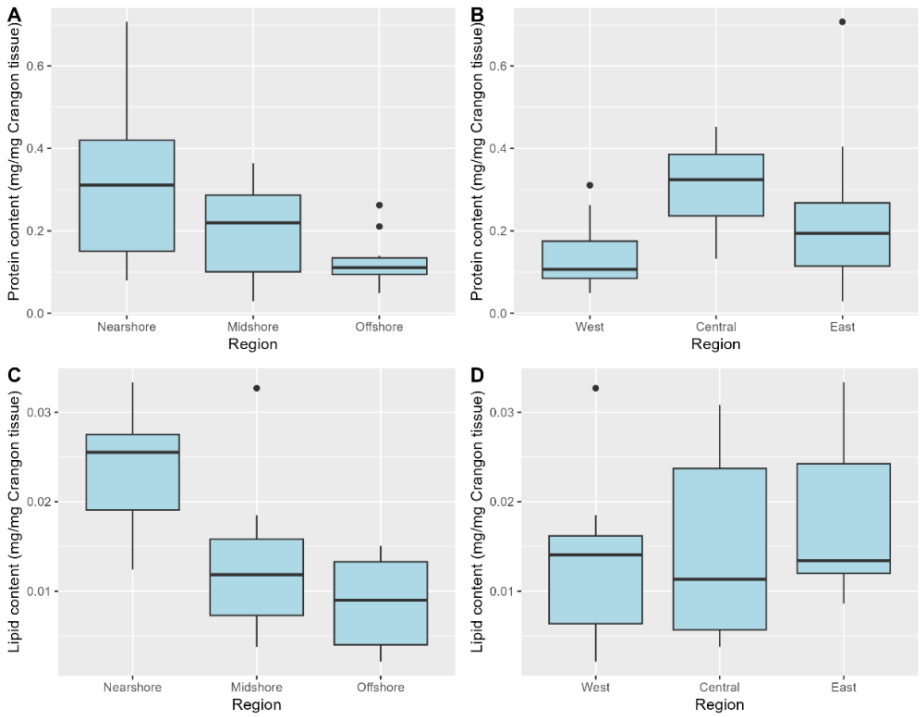

Figure 11-1 *Boxplots showing the variation in [A;B] protein and [C;D] lipid content of C. crangon in different areas of the BPNS. Graph A and C show the variation by a near-offshore gradient, while graph B and D show the variation from the west to east part of the BPNS. Samples were taken during the 2023-DYFS campaign in September. Protein and lipid content is expressed as (mg protein/mg C. crangon tissue) and (mg lipid/mg C. crangon tissue), respectively.*

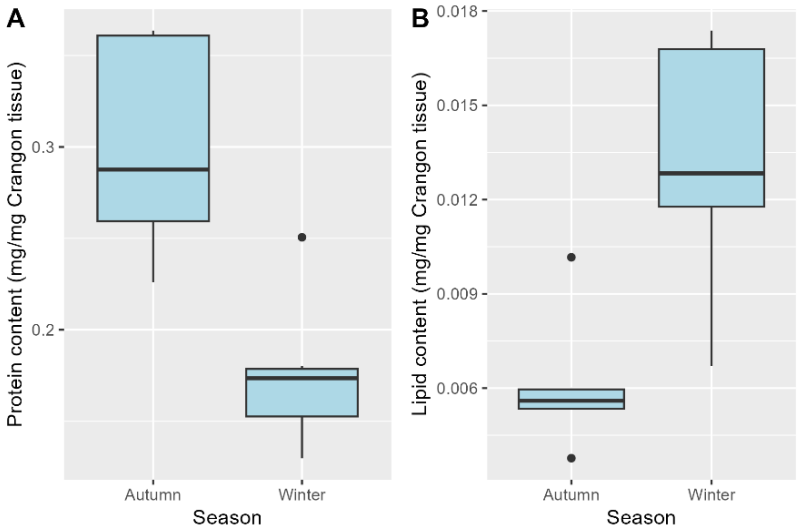

Figure 11-2 Seasonal [A] protein and [B] lipid content of sampled C. crangon. Samples were taken in autumn (September) and winter (November).

Table 11-1 Average protein and lipid content according to the region or season of sampling. The average nearshore concentration is for example the average protein content of all shrimp sampled in stations located in the nearshore area.

	Protein content (mg/mg shrimp)	Lipid content (mg/mg shrimp)
Spatial		
Nearshore	0.316	0.0232
Midshore	0.207	0.0126
Offshore	0.125	0.0088
West	0.136	0.0126
Central	0.313	0.0145
East	0.235	0.0176
Seasonal		
Autumn	0.300	0.0061
Winter	0.176	0.0134

DISCUSSION

12 SPATIOTEMPORAL TRENDS OF *C. CRANGON*

A Kruskal-Wallis test revealed a significant difference in relative abundance over the stations as throughout the year. However, after performing the post hoc Dunn test, no year showed a significant difference in relative abundance. This contradicts the initial expectation, where higher abundances were anticipated for 2018 and 2022 due to the recorded increased annual landings during those years (**Figure 4-11**). Nonetheless, the combination of these tests suggests that the year of sampling does influence the relative abundance of *C. crangon*. However, the available data is insufficient to determine the precise nature of this influence. In order to give a more conclusive result, more datapoints on different timestamps within the same year should be taken, as well as more years should be included.

Additionally, the GAMs reveal a significantly negative correlation between the *C. crangon* abundance and present depth. This seems a logical correlation since, during this time of the year, shrimp are generally located in shallow, nearshore waters (Campos & Van Der Veer, 2008). This correlation is however time depend. In other months, such as December or January, this correlation may be reversed as shrimp migrate to deeper waters (Campos & Van Der Veer, 2008). This underscores the fact that correlations between environmental variables and shrimp abundances are time-dependent, and that every variable should be considered within its specific temporal context.

13 (A)BIOTIC INFLUENCES ON *C. CRANGON* RECRUITMENT

13.1 Increased water temperatures

13.1.1 General trends

In the BPNS, the highest mean and max water temperatures were recorded in July and August 2018 and 2022 (**Figure 9-2**). Other studies, such as Semmouri et al. (2023) found similar results, and also reported that, during the latter years, the most intense heatwaves in the BPNS were recorded. These heatwaves caused a relative short, but very intense heating of the water temperature. In 2022 for example, the water temperature increased in eight days from 19.42°C to 21.05°C, which is an increase of 8.4% (Semmouri et al., 2023). This illustrates the degree of intensity of the heatwaves during these years. Contrary to the short and intense increase during the marine heatwave event, water temperatures stayed elevated for a prolonged time during the following months. After the 2022 MHW for instance, temperatures still remained around 15°C in November, which is ±2°C higher than the average temperature for November during the studied period (2014-2023).

Another remarkable trend is the water temperature of 2023. Despite the fact that in this year, no "official" marine heatwave was recorded during July and August in the BPNS, water temperatures were similar to the years in which MHWs were present (2018, 2022) (**Figure 9-2**) (Koninklijk Meteorologisch Instituut van België (KMI), 2023). This is likely the result of general elevated water temperatures in the entire North Atlantic region, as illustrated in **Figure D- 1** and **Figure D- 2**. During the beginning of 2023, scientist already expected elevated water temperatures during the second half of the year as a result of the El Niño phenomenon (Flanders Marine Institute (VLIZ), 2023). However, elevated temperatures in the northern Atlantic region were already visible from May and continued to June. So even before the official start of El Niño on the 4th of July 2023, temperatures were already anomalously high (Copernicus, 2023). The major contributor to this anomaly is a strongly weakened high pressure area around the Azores, which is part of the North Atlantic Oscillation (NAO). This resulted in a strongly negative NAO-index, which was also observed in this study (see §2.2.1 and

§13.3.3) (**Figure 9-10**). As a result of this negative NAO index, wind activity over the northeastern Atlantic region was strongly diminished, leading to a reduced mixing of the ocean. Warm sea surface water could therefore not be mixed with deeper, colder waters, hence the strong anomalies (Copernicus, 2023).

As described in §1.2.2, marine heatwaves are not only caused by anomalous air-sea heat fluxes, but also through horizontal advection, caused by anomalously temperature gradients, such as described above. In July and August 2023, there was no recording of a (terrestrial) heatwave in the BPNS, but, due to the observed elevated water temperatures and the anomalously high water temperatures in the northeastern Atlantic, the authors believe that a marine heatwave was present in the BPNS in the summer of 2023. However, this heatwave was not primarily caused by an anomalously air-sea heat flux, such as the previous ones (e.g. 2022), but due to horizontal advection. In September 2023 however, a terrestrial heatwave was recorded, which possibly contributed to the already elevated water temperatures (Vlaamse Milieu Maatschappij (VMM), 2023). Normally, water temperature shows a decrease after August; however, in 2023, an increase in temperature was observed, with temperatures up to 21.56°C. In comparison, the maximum temperature recorded in August 2023 was ±20°C. This anomaly could be attributed to the recorded terrestrial heatwave that was present during that month.

Because of the anomalously high temperatures in June and the heatwave in September 2023, water temperatures in 2023 stayed relatively high during autumn. This matches the pattern which is displayed by the years during which intense heatwaves occurred (**Figure 9-2**).

In general, no direct correlation was found between the *Crangon crangon* abundance and the water temperature. However, as shown in **Figure 10-3**, the water temperature has a significant (negative) contribution in explaining the variance of the GAM (**Table 10-1**). Specifically for temperatures exceeding ±17°C, there appears to be a negative correlation between the *C. crangon* abundance and water temperature. Given that the thermal limits of shrimp are estimated at ±30°C, this decrease in abundance can't be attributed to thermal stress (Campos & Van Der Veer, 2008). A possible explanation may lie in the deoxygenation of coastal waters, which is reinforced by increasing water temperatures and could, therefore, occur more frequently at higher temperatures (Keeling et al., 2010). The possible link with deoxygenation is further discussed in §13.1.4.

13.1.2 Influences of marine heatwaves on *C. crangon* abundance

13.1.2.1 Seasonal migrations and maturation rate

During the observed period of 2014-2023, two years -2018 and 2022- had a significant amount of days above 20°C (**Table C- 1**). These years are noted in literature as the years during which the most intense MHWs in the BPNS occurred (Mortelmans et al., 2024; Semmouri et al., 2023). However, when examining the water temperatures during the spring months, such as March or April, it is remarkable that these temperatures are located around, or sometimes even below the average (**Figure 9-2-B**). Conversely, in autumn, the monthly mean temperatures remained relatively high, as described in the previous section. Based on these two observations, MHWs can be described as a very sudden but intense events during which the sea warms in a relative short time period, followed by a prolonged period of elevated water temperatures as the water gradually cools down. This prolonged cooling period accounts for the observed higher-than-normal water temperatures in autumn.

The elevated nearshore water temperatures in autumn, induced by MHW events, likely cause *C. crangon* to reside longer than usual in these waters, delaying the seasonal migration to more offshore waters that usually takes place around this time. As a result, *C. crangon* will be longer available to be fished (see also §13.5).

Given that the development- and growth rates of larval, juvenile and adult shrimp depend on water temperature (Campos & Van Der Veer, 2008), it is likely that they are influenced by the MHW events. According to Boddeke (1976, 1982), the summer brood was the main contributor to autumn stock due to a high maturation rate of larval and juvenile shrimp during warmer periods. The elevated water temperature may potentially accelerate the maturation rate of larval and juvenile shrimp and the growth rate of adult shrimp, resulting in a higher amount of commercial-sized *C. crangon* compared to "normal" years. However, no significant correlations were found to prove this hypothesis. The authors however believe that is due to a lack of data, rather than that there are effectively no correlations. Further research, which includes an intense sampling of *C.crangon* during summer months, is needed to test these hypotheses (see also §15.1).

13.1.2.2 Food availability: phytoplankton abundance

Phytoplankton abundance, quantified by the chlorophyll *a* and beta carotene concentrations, shows both in September (**Figure 9-6-A**, **Figure 9-6-B**) and in spring (**Figure 9-6-D, Figure 9-6-E**) a significant positive correlation with the *C. crangon* abundance. However, the higher Spearman Rho values suggest that the influence of the average spring concentrations is more substantial than the September concentrations. Phytoplankton is namely considered to be the main food source of larval *C. crangon*, the life stage of shrimp just after hatching. These larval shrimp develop during the two or five months after the hatching of the egg, which mostly occurs during winter. Food availability in spring, particularly the presence of phytoplankton, is therefore crucial for the development and/or the mortality rate of larval shrimp, and consequently also the present stock in autumn (Campos et al., 2010; Hünerlage et al., 2019; Tulp et al., 2012).

Similar observations already exist in literature, but there is uncertainty if food availability influences the mortality rate or just the growth rate. Hufnagl et al. (2010) concluded for example that food limitations had predominantly an influence on the growth rate of larval shrimp rather than on the mortality. This could mean that, when food is limited, the same number of individuals develop, but that less reach the commercial sizes, resulting in less landings.
To illustrate the importance of food availability in spring, a GAM was constructed with the average chlorophyll *a* concentration as one of the explaining parameters (**Figure 10-3**). In this GAM, a positive trend is observed between the log10-transformed *C. crangon* abundance and the chlorophyll *a* concentration, confirming the above discussed correlation. Furthermore, in this model, the average spring chlorophyll *a* concentration has a significant contribution in explaining the variance ($p < 0.05$) (**Table 10-1**).

Both these findings highlight the importance of food availability in the recruitment process of *C. crangon* and underscore the importance to consider this parameter if one wants to explain variations in the autumn stock. However, the average spring phytoplankton abundance itself is influenced by several parameters, such as the presence of zooplankton.

13.1.2.3 Food availability: zooplankton

The most dominant zooplankton group in the BPNS, the copepods, play an important role as grazers on phytoplankton (Campos & Van Der Veer, 2008; Semmouri, 2022). High copepod densities in spring are negatively correlated with *C. crangon* abundances in September, illustrating that zooplankton acts as an important competitor of the larval shrimp during their development in spring (**Figure 9-7**). The higher the zooplankton abundance, the stronger the competition between zooplankton and larval shrimp and consequently leading to a reduced food availability. Given the previously discussed positive correlation between food availability and the autumn *C. crangon* stock, high zooplankton abundance in spring may potentially inflict a decrease in the *C. crangon* autumn stock. Fluctuations in copepod abundance, induced by for example MHWs, could thus have indirect effects on the shrimp stock.

Besides water temperature, MHWs also have a significant impact on zooplankton abundances. Semmouri et al. (2023) reported a sharp decline in copepod abundance in 2018 and 2022, induced by severe MHW events which were present that year. In addition, a strong increase in *Bellerochea*, a diatom genus present in the BPNS, was noticed in the same time

frame as the decline of the copepod community (Mortelmans et al., 2024). This combination of both a decrease of zooplankton and an increase of phytoplankton in late summer/early autumn, complemented with elevated water temperatures, could stimulate the growth rate of present larval and /or juvenile shrimp, resulting in increased number of *C. crangon* individuals that reach commercial sizes in autumn.

Additionally, Semmouri et al. (2023) reported that zooplankton communities recovered relatively fast and that normal levels were reached again in October 2018 and November 2022, respectively. Larval shrimp hatched during the following winter would thus not experience a decreased copepod community and thus not an increase in food availability. In other words, the indirect effect of a decrease in copepods abundances on shrimp abundances, induced by MHWs, would only be visible during summer and/or autumn and not in the following winter or spring. In this dissertation, the influence of zooplankton abundances could only be studied to a limited extent due to a constrained data series. In order to fully understand the correlation between zooplankton abundance and *C. crangon* abundance, more comprehensive data series are needed that include several datapoints spread over the year. In this way, the influence of the zooplankton can be directly correlated with the different life stages of *C. crangon*. Future research should therefore focus on more intense sampling efforts in order to expand existing data series.

13.1.3 Average winter temperatures

Water temperature plays a crucial role in the development of *C. crangon* eggs, larval and juvenile stages, not only during summer but also throughout winter. In this dissertation, a direct negative correlation between the 6-month average winter temperature and *C. crangon* was observed, meaning that the autumn stock decreases with increasing average winter temperatures (**Figure 9-7-B**). During a more severe winter (i.e. colder water temperatures), egg- and larval development will slow down, resulting in a delayed peak spawning. Consequently, larvae and juveniles will only reach commercial sizes in autumn, contributing to the autumn stock. Additionally, if water temperatures are too cold, adult shrimp tend to migrate to even deeper and warmer waters, which prolongs the time for adults to return to more shallow waters (Hünerlage et al., 2019). In contrast, during milder winters with relatively high water temperatures, hatching and development will be accelerated, resulting in a higher amount of commercial-sized shrimp in the spring stock and less in the autumn stock (Hünerlage et al., 2019). Additionally, if winter temperatures are too high, maturation rates will consequently increase, leading to a potential mismatch between the larval bloom and the spring phytoplankton bloom (Hünerlage et al., 2019).
(Retired) fisherman also confirmed this patten, claiming that severe winters equal high shrimp landings in autumn (Vertongen, 2024).

13.1.4 Average summer temperatures

Contrary to the 6-month average winter temperatures, no linear correlation was found between the *C. crangon* abundance in September and the 6-month summer average temperature. However, as illustrated by **Figure 10-1** and **Table 10-1**, the parameter has a significant contribution in explaining the variance of the log10-transformed *C. crangon* abundance. The shape of the curve has a similar trend compared to the one of the water temperatures in **Figure 10-3**, and indicates that there is an optimal temperature average which leads to the highest shrimp stock. The shape of this curve is however rather surprising because for average summer temperatures higher than ± 16.5°C, the abundance seems to decrease. This does not correspond to the upper thermal limit, which is estimated at ± 30°C (see also §13.1.1) (Campos & Van Der Veer, 2008). Further, one would expect that the elevated temperatures would accelerate growth and development rates, which would result in an increased stock in autumn.

In literature, no studies were found that also described this trend, and therefore, it is hard to find a correct explanation. A possible suggestion is that these increased summer averages are related to an increased deoxygenation of the BPNS. As described by Keeling et al. (2010), deoxygenation is temperature related, meaning that increased water temperatures

enhance the presence of anoxic zones in the sea, particularly in more deeper areas. *C. crangon,* who lives during (late) spring and summer on the seafloor, could be directly affected by these anoxic zones. However, further research will be needed to investigate this deoxygenation potential.

On a 3-monht scale, no significant correlations are found, neither via a scatterplot or a GAM. This could indicate that the mean temperatures of July-September do not significantly impact the abundance of *C. crangon* in September, and that higher (or lower) temperatures in other months such as March or April have a more significant influence. These months coincide with the phytoplankton bloom, which potentially underscores the importance of food availability during the recruitment process.

The influence of water temperature in summer is, contrary to winter water temperature, poorly described in literature, which make it hard to draw any hard conclusions.

13.2 Nutrient abundance and salinity levels

Another direct effect on phytoplankton abundance is nutrient availability, particularly through the run-off of rivers into the sea. High nutrient availabilities have a positive effect on the presence of phytoplankton abundances, such as *Bellerochea*. Mortelmans et al. (2024) reported a gradient in abundance of this phytoplankton species across the BPNS, with highest concentrations observed near the Scheldt estuary, which is an eutrophicated system. Additionally, Siegel et al. (2005) reported a significant positive correlation between the run-off of the Elbe River in the German Bight of the North Sea and the autumn shrimp stock the following year. This suggests that nutrient run-off of, for example, the Scheldt Rivier into the BPNS could potentially enhance phytoplankton abundances and, indirectly, *Crangon* abundances. During an interview, some (retired) fisherman endorsed this hypothesis, claiming that influxes of for examples human faeces into the sea had a positive effect on the shrimp abundances (Vertongen, 2024).

The run-off of nutrients towards the BPNS may thus directly boost phytoplankton abundances and indirectly *Crangon* abundances. However, despite the relations described in literature, the direct correlation plots (**Figure 9-5**) and constructed GAMs (**Figure 10-1**, **Figure 10-2**, **Figure 10-3**) did not exhibit any significant correlations, except for phosphate concentrations (**Figure 9-5-D**). The lack of correlations could be attributed to the fact that in these correlation plot, nutrient concentrations from September were used. In this period, the *Crangon* stock predominantly exists out of juveniles and adults, which primarily feed on juvenile fish as main food resource (Campos & Van Der Veer, 2008). Therefore, shrimp show no correlation with nutrients, since these are associated with phytoplankton abundance.

In addition, a distinct affinity of *C. crangon* for lower salinity areas was observed, as illustrated by the negative correlation in **Figure 9-4**. This aligns with the findings of Campos et al. (2010), who also reported a similar negative correlation between salinity levels and shrimp populations during summer. In the BPNS, these lower-salinity areas are predominantly found near the Scheldt estuary, where the influx of freshwater from the Scheldt River reduces the salinity levels.

Additionally to the latter negative correlation, **Figure 9-4** also reveals a clear geographical pattern of shrimp abundance relative to longitude. Specifically, areas with higher salinity levels are located at lower longitudes and thus further away from the Scheldt estuary, which is located in the most eastern part of the BPNS. This pattern suggest that shrimp abundances will increase closer to the Scheldt estuary, as water will become less saline.
The study of Tulp et al. (2012) supports this observation, noting a difference in salinity level between the Eastern and Western Dutch Wadden Sea, driven by the freshwater inflow from the IJsselmeer. A similar salinity gradient is likely present in the BPNS, with higher salinity levels in the west and lower in the east.

Despite the observed negative correlation, the salinity preferences of *C. crangon* depend on additional factors such as the present life stage and the water temperature (see §4.5) (Campos & Van Der Veer, 2008; Tulp et al., 2012). For instance, larval shrimp may favour different environmental conditions than adult shrimp. Generally, *C. crangon* prefers low salinity levels when water temperatures are higher, and vice versa (Campos & Van Der Veer, 2008). In September, nearshore waters are relatively warm, hence the observed negative correlation towards salinity. However, this correlation will probably be reversed during winter months when nearshore waters are relatively cold, and shrimp prefer the more saline offshore waters.

13.3 Relation to the North Atlantic Oscillation

13.3.1 General trends

Generally, the NAO index follows a fixed trend. However, for the year 2018, this trend is completely broken and even reversed (**Figure 9-8**). It is the only year with a positive NAO index for all seasons. In 2022, the NAO index reached negative values for spring, summer and autumn, but no large variations are witnessed between these seasons, which can be seen in other years. The NAO index of 2015 for example ranges from strong positive values to strong negative values in summer. The two mentioned years -2018 & 2022- are, coincidentally, the two years with the most intense heatwave events. Especially the pattern in 2018 is very remarkable. According to literature, the effects of the NAO are however most prominent during winter, and thus is the significance of this unusual trend is uncertain (Stenseth et al., 2003).

13.3.2 Winter NAO index

A positive NAO index is associated with an influx of Atlantic winds in the North Sea, resulting in warmer and wetter winters than usual (Wanner et al., 2001). But, as discussed in §2.3.3, a warm winter is associated with a decreased autumn stock. It is thus expected that in case of a positive NAO, a decrease in autumn stock would be noted. However, the opposite correlation is observed. In this dissertation, a positive correlation between the *C. crangon* abundance in September and the winter NAO (January-March) and the extended winter NAO index (December-March) is noted (**Figure 9-9**, **Figure 10-3**).

Both Siegel et al. (2005) and Henderson et al. (2006) reported a negative correlation between the *C. crangon* recruitment in respectively the German Wadden Sea and the Bristol Channel, and the winter NAO-index. However, Siegel et al. (2005) reported an 18-month lag of the effects of the fluctuation of the inter NAO index on the autumn abundance, which is hard to explain since most shrimp have a one-year lifespan. Additionally, Hünerlage et al. (2019) reported a negative correlation with the winter NAO index.

The observed positive correlation in **Figure 9-9** is therefore a rather surprising result and is contradicted to the above discussed hypothesis. A possible explanation can maybe be found in the other effects of the NAO. A positive NAO does not only bring warmer Atlantic winds, but also wetter ones, resulting in more wetter winters than usual. Campos et al. (2010) stated however that autumn recruitment was rather favoured by low precipitation in winter.
Another possible explanation for this unusual correlation is the increased storm activity related with a positive NAO index. These storms could cause turbulences in the seas, creating a good mixing of nutrients, which could maybe favour larval development. However, these are just suggestions, and further research needs to be conducted in order to clearly explain the relation between the winter NAO and the autumn recruitment in the BPNS.

13.3.3 Summer NAO index

Despite being most prominent in winter, the correlation between the average summer (July-September) NAO index is also studied (**Figure 9-10**). Just as the winter NAO index, the summer NAO index shows a positive correlation with the *C. crangon* abundance in September. Remarkable is that years with high annual landings, such as 2014, 2018 and 2022, have

a summer NAO index which is either positive or close to zero. Years with a low annual landing, such as 2019 or 2023, have a rather negative summer NAO index. This may indicate that under a rather positive or close -to-zero summer NAO index, more favourable environmental conditions are present (e.g. elevated water temperature).

In literature, the effect of the NAO in the BPNS is poorly described. It is unclear of the geographical region of the BPNS has a significant influence on the present effects of the NAO compared to other regions such as the German Wadden Sea. It is however clear that the NAO has a significant influence on the recruitment process of *C. crangon*, and that future research is needed in order to fully understand the underlying relations.

13.4 Juvenile whiting abundance

Based on **Figure C- 4**, three remarkable years can be identified regarding juvenile whiting abundance. In 2018 and especially 2023, whiting was very abundant in the BPNS. On the contrary, in 2022, the lowest amount was sampled during the observed period. An unambiguous explanation for these peaks and lows is hard to formulate since the mechanism behind fish recruitment and migrations is not (yet) well understood.

In this dissertation, a direct negative linear correlation was found between the juvenile whiting abundance and the *C. crangon* abundance (**Figure C- 5**). In the presented GAMs however, this parameter did not show a significant contribution in explaining the variance (**Figure 10-1**, **Figure 10-2**). Nevertheless, the observed negative correlation is also reported by several other studies. Temming & Hufnagl (2015) observed for instance a regime shift in the southern North Sea between 1960-2010. In the decades before the year 2000, a significant amount of whiting was present in the southern North Sea because the so-called "gadoid outburst" during 1960-1970. As a result, brown shrimp stocks were subjected to a high predation pressure (Welleman & Daan, 2001). However, after 2000, the population of whiting and other predators (e.g. cod) decreased due to intense fishing and climate change, promptly leading to an increase of 39% in commercial shrimp landings over a period of 10 years (Temming & Hufnagl, 2015). Hünerlage et al. (2019) presented a similar case study in which the autumn *C crangon* stock in the German Bight of the North Sea was heavily subjected to predation by juvenile whiting during summer 2016. During September of that year, very low numbers of juvenile and adult *C. crangon* were noted.
Additionally, Campos et al. (2010) reported the importance of predators by concluding that the predator abundance explained up to 85% of the variance of the *C. crangon* abundance in autumn. An important note is that (juvenile) whiting is not the only important predator of *Crangon.* Other fish species, such as herring or cod, or swimming crabs of the genus *Liocarcinus,* may also have a significant influence on *Crangon* abundances. This will however be further discussed in §15.1.3.

Nevertheless, it can be concluded that (juvenile) whiting abundance exerts a strong negative influence on *C. crangon* stocks. Additionally, whiting are adapted to withstand relative high water temperatures, especially compared to for example cod. This adaptation is however age-dependent, with older individuals being less resistant to relative high temperatures (Temming & Hufnagl, 2015). This could explain the high amount of juvenile- and low amount of adult whiting observed in the BPNS in September 2023 (*Author's observation*).

During 2022 and 2023, the above described correlations appeared to be valid in both years: low whiting abundances were accompanied by high *C. crangon* abundances (**Figure 4-11**, **Figure C- 4**). However, in 2018, a contradictory trend was observed, with both high *C. crangon* and juvenile whiting abundances present. It is possible that the shrimp stock was sufficiently large that the impact of whiting abundance was negligible, but no definitive explanation was identified in this dissertation.

13.5 Impacts of fishing activities

Additionally to the increased maturation rate, the increased water temperature during the summer months in 2018 and 2022 resulted also in an increased average autumn temperature (**Figure 9-2**). When warmed up, the BPNS cools down at a slow rate, resulting in relatively high mean water temperatures in October (2018: 16.82°C; 2022: 16.34°C) and November (2018: 12.72°C; 2022: 15°C) (Flanders Marine Institute (VLIZ), 2015). Around this time, *C. crangon* normally migrates back to deeper and more offshore water to flee from the colder, nearshore waters and to reproduce (see §4.7.1). However, when water temperatures are warmer than normal, such as in 2022, shrimp will remain longer in the shallower nearshore waters, making them longer available for (commercial) fishers. According to local sport fisherman, the fishing season in 2022 lasted until the 18th of December, with hauls up to 15-20 kg shrimp day^{-1}. In comparison, these fishermen usually haul 40-70 kg shrimp day^{-1} during the high season (September-October) with their small sportfishing vessel (Vertongen, 2024). This prolonged fishing season could be one explanation for the high annual landings in 2022 and 2018.

This prolonged fishing season could however have a negative impact on the shrimp stock of the subsequent years. A significant share of the caught shrimp during the prolonged season are adult females which carry eggs on their tails (Respondek et al., 2022), which was also observed by the interviewed sport fishermen (Vertongen, 2024). An increase in caught egg-carrying females could directly results in a decrease of present eggs during winter, which in their turn, could result in a reduced autumn stock the following year. This might explain the observed decline in annual landings in the years following those with MHWs, such as 2019 and 2023 .

However, in a long-term study, ranging from 1973 to 2003, Siegel et al. (2005) found that fishery activities only explained <5% of the variance of the present autumn stock, and that most of the variability was explained by (a)biotic parameters such as water temperature and predator abundance. In their study, they concluded that fisheries did not have any significant influence on the autumn stock. A similar trend was reported by Temming & Hufnagl (2015), who reported that no signs of overfishing in the Dutch Wadden Sea were present.

In contrast, this dissertation found a significant negative correlation between the present *C. crangon* stock in September and the annual landings of the previous year in the BPNS (**Figure 9-11**). This suggests that, contrary to previous studies, fishing activities may indeed have a significant impact. A more recent study of Respondek et al. (2022) which studied the impact of fishing activities on the shrimp stocks in the Dutch Wadden Sea and the German Bight, supports this observation. They reported that the landings during winter time explained up to 86% of the abundance variance during summer (July-August). Moreover, their linear model, which was based on the landings during the winter period, explained up to 70% of variance in the shrimp abundances in summer. This is 13% more than previous models from for example Siegel et al. (2005), which included the winter NAO, winter temperature of nutrient run-off (Respondek et al., 2022; Siegel et al., 2005). They concluded that a reduced spawning stock in winter, induced by fishing activities, had a significant negative influence on the *C. crangon* stock in summer (Respondek et al., 2022).

Based on these observations, the influence of fishing activities in the BPNS appears to be significant and is likely reinforced by the occurrence of MHWs. These events prolong the fishing season significantly (e.g. 2022), resulting in a higher amount of egg-bearing females being caught, ultimately leading to a reduced winter spawning stock. Without marine heatwaves, these impacts would likely be less severe because of the earlier migration of *C. crangon* to deeper waters. Further research will however be needed to fully comprehend the significance of the fishing activities, whether or not in combination with MHWs.

14 NUTRITIONAL CONTENT

14.1 Method validation

According to Mæhre et al. (2018), the protein determination based on the Bradford method is often influenced by interferences, potentially leading to an overestimation of the protein level in marine tissues. However, the results in this study, which were obtained from various extractions, did not show any significant differences with the reported value of ±0.20 mg (mg *Crangon* tissue)$^{-1}$ in literature (**Table 4-1**) (Turan et al., 2011). The discrepancies between extracting results and the average value reported in literature are generally smaller than the differences noted by Mæhre et al. (2018). Therefore, any observed anomalous values are more likely attributable to human errors rather than methodological issues.

The results of the lipid extractions generally align with the average value of ±0.01 mg (mg *Crangon* tissue)$^{-1}$ reported by Turan et al. (2011) (**Table 4-1**). Additionally, Iverson et al. (2001) found that the Bligh and Dyer method provided accurate result for low-lipid tissue (< 2% of total wet weight). However, for lipid contents exceeding a concentration of 2% of the wet weight, the Bligh and Dyer method systematically estimated a lower lipid content compared to, for example, the Folch-method. This underestimation increased significantly with the lipid content (Iverson et al., 2001). The majority of the results of this assessment however were estimated at a lipid concentration of ± 1% of the total (wet) weight of the shrimp. Nevertheless, some results exceeded the 2% mark, and therefore these should be interpreted with caution. However, given that the lipid content does not significantly deviate from 2%, any underestimation of these concentrations is likely negligible.

14.2 Spatiotemporal trends

14.2.1 Spatial differences

Generally, there is a decreasing gradient of protein and lipid content when individuals are more located offshore. Hereby, a significant higher protein content is observed in nearshore individuals compared to offshore shrimp (**Figure 11-1-A**). Protein content of individuals that were sampled in the midshore area showed a concentration that was close to the reported values in literature (Turan et al., 2011). The protein content of nearshore shrimp is higher than the content found in literature, while offshore shrimp show a lower protein level compared to literature (**Table 11-1**) (Turan et al., 2011). Regarding lipid contents, the same gradient can be observed. Significant higher lipid concentrations were found in shrimp close to the coast (nearshore), while more offshore individuals exhibited lower levels. This gradient is not (yet) described in literature and is very remarkable. After all, all samples had similar weights and lengths. However, since the small number of samples (n = 35), these results should be interpreted with caution.

Less pronounced patterns are visible over the east-west gradient. Only centrally located individuals showed a significant higher protein content than western located shrimp. No other significant differences were observed. This could indicate that a near-offshore gradient plays a more significant role in the nutritional content of shrimp compared to the east-west gradient.

This type of gradient has not yet been documented in the literature. However, as reported by Hufnagl et al. (2010) and Mika et al. (2014), food availability is a significant driver of protein and lipid levels in *C. crangon.* One possible explanation for the increased protein and lipid levels in nearshore shrimp could be the higher food availability in these regions. Shallow areas tend to experience higher eutrophication compared to more offshore areas, leading (in)directly to a higher food availability. Additionally, adult shrimp may also prey on newly settled juvenile shrimp in these regions. Pihl & Rosenberg (1982) observed that the diet of adult shrimp in Swedish shallow waters consisted for more than 20% out of

young shrimp. Since settlement of juveniles only occurs in shallow waters, this food source may not be available in more offshore regions (Campos & Van Der Veer, 2008).

14.2.2 Seasonal differences

A significantly higher protein content was found in *C. crangon* individuals sampled in autumn compared to those collected during winter. In contrast, the pattern for lipids is reversed, with shrimp sampled in winter exhibiting significantly higher lipid levels than those sampled in autumn.

Mika et al. (2014) observed a similar trend, noticing an increase in lipid contents after the summer season. After summer, lipid levels are low due to the past reproduction period (see §4.5), and therefore need to be replenished during autumn and early winter before *C. crangon* migrates back to deeper waters. During winter and in these deeper waters, a lack of food is present, requiring *C. crangon* to build up lipid reserves (Mika et al., 2014). Additionally, Ayas et al. (2013) also reported that lipid content in shrimp is mainly driven by food availability. In both studies, lipid content peaked in the spring, coinciding with the phytoplankton bloom and the resulting abundance of food. Food availability does seem to play an important role in the lipid content, as well as the present life stage of *C. crangon.*

Despite not noticing any seasonal patterns, Hufnagl et al. (2010) suggested that proteins are being used as main energy source when lipid levels are low. This could explain the reversed pattern that was observed during this assessment. In autumn, lipid levels are low due to the past reproduction period, and therefore, *C. crangon* may shift to proteins as energy source. During autumn, the lipid reserves are slowly restored, resulting in increased lipid levels and reduced protein levels.

Despite the limited sampled size (n = 5), this assessment gives a rough indication of the seasonal nutritional distribution of *C. crangon*. Some first and tentative trends are visible, but further research is necessary to investigate the observed trends and to form any comprehensive conclusions.

15 FUTURE RECOMMENDATIONS

15.1 Data Expansion

Because the results of this dissertation are primarily limited by the available date, several suggestions are made to expand the current available data series in order to have more comprehensive results.

15.1.1 Samples

The LifeWatch framework provided several datasets which compromised several abiotic and biotic parameters such as water temperature, pigment and nutrient concentrations and zooplankton densities. However, information about *C. crangon* abundances were lacking, and therefore, data series provided by ILVO were used. ILVO samples each year the *C. crangon* abundance at various stations in September. However, the recruitment process of *C. crangon* is subjected to several influences on different time stamps. Therefore, in order to get a more comprehensive image of the recruitment process and its influences, more samples throughout the year should be taken. In this way, influences such as food availability could be directly linked to the present larval, juvenile or adult abundance.

In addition, because ILVO and LifeWatch use different sampling protocols and stations, several assumptions needed to be made in order to couple both datasets. This resulted in data losses and limited results since the data series of ILVO

was only available for September. A more generalized sample protocol and locations could prevent these latter data losses.

15.1.2 Research area

In this dissertation, only the BPNS was part of the research area. The North Sea however does not know any boundaries, and therefore, the *C. crangon* abundance in the BPNS could be subjected to external influences, such as fish migrations. Due to its geographical location, effects on *C. crangon* abundances in other parts of the North Sea could affect the *Crangon* abundance in the BPNS in a different way. This was already shortly discussed in §13.3, where a different correlation was found for the winter NAO index compared to other part of the North Sea.

15.1.3 Predation

Because its remarkable presence in 2023, whiting was selected as a parameter to explain the *C. crangon* fluctuations. However, other species besides whiting, such as herring or flatfish, also need to be studied since they also potentially could influence the autumn stock in a significant way. Campos et al. (2010) observed for example a significant influence of Pleuronectiforms on the *Crangon* abundance in autumn. Therefore, in future studies, other predator species than whiting should also be considered.

15.1.4 Precipitation data

As discussed in §13.3, the NAO index does not only tell something about the water temperature, it gives also an indication of the precipitation. Since *C. crangon* abundances are significantly correlated to the NAO index -both in this dissertation as in literature-, the influence of precipitation on the recruitment process should also be investigated. Additionally, precipitation could also influence the salinity levels of the sea, and consequently also the development rates of eggs, larval and juvenile shrimp (Campos et al., 2010).

15.2 Acidification potential

The increasing anthropogenic carbon dioxide emissions result in a steady decrease of the oceans pH-level. From 1980 to 2010, the pH level of the oceans dropped with 0.02 pH unit every decade, and since the pre-industrial period, a decrease of 0.1 pH units is noticed (Kroeker et al., 2013). Although this difference looks irrelevant at first glance it still has a big impact on marine ecology. Together with the pH, a decline in concentration of carbonate ions (CO_3^{2-}) and an increase in hydrogen carbonate (HCO_3^-) is observed. Carbonate ions are crucial for so-called calcifiers, marine organisms that built shells or other skeletal structures out of calcium carbonate. As a calcifier, *C. crangon* is very sensitive to pH changes, and thus even small changes in pH could alter their natural behaviour (Delbare et al., 2015).

The CO_2-uptake and consequently the acidification will be higher when the temperature of the water is lower. Effects of acidification will thus increase when moving away from the equator (Hoegh-Guldberg et al., 2017). Acidification is already occurring in the northern part of the North Sea, and with no direct signs of a reduction in anthropogenic emissions, it is expected that acidification will start to occur in the BPNS in the near future (Hoegh-Guldberg et al., 2017). Just as MHWs, acidification will have a significant influence on future *C. crangon* stocks and therefore also crucial to understand.

15.3 Deoxygenation potential

As seen in §1.1, deoxygenation forms besides increasing water temperatures and acidification a third major threat to the seas and oceans.

In deeper waters, multiple factors contribute to the deoxygenation process. The most important one is the solubility of oxygen in water, which is negatively correlated with temperature. Consequently, if water temperature rises, less O_2 can be dissolved. Warmer water additionally shows an increased stratification pattern, resulting in a reduced "ventilation" of the sea. An increased stratification mitigates the mixing of oxygen-rich surface waters with oxygen-poor deeper waters, resulting in a reduced supply of oxygen to deeper waters (Keeling et al., 2010; Oschlies et al., 2018). Each year, adult shrimp migrate back towards deeper water to reproduce. Anoxic deeper waters could significantly impact the reproduction pattern of *C. crangon* and consequently the size of the autumn stock.

In more shallow, nearshore waters, oxygen depletion is caused by eutrophication by run-off of nutrients, originating from e.g. agriculture (Bijma et al., 2013).

15.4 Predictive modelling of *Crangon crangon* abundances

As a final recommendation, the authors suggest developing a predictive model for the *C. crangon* abundance in September. In this dissertation, several crucial influences, such as water temperature or food availability were identified. These parameters could, with good and sufficient data collection, be used to construct a predictive model. By measuring these parameters in the timeframes where they have the most influence, a prediction could be made on the expected size of the autumn stock. In this way, if the model predicts a smaller-than-usual autumn stock, preventive measurements can be made to protect the fisherman and the shrimp stock. Today's limitation for this model is the available data. Current data series are too short and/or insufficient to create valid predictions. Hence, before constructing such a model, the current data series of, for example, *C. crangon* abundances needs to be extended.

CONCLUSION

The initial aim of this exploratory study was to investigate the relation between the occurrence of marine heatwaves and the fluctuations in *C. crangon* abundance in the Belgian Part of the North Sea. However, a more detailed study of the lifecycle and recruitment of the European brown shrimp learned that, besides water temperature, several other environmental variables have a significant impact. The most significant parameters showing a strong correlation to shrimp abundances include food availability, zooplankton density, salinity and whiting abundance. The (winter) NAO index showed an unexpected result compared to results from literature and therefore, the influence is uncertain. Although no direct correlations were found between nutrient concentrations and shrimp abundances, the authors believe that the concentrations could still have an indirect effect on the recruitment via the phytoplankton abundance. Future research will be needed to explore this hypothesis.
The recruitment of *C. crangon* is thus subjected to several environmental variables, meaning that fluctuations in each of these variables could cause a variation in shrimp abundance. Consequently, no single, straightforward explanation can account for the observed trends which were described in this dissertation.

Despite no direct correlations, there are some indirect indications that marine heatwaves could influence the *C. crangon* abundances in September. The most plausible track seems to be that because of the prolonged period of elevated water temperatures, shrimp remain longer in more shallow waters, making them longer available for fisherman. However, increased capture of adults, and more specifically, egg-carrying females, may result in a lower winter brood and consequently a lower autumn stock in the following year. Other potential consequences of MHWs include accelerated maturation rates or deoxygenation of the BPNS, but further research will be necessary to investigate these.

Preliminary trends were also observed regarding the protein and lipid content of shrimp, with indications of both seasonal and spatial differences. However, further research will be necessary to confirm these findings.

In summary, the observed variability of *C. crangon* in the BPNS is a combination of several environmental factors that all exert their own influence in a specific time period on a specific stage in the lifecycle of *C. crangon*. In order to fully understand the abundance variability, all of these influences need to be studied in the right period, while looking at the right life stage of *C. crangon*. In order to do so, more comprehensive and consistent data series will be necessary. Despite its limited results, this master thesis serves as an initial, exploratory study to describe the major influences on the lifecycle and recruitment process of *C. crangon* and could act as a foundation for further research. A better understanding of these parameters could enhance the prediction of *C. crangon* fluctuations, enabling the implementation of preventive measures to safeguard both human and marine interests.

REFERENCES

Andrews, O. D., Bindoff, N. L., Halloran, P. R., Ilyina, T., & Le Quéré, C. (2013). Detecting an external influence on recent changes in oceanic oxygen using an optimal fingerprinting method. *Biogeosciences*, *10*(3), 1799–1813. https://doi.org/10.5194/bg-10-1799-2013

Aviat, D., Diamantis, C., Neudecker, T., Berkenhagen, J., & Müller, M. (2011). *The North Sea Brown Shrimp fisheries*.

Ayas, D., Ozogul, Y., & Yazgan, H. (2013). The effects of season on fat and fatty acids contents of shrimp and prawn species. *European Journal of Lipid Science and Technology*, *115*(3), 356–362. https://doi.org/10.1002/ejlt.201200081

Barnston, A. G., & Livezey, R. E. (1987). Classification, Seasonality and Persistence of Low-Frequency Atmospheric Circulation Patterns. *Monthly Weather Review*, *115*(6), 1083–1126. https://doi.org/10.1175/1520-0493(1987)115<1083:CSAPOL>2.0.CO;2

Beaugrand, G., Ibañez, F., & Reid, P. (2000). Spatial, seasonal and long-term fluctuations of plankton in relation to hydroclimatic features in the English Channel, Celtic Sea and Bay of Biscay. *Marine Ecology Progress Series*, *200*, 93–102. https://doi.org/10.3354/meps200093

Belga. (2024, May 15). De tomate crevette is gered: opnieuw voldoende voorraad grijze noordzeegarnalen. *Gazet van Antwerpen*. https://www.hln.be/binnenland/de-tomate-crevette-is-gered-schaarste-bij-garnalen-is-voorbij~ac39fb66/

Belkin, I. M. (2009). Rapid warming of Large Marine Ecosystems. *Progress in Oceanography*, *81*(1–4), 207–213. https://doi.org/10.1016/j.pocean.2009.04.011

Bensoussan, N., Romano, J.-C., Harmelin, J.-G., & Garrabou, J. (2010). High resolution characterization of northwest Mediterranean coastal waters thermal regimes: To better understand responses of benthic communities to climate change. *Estuarine, Coastal and Shelf Science*, *87*(3), 431–441. https://doi.org/10.1016/j.ecss.2010.01.008

Benthuysen, J., Feng, M., & Zhong, L. (2014). Spatial patterns of warming off Western Australia during the 2011 Ningaloo Niño: Quantifying impacts of remote and local forcing. *Continental Shelf Research*, *91*, 232–246. https://doi.org/10.1016/j.csr.2014.09.014

Bijma, J., Pörtner, H. O., Yesson, C., & Rogers, A. D. (2013). Climate change and the oceans – What does the future hold? *Marine Pollution Bulletin*, *74*(2), 495–505. https://doi.org/10.1016/J.MARPOLBUL.2013.07.022

Bligh, E. G., & Dyer, W. J. (1959). A rapid method of total lipid extraction and purification. *Canadian Journal of Biochemistry and Physiology*, *37*(8), 911–917. https://doi.org/10.1139/o59-099

Boddeke, R. (1976). The seasonal migration of the brown shrimp crangon crangon. *Netherlands Journal of Sea Research*, *10*(1), 103–130. https://doi.org/10.1016/0077-7579(76)90006-5

Boddeke, R. (1982). The occurrence of winter and summer eggs in the brown shrimp (crangon crangon) and the pattern of recruitment. *Netherlands Journal of Sea Research*, *16*, 151–162. https://doi.org/10.1016/0077-7579(82)90026-6

Bradford, M. M. (1976). A rapid and sensitive method for the quantitation of microgram quantities of protein utilizing the principle of protein-dye binding. *Analytical Biochemistry*, *72*(1), 248–254. https://doi.org/https://doi.org/10.1016/0003-2697(76)90527-3

Caldeira, K. (2007). What Corals are Dying to Tell Us About CO2 and Ocean Acidification. *Oceanography*, *20*(2), 188–195. https://doi.org/10.5670/oceanog.2007.69

Caldeira, K., & Wickett, M. E. (2003). Anthropogenic carbon and ocean pH. *Nature*, *425*(6956), 365–365. https://doi.org/10.1038/425365a

Camp, E. V., Ahrens, R. N., Collins, A. B., & Lorenzen, K. (2020, March 27). *Fish populations recruitment: what recruitment means and why it matters*. FA222. https://edis.ifas.ufl.edu/publication/FA222

Campos, J., Bio, A., Cardoso, J. F. M. F., Dapper, R., Witte, J. I. J., & Van Der Veer, H. W. (2010). Fluctuations of brown shrimp Crangon crangon abundance in the western Dutch Wadden Sea. *Marine Ecology Progress Series*, *405*, 203–219. https://doi.org/10.3354/meps08493

Campos, J., Bio, A., Freitas, V., Moreira, C., & van der Veer, H. (2013). Age estimation of brown shrimp Crangon crangon: comparison of two approaches applied to populations at the biogeographic edges. *Aquatic Biology*, *19*(2), 167–184. https://doi.org/10.3354/ab00524

Campos, J., & Van Der Veer, H. W. (2008). Autecology of Crangon Crangon (L.) with an emphasis on latitudinal trends. *Oceanography and Marine Biology*, *46*, 65–104. https://doi.org/10.1201/9781420065756.ch3

Campos, J., Van der Veer, H. W., Freitas, V., & Kooijman, S. A. L. M. (2009). Contribution of different generations of the brown shrimp Crangon crangon (L.) in the Dutch Wadden Sea to commercial fisheries: A dynamic energy budget approach. *Journal of Sea Research*, *62*(2–3), 106–113. https://doi.org/10.1016/j.seares.2009.07.007

Cao, L., & Caldeira, K. (2008). Atmospheric CO ₂ stabilization and ocean acidification. *Geophysical Research Letters*, *35*(19). https://doi.org/10.1029/2008GL035072

Cavanaugh, J. E., & Neath, A. A. (2019). The Akaike information criterion: Background, derivation, properties, application, interpretation, and refinements. *WIREs Computational Statistics*, *11*(3). https://doi.org/10.1002/wics.1460

Centrum Agrarische Geschiedenis (CAG). (2021a). *Garnalen vissen te voet en te paard*. https://cagnet.be/page/garnalen-vissen

Centrum Agrarische Geschiedenis (CAG). (2021b). *Van jolletje tot eurokotter*. https://cagnet.be/page/garnalen-jolletje

Chen, K., Gawarkiewicz, G. G., Lentz, S. J., & Bane, J. M. (2014). Diagnosing the warming of the Northeastern U.S. Coastal Ocean in 2012: A linkage between the atmospheric jet stream variability and ocean response. *Journal of Geophysical Research: Oceans*, *119*(1), 218–227. https://doi.org/10.1002/2013JC009393

Chen, K., Gawarkiewicz, G., Kwon, Y., & Zhang, W. G. (2015). The role of atmospheric forcing versus ocean advection during the extreme warming of the Northeast U.S. continental shelf in 2012. *Journal of Geophysical Research: Oceans*, *120*(6), 4324–4339. https://doi.org/10.1002/2014JC010547

Chen, W., Staneva, J., Grayek, S., Schulz-Stellenfleth, J., & Greinert, J. (2022). The role of heat wave events in the occurrence and persistence of thermal stratification in the southern North Sea. *Natural Hazards and Earth System Sciences*, *22*(5), 1683–1698. https://doi.org/10.5194/nhess-22-1683-2022

Conversi, A., Piontkovski, S., & Hameed, S. (2001). Seasonal and interannual dynamics of Calanus finmarchicus in the Gulf of Maine (Northeastern US shelf) with reference to the North Atlantic Oscillation. *Deep Sea Research Part II: Topical Studies in Oceanography*, *48*(1–3), 519–530. https://doi.org/10.1016/S0967-0645(00)00088-6

Copernicus. (2023, July 6). *Record North Atlantic warmth– Hottest June on record globally*. https://climate.copernicus.eu/record-breaking-north-atlantic-ocean-temperatures-contribute-extreme-marine-heatwaves

Cronin, M. F., Gentemann, C. L., Edson, J., Ueki, I., Bourassa, M., Brown, S., Clayson, C. A., Fairall, C. W., Farrar, J. T., Gille, S. T., Gulev, S., Josey, S. A., Kato, S., Katsumata, M., Kent, E., Krug, M., Minnett, P. J., Parfitt, R., Pinker, R. T., … Zhang, D. (2019). Air-Sea Fluxes With a Focus on Heat and Momentum. *Frontiers in Marine Science*, *6*. https://doi.org/10.3389/fmars.2019.00430

De Hauwere, N. (2017, January 18). *The North Sea*. Marine Regions. https://marineregions.org/gazetteer.php?p=details&id=2350

De Redactie. (2017, July 28). *Garnalen zijn nog nooit zo duur geweest*. HLN. https://www.hln.be/consument/garnalen-zijn-nog-nooit-zo-duur-geweest~a5f9d89b/

De Rijcke, M. (2017). *The current and future risk of harmful algal blooms in the North Sea* [PhD]. Faculty of Bioscience Engineering.

Delbare, D., Cooreman, K., & Smagghe, G. (2015). Rearing European brown shrimp (Crangon crangon, Linnaeus 1758): A review on the current status and perspectives for aquaculture. *Reviews in Aquaculture*, *7*(4), 262–282. https://doi.org/10.1111/raq.12068

Denne, R. A. (2018). Plankton. In R. Sorkhabi (Ed.), *Encyclopedia of Petroleum Geoscience* (pp. 1–11). Springer International Publishing. https://doi.org/10.1007/978-3-319-02330-4_55-1

Depestele, J., Ivanović, A., Degrendele, K., Esmaeili, M., Polet, H., Roche, M., Summerbell, K., Teal, L. R., Vanelslander, B., & O'Neill, F. G. (2015). Measuring and assessing the physical impact of beam trawling. *ICES Journal of Marine Science*, *73*(suppl_1), i15–i26. https://doi.org/10.1093/icesjms/fsv056

Deruytter, D. (2018). *Determination of energy available (protein, carbohydrate and lipids) and energy consumption (ETS activity) in Mytilus edulis* (Vol. 2, pp. 2–6). Laboratory of Environmental Toxicology and Aquatic Ecology (GhEnToxLab) .

Drinkwater, K. F., Belgrano, A., Borja, A., Conversi, A., Edwards, M., Greene, C. H., Ottersen, G., Pershing, A. J., & Walker, H. (2003). *The response of marine ecosystems to climate variability associated with the North Atlantic Oscillation* (pp. 211–234). https://doi.org/10.1029/134GM10

Echevin, V., Colas, F., Espinoza-Morriberon, D., Vasquez, L., Anculle, T., & Gutierrez, D. (2018). Forcings and Evolution of the 2017 Coastal El Niño Off Northern Peru and Ecuador. *Frontiers in Marine Science*, *5*. https://doi.org/10.3389/fmars.2018.00367

Elias, S. (2021). Changes in Ocean Circulation Patterns. In *Threats to the Arctic* (pp. 27–44). Elsevier. https://doi.org/10.1016/B978-0-12-821555-5.00001-2

EMODnet Bathymetry Consortium. (2022). *EMODnet Digital Bathymetry (DTM 2022)*. EMODnet Bathymetry Consortium. https://emodnet.ec.europa.eu/geoviewer/#!

European Marine Observation and Data Network (EMODnet). (2023). *Seabed substrates: Multiscale folk 7*. EMODnet Map Viewer. https://emodnet.ec.europa.eu/geoviewer/#!

Evans, S. (1984). Energy budgets and predation impact of dominant epibenthic carnivores on a shallow soft bottom community at the Swedish west coast. *Estuarine, Coastal and Shelf Science*, *18*(6), 651–672. https://doi.org/10.1016/0272-7714(84)90037-4

FAO. (n.d.). *Species Fact Sheet: Crangon crangon (Linnaeus, 1758)*. FAO.

Feng, M., McPhaden, M. J., Xie, S.-P., & Hafner, J. (2013). La Niña forces unprecedented Leeuwin Current warming in 2011. *Scientific Reports*, *3*(1), 1277. https://doi.org/10.1038/srep01277

Flanders Marine Institute (VLIZ). (2015). *ICOS and LifeWatch observatory data: buoy data*. https://rshiny.lifewatch.be/buoy-data/

Flanders Marine Institute (VLIZ). (2017). *Marine Information and Data Acquisition System: Underway & Cruise data*.

Flanders Marine Institute (VLIZ). (2020). *LifeWatch observatory data: nutrient, pigment, suspended matter and secchi measurements in the Belgian Part of the North Sea*. https://rshiny.lifewatch.be/station-data/

Flanders Marine Institute (VLIZ). (2023, July 28). *Noord-Atlantische Oceaan heeft koorts*. Testerep Magazine. https://www.vliz.be/testerep/nl/2023-07-noord-atlantische-oceaan-met-koorts

FOD Volksgezondheid. (2023, December 21). *Onze Natuur: Ontdek de Noordzee* [Video recording]. YouTube.

Folk, R. L. (1954). The Distinction between Grain Size and Mineral Composition in Sedimentary-Rock Nomenclature. *The Journal of Geology*, *62*(4), 344–359. http://www.jstor.org/stable/30065016

Freitas, V., Campos, J., Fonds, M., & Van der Veer, H. W. (2007). Potential impact of temperature change on epibenthic predator–bivalve prey interactions in temperate estuaries. *Journal of Thermal Biology*, *32*(6), 328–340. https://doi.org/10.1016/j.jtherbio.2007.04.004

Frölicher, T. L., Fischer, E. M., & Gruber, N. (2018). Marine heatwaves under global warming. *Nature*, *560*(7718), 360–364. https://doi.org/10.1038/s41586-018-0383-9

Fromentin, J., & Planque, B. (1996). Calanus and environment in the eastern North Atlantic. II. Influence of the North Atlantic Oscillation on C. finmarchicus and C. helgolandicus. *Marine Ecology Progress Series*, *134*, 111–118. https://doi.org/10.3354/meps134111

Garrabou, J., Coma, R., Bensoussan, N., Bally, M., Chevaldonné, P., CIGLIANO, M., Díaz, D., Harmelin, J.-G., Gambi, M. C., Kersting, D., Ledoux, J.-B., Lejeusne, C., Linares, C., Marschal, C., Pérez, T., Ribes, M., ROMANO, J., Serrano, E., Teixidó, N., & Cerrano, C. (2008). Mass mortality in Northwestern Mediterranean rocky benthic communities: Effects of the 2003 heat wave. *Global Change Biology*, *15*, 1090–1103. https://doi.org/10.1111/j.1365-2486.2008.01823.x

Genin, A., Levy, L., Sharon, G., Raitsos, D., & Diamant, A. (2020). Rapid onsets of warming events trigger mass mortality of coral reef fish. *Proceedings of the National Academy of Sciences of the United States of America*, *117*. https://doi.org/10.1073/pnas.2009748117

Greene, C. (2000). The response of Calanus finmarchicus populations to climate variability in the Northwest Atlantic: basin-scale forcing associated with the North Atlantic Oscillation. *ICES Journal of Marine Science*, *57*(6), 1536–1544. https://doi.org/10.1006/jmsc.2000.0966

Gruber, N. (2008). The Marine Nitrogen Cycle. In *Nitrogen in the Marine Environment* (pp. 1–50). Elsevier. https://doi.org/10.1016/B978-0-12-372522-6.00001-3

Health Belgium. (2020, June 20). *Facts about our North Sea*. https://www.health.belgium.be/en/facts-about-our-north-sea#article

Henderson, P. A., Seaby, R. M., & Somes, J. R. (2006). A 25-year study of climatic and density-dependent population regulation of common shrimp *Crangon crangon* (Crustacea: Caridea) in the Bristol Channel. *Journal of the Marine Biological Association of the United Kingdom*, *86*(2), 287–298. https://doi.org/10.1017/S0025315406013142

Henry, J., Patterson, J., & Krimsky, L. (n.d.). *Ocean Acidification: Calcifying Marine Organisms 1*. https://doi.org/10.1016/j

Hernandez, F., Dillen, N., & Fernández-Bejarano, S. (2021). *lwdataexplorer: Access to data from the LifeWatch Data Explorer* (R package version 0.0.0.9000). https://lifewatch.github.io/lwdataexplorer

Heylen, K. (2024, February 28). *Worden garnaalkroketten stilaan onbetaalbaar? "Tekort aan noordzeegarnalen nooit zo erg."* VRT NWS. https://www.vrt.be/vrtnws/nl/2024/02/28/garnaalkroketten-op-restaurant-worden-stilaan-onbetaalbaar/

Histories. (n.d.). *Als een paard in het water*. Retrieved July 10, 2024, from https://histories.be/ritueel/strandvisserij/

Hobday, A. J., Alexander, L. V., Perkins, S. E., Smale, D. A., Straub, S. C., Oliver, E. C. J., Benthuysen, J. A., Burrows, M. T., Donat, M. G., Feng, M., Holbrook, N. J., Moore, P. J., Scannell, H. A., Sen Gupta, A., & Wernberg, T. (2016). A hierarchical approach to defining marine heatwaves. *Progress in Oceanography*, *141*, 227–238. https://doi.org/10.1016/j.pocean.2015.12.014

Hoegh-Guldberg, O., & Bruno, J. F. (2010). The impact of climate change on the world's marine ecosystems. *Science*, *328*(5985), 1523–1528. https://doi.org/10.1126/SCIENCE.1189930/ASSET/F23D4D51-3B99-42AD-A2B7-C0B9B167A930/ASSETS/GRAPHIC/328_1523_B1.JPEG

Hoegh-Guldberg, O., Poloczanska, E. S., Skirving, W., & Dove, S. (2017). Coral reef ecosystems under climate change and ocean acidification. In *Frontiers in Marine Science* (Vol. 4, Issue MAY). Frontiers Media S. A. https://doi.org/10.3389/fmars.2017.00158

Hufnagl, M., Temming, A., Dänhardt, A., & Perger, R. (2010). Is Crangon crangon (L. 1758, Decapoda, Caridea) food limited in the Wadden Sea? *Journal of Sea Research*, *64*(3), 386–400. https://doi.org/10.1016/j.seares.2010.06.001

Hünerlage, K., Siegel, V., & Saborowski, R. (2019). Reproduction and recruitment of the brown shrimp Crangon crangon in the inner German Bight (North Sea): An interannual study and critical reappraisal. *Fisheries Oceanography*, *28*(6), 708–722. https://doi.org/10.1111/fog.12453

Hurrell, J. W., & Deser, C. (2010). North Atlantic climate variability: The role of the North Atlantic Oscillation. *Journal of Marine Systems*, *79*(3–4), 231–244. https://doi.org/10.1016/j.jmarsys.2009.11.002

Hurrell, J. W., Kushnir, Y., Ottersen, G., & Visbeck, M. (2003). *An overview of the North Atlantic Oscillation* (pp. 1–35). https://doi.org/10.1029/134GM01

Iampietro, P. J., & Kvitek, R. (2002). *Quantitative seafloor habitat classification using GIS terrain analysis: Effects of data density, resolution, and scale*. http://www.jennessent.com

Intergovernmental Panel on Climate Change (IPCC). (2023). *Climate Change 2021 – The Physical Science Basis*. Cambridge University Press. https://doi.org/10.1017/9781009157896

Intergovernmental Panel on Climate Change (IPCC). (2007). *Climate Change 2007: The Physical Science Basis*.

Iverson, S. J., Lang, S. L. C., & Cooper, M. H. (2001). Comparison of the bligh and dyer and folch methods for total lipid determination in a broad range of marine tissue. *Lipids*, *36*(11), 1283–1287. https://doi.org/10.1007/s11745-001-0843-0

Kamykowski, D., & Zentara, S.-J. (1986). Predicting plant nutrient concentrations from temperature and sigma-t in the upper kilometer of the world ocean. In *Deep-Sea Research* (Vol. 33, Issue 1).

Kassambara, A. (2023). *ggpubr: "ggplot2" Based Publication Ready Plots* (R package version 0.6.0}). https://CRAN.R-project.org/package=ggpubr

Kassambara A. (2023). *ggpubr: "ggplot2" Based Publication Ready Plots* (R package version 0.6.0). https://CRAN.R-project.org/package=ggpubr

Keeling, R. F., Körtzinger, A., & Gruber, N. (2010). Ocean Deoxygenation in a Warming World. *Annual Review of Marine Science*, *2*(1), 199–229. https://doi.org/10.1146/annurev.marine.010908.163855

Knight, J. R., Allan, R. J., Folland, C. K., Vellinga, M., & Mann, M. E. (2005). A signature of persistent natural thermohaline circulation cycles in observed climate. *Geophysical Research Letters*, *32*(20). https://doi.org/10.1029/2005GL024233

Knight, J. R., Folland, C. K., & Scaife, A. A. (2006). Climate impacts of the Atlantic Multidecadal Oscillation. *Geophysical Research Letters*, *33*(17). https://doi.org/10.1029/2006GL026242

Koninklijk Meteorologisch Instituut van België (KMI). (2023). *Eerste hittegolf ooit tijdens een septembermaand*. https://www.meteo.be/nl/info/nieuwsoverzicht/eerste-hittegolf-ooit-tijdens-een-septembermaand

Kroeker, K. J., Kordas, R. L., Crim, R., Hendriks, I. E., Ramajo, L., Singh, G. S., Duarte, C. M., & Gattuso, J. P. (2013). Impacts of ocean acidification on marine organisms: Quantifying sensitivities and interaction with warming. *Global Change Biology*, *19*(6), 1884–1896. https://doi.org/10.1111/gcb.12179

Kuhl, H. (1972). Hydrography and biology of the Elbe estuary. *Oceanography and Marine Biology An Annual Review 10*, 225–309.

Kuipers, B. R., & Dapper, R. (1981). Production of Crangon crangon in the tidal zone of the Dutch Wadden Sea. *Netherlands Journal of Sea Research*, *15*(1), 33–53. https://doi.org/10.1016/0077-7579(81)90004-1

Kuipers, B. R., & Dapper, R. (1984). Nursery function of Wadden Sea tidal flats for the brown shrimp Crangon crangon. *Marine Ecology Progress Series*, *17*(2), 171–181. http://www.jstor.org/stable/24815809

LaRiviere, J. P., Ravelo, A. C., Crimmins, A., Dekens, P. S., Ford, H. L., Lyle, M., & Wara, M. W. (2012). Late Miocene decoupling of oceanic warmth and atmospheric carbon dioxide forcing. *Nature*, *486*(7401), 97–100. https://doi.org/10.1038/nature11200

LifeWatch Belgium. (2023). *Data*. VLIZ. https://www.lifewatch.be/en/data

Lindsey, R., & Dahlman, L. (2009, August 30). *Climate Variability: North Atlantic Oscillation*. https://www.climate.gov/news-features/understanding-climate/climate-variability-north-atlantic-oscillation

Linnaeus, C. (1758). *Systema Naturae per regna tria naturae, secundum classes, ordines, genera, species, cum characteribus, differentiis, synonymis, locis* (L. Salvius, Ed.; 10th ed., Vol. 1).

Liu, G., Heron, S., Eakin, C., Muller-Karger, F., Vega-Rodriguez, M., Guild, L., De La Cour, J., Geiger, E., Skirving, W., Burgess, T., Strong, A., Harris, A., Maturi, E., Ignatov, A., Sapper, J., Li, J., & Lynds, S. (2014). Reef-Scale Thermal Stress Monitoring of Coral Ecosystems: New 5-km Global Products from NOAA Coral Reef Watch. *Remote Sensing*, *6*(11), 11579–11606. https://doi.org/10.3390/rs61111579

Lloyd, A. J., & Yonge, C. M. (1947). The biology of Crangon vulgaris L. in the Bristol Channel and Severn Estuary. *Journal of the Marine Biological Association of the United Kingdom*, *26*, 626–661.

Loaiza Cerón, W., Andreoli, R. V., Kayano, M. T., Ferreira de Souza, R. A., Jones, C., & Carvalho, L. M. V. (2020). The Influence of the Atlantic Multidecadal Oscillation on the Choco Low-Level Jet and Precipitation in Colombia. *Atmosphere*, *11*(2), 174. https://doi.org/10.3390/atmos11020174

Luttikhuizen, P. C., Campos, J., Bleijswijk, J. van, Peijnenburg, K. T. C. A., & van der Veer, H. W. (2008). Phylogeography of the common shrimp, Crangon crangon (L.) across its distribution range. *Molecular Phylogenetics and Evolution*, *46*(3), 1015–1030. https://doi.org/10.1016/j.ympev.2007.11.011

Mæhre, H., Dalheim, L., Edvinsen, G., Elvevoll, E., & Jensen, I.-J. (2018). Protein Determination—Method Matters. *Foods*, *7*(1), 5. https://doi.org/10.3390/foods7010005

Mauchline, J. (1998). *The biology of calanoid copepods* (1st ed., Vol. 33). Advances in Marine Biology.

Mauroo, T. (2018, September 18). *Grijze garnalen uit de Noordzee zijn momenteel erg goedkoop*. VRT NWS. https://www.vrt.be/vrtnws/nl/2018/09/18/grijze-garnalen-uit-de-noordzee-zijn-momenteel-erg-goedkoop/

Mejía-Ortíz, L. M. (2019). Crustacea. In *Encyclopedia of Caves* (pp. 333–347). Elsevier. https://doi.org/10.1016/B978-0-12-814124-3.00037-6

Mika, A., Gołębiowski, M., Skorkowski, E., & Stepnowski, P. (2014). Lipids of adult brown shrimp, *Crangon crangon* : seasonal variations in fatty acids class composition. *Journal of the Marine Biological Association of the United Kingdom*, *94*(5), 993–1000. https://doi.org/10.1017/S0025315414000162

Millar, C., Kvaavik, C., Villamor, A., Large, S., & Magnusson, A. (2023). *icesDatras: DATRAS Trawl Survey Database Web Services* (R package version 1.4.1). https://CRAN.R-project.org/package=icesDatras

Mohamed, B., Barth, A., & Alvera-Azcárate, A. (2023). Extreme marine heatwaves and cold-spells events in the Southern North Sea: classifications, patterns, and trends. *Frontiers in Marine Science*, *10*. https://doi.org/10.3389/fmars.2023.1258117

Mohamed, B., Nilsen, F., & Skogseth, R. (2022). Interannual and Decadal Variability of Sea Surface Temperature and Sea Ice Concentration in the Barents Sea. *Remote Sensing*, *14*(17), 4413. https://doi.org/10.3390/rs14174413

Moisan, J. R., & Niiler, P. P. (1998). The Seasonal Heat Budget of the North Pacific: Net Heat Flux and Heat Storage Rates (1950–1990). *Journal of Physical Oceanography*, *28*(3), 401–421. https://doi.org/10.1175/1520-0485(1998)028<0401:TSHBOT>2.0.CO;2

Montgomerie, M. (2022). *Basic fishing methods: a comprehensive guide to commercial fishing methods*. https://doi.org/https://doi.org/10.25607/obp-1937

Moreira, C., Campos, J., Freitas, F., & van der Veer, H. W. (2012). Short Review of the Eco-geography of Crangon. *Journal of Crustacean Biology*, *32*(2), 159–169. https://doi.org/10.1163/193724011X615569

Mortelmans, J., Aubert, A., Reubens, J., Otero, V., Deneudt, K., & Mees, J. (2021). Copepods (Crustacea: Copepoda) in the Belgian part of the North Sea: Trends, dynamics and anomalies. *Journal of Marine Systems*, *220*. https://doi.org/10.1016/j.jmarsys.2021.103558

Mortelmans, J., Deneudt, K., Cattrijsse, A., Beauchard, O., Daveloose, I., Vyverman, W., Vanaverbeke, J., Timmermans, K., Peene, J., Roose, P., Knockaert, M., Chou, L., Sanders, R., Stinchcombe, M., Kimpe, P., Lammens, S., Theetaert, H., Gkritzalis, T., Hernandez, F., & Mees, J. (2019). Nutrient, pigment, suspended matter and turbidity measurements in the Belgian part of the North Sea. *Scientific Data*, *6*(1), 22. https://doi.org/10.1038/s41597-019-0032-7

Mortelmans, J., Goossens, J., Amadei Martínez, L., Deneudt, K., Cattrijsse, A., & Hernandez, F. (2019). LifeWatch observatory data: Zooplankton observations in the Belgian part of the North Sea. *Geoscience Data Journal*, *6*(2), 76–84. https://doi.org/https://doi.org/10.1002/gdj3.68

Mortelmans, J., Semmouri, I., Perneel, M., Lagaisse, R., Martínez, L. A., Rommelaere, Z., Hablützel, P. I., & Deneudt, K. (2024). Temperature-induced copepod depletion and the associated wax of Bellerochea in Belgian coastal waters: Implications and shifts in plankton dynamics. *Journal of Sea Research*, *201*, 102523. https://doi.org/10.1016/j.seares.2024.102523

Muus, B. J. (1967). The Fauna of Danish Estuaries and Lagoon. Distribution and ecology of dominating species in the shallow reaches of the mesohaline zone. *Meddelelser Fra Kommissionen for Danmarks Fiskeri- Og Havunder Soegelser* , *5*, 1–316.

National Oceanic and Atmospheric Administration. (2023). *North Atlantic Oscilation (NAO)*. https://www.ncei.noaa.gov/access/monitoring/nao/

Neuwirth, E. (2022). *RColorBrewer: ColorBrewer Palettes* (R package version 1.1-3). https://CRAN.R-project.org/package=RColorBrewer

Olita, A., Sorgente, R., Natale, S., Gaberšek, S., Ribotti, A., Bonanno, A., & Patti, B. (2007). Effects of the 2003 European heatwave on the Central Mediterranean Sea: surface fluxes and the dynamical response. *Ocean Science*, *3*(2), 273–289. https://doi.org/10.5194/os-3-273-2007

Oliver, E. C. J., Benthuysen, J. A., Bindoff, N. L., Hobday, A. J., Holbrook, N. J., Mundy, C. N., & Perkins-Kirkpatrick, S. E. (2017). The unprecedented 2015/16 Tasman Sea marine heatwave. *Nature Communications*, *8*(1), 16101. https://doi.org/10.1038/ncomms16101

Oliver, E. C. J., Benthuysen, J. A., Darmaraki, S., Donat, M. G., Hobday, A. J., Holbrook, N. J., Schlegel, R. W., & Gupta, A. Sen. (2021). Marine Heatwaves. *Annual Review OfMarine Science*, *13*(31), 3–42. https://doi.org/10.1146/annurev-marine-032720

Oliver, E. C. J., Perkins-Kirkpatrick, S. E., Holbrook, N. J., & Bindoff, N. L. (2018). Anthropogenic and Natural Influences on Record 2016 Marine Heat waves. *Bulletin of the American Meteorological Society*, *99*(1), S44–S48. https://doi.org/10.1175/BAMS-D-17-0093.1

Ooms, J. (2023). *writexl: Export Data Frames to Excel "xlsx" Format* (R package version 1.4.2). https://CRAN.R-project.org/package=writexl

Oschlies, A., Brandt, P., Stramma, L., & Schmidtko, S. (2018). Drivers and mechanisms of ocean deoxygenation. *Nature Geoscience*, *11*(7), 467–473. https://doi.org/10.1038/s41561-018-0152-2

Oset Garcia, P. (2016, December 16). *Belgian Part of the North Sea*. Marine Regions. https://marineregions.org/gazetteer.php?p=details&id=26567

Pearce, A., Lenanton, R., Jackson, G., Moore, J., Feng, M., & Gaughan, D. (2011). The "marine heat wave" off Western Australia during the summer of 2010/11. In *Fisheries Research Report* (Vol. 22). Department of Fisheries, Western Australia.

Penning, E., Govers, L. L., Dekker, R., & Piersma, T. (2021). Advancing presence and changes in body size of brown shrimp Crangon crangon on intertidal flats in the western Dutch Wadden Sea, 1984–2018. *Marine Biology*, *168*(11), 160. https://doi.org/10.1007/s00227-021-03967-z

Perkins-Kirkpatrick, S. E., King, A. D., Cougnon, E. A., Holbrook, N. J., Grose, M. R., Oliver, E. C. J., Lewis, S. C., & Pourasghar, F. (2019). The Role of Natural Variability and Anthropogenic Climate Change in the 2017/18 Tasman Sea Marine Heatwave. *Bulletin of the American Meteorological Society*, *100*(1), S105–S110. https://doi.org/10.1175/BAMS-D-18-0116.1

Petrie, A. (2020). *regclass: Tools for an Introductory Class in Regression and Modeling* (R package version 1.6). https://CRAN.R-project.org/package=regclass

Pihl, L., & Rosenberg, R. (1982). Production, abundance, and biomass of mobile epibenthic marine fauna in shallow waters, Western Sweden. *Journal of Experimental Marine Biology and Ecology*, *57*(2–3), 273–301. https://doi.org/10.1016/0022-0981(82)90197-6

Pihl, L., & Rosenberg, R. (1984). Food selection and consumption of the shrimp Crangon crangon in some shallow marine areas in western Sweden. *Marine Ecology Progress Series*, *15*, 159–168. https://doi.org/10.3354/meps015159

Planque, B., & Reid, P. C. (1998). Predicting *Calanus Finmarchicus* Abundance from a Climatic Signal. *Journal of the Marine Biological Association of the United Kingdom*, *78*(3), 1015–1018. https://doi.org/10.1017/S0025315400044969

Poloczanska, E. S., Burrows, M. T., Brown, C. J., Molinos, J. G., Halpern, B. S., Hoegh-Guldberg, O., Kappel, C. V., Moore, P. J., Richardson, A. J., Schoeman, D. S., & Sydeman, W. J. (2016). Responses of marine organisms to climate change across oceans. In *Frontiers in Marine Science* (Vol. 3, Issue MAY). Frontiers Media S. A. https://doi.org/10.3389/fmars.2016.00062

Posit team. (2023). *RStudio: Integrated Development Environment for R* (2023.12.0.369). Posit Software, PBC. http://www.posit.co/

QGIS.org. (2023). *QGIS Geographic Information System* (3.28.12-Firenze). Open Source Geospatial Foundation Project. http://qgis.org

R Core Team. (2023). *R: A Language and Environment for Statistical Computing* (4.3.1). R Foundation for Statistical Computing. https://www.R-project.org/

Raat, H. (2023). *Bemonsteringsprotocol Demersal Young Fish & Brown Shrimp Survey (DYFS) met RV Simon Stevin*.

Rayner, N. A., Parker, D. E., Horton, E. B., Folland, C. K., Alexander, L. V., Rowell, D. P., Kent, E. C., & Kaplan, A. (2003). Global analyses of sea surface temperature, sea ice, and night marine air temperature since the late nineteenth century. *Journal of Geophysical Research: Atmospheres*, *108*(D14). https://doi.org/10.1029/2002JD002670

Redant, F. (1978). *Komsumptie en produktie van post-larvale Crangon crangon in de Belgische kustwateren*. Vrije Universiteit Brussel.

Reid, J. W., & Williamson, C. E. (2010). Ecology and Classification of North American Freshwater Invertebrates Chapter 21. In *Ecology and Classification of North American Freshwater Invertebrates*. https://doi.org/10.1016/10.1016/B978-0-12-374855-3.00021-2

Reid, P. C., & Beaugrand, G. (2012). Global synchrony of an accelerating rise in sea surface temperature. *Journal of the Marine Biological Association of the United Kingdom*, *92*(7), 1435–1450. https://doi.org/10.1017/S0025315412000549

Respondek, G., Günther, C., Beier, U., Bleeker, K., Pedersen, E. M., Schulze, T., & Temming, A. (2022). Connectivity of local sub-stocks of Crangon crangon in the North Sea and the risk of local recruitment overfishing. *Journal of Sea Research*, *181*, 102173. https://doi.org/10.1016/j.seares.2022.102173

Revelle, W. (2023). *psych: Procedures for Psychological, Psychometric, and Personality Research* (R package version 2.3.9). Northwestern University. https://CRAN.R-project.org/package=psych

Richardson, A. J. (2008). *In hot water: zooplankton and climate change*. https://academic.oup.com/icesjms/article/65/3/279/787309

Rosenzweig, C., Karoly, D., Vicarelli, M., Neofotis, P., Wu, Q., Casassa, G., Menzel, A., Root, T. L., Estrella, N., Seguin, B., Tryjanowski, P., Liu, C., Rawlins, S., & Imeson, A. (2008). Attributing physical and biological impacts to anthropogenic climate change. *Nature*, *453*(7193), 353–357. https://doi.org/10.1038/nature06937

Rouault, M., Illig, S., Bartholomae, C., Reason, C. J. C., & Bentamy, A. (2007). Propagation and origin of warm anomalies in the Angola Benguela upwelling system in 2001. *Journal of Marine Systems*, *68*(3–4), 473–488. https://doi.org/10.1016/j.jmarsys.2006.11.010

Salinger, M. J., Renwick, J., Behrens, E., Mullan, A. B., Diamond, H. J., Sirguey, P., Smith, R. O., Trought, M. C. T., Alexander, L., Cullen, N. J., Fitzharris, B. B., Hepburn, C. D., Parker, A. K., & Sutton, P. J. (2019). The unprecedented coupled ocean-atmosphere summer heatwave in the New Zealand region 2017/18: drivers, mechanisms and impacts. *Environmental Research Letters*, *14*(4), 044023. https://doi.org/10.1088/1748-9326/ab012a

Scannell, H. A., Pershing, A. J., Alexander, M. A., Thomas, A. C., & Mills, K. E. (2016). Frequency of marine heatwaves in the North Atlantic and North Pacific since 1950. *Geophysical Research Letters*, *43*(5), 2069–2076. https://doi.org/10.1002/2015GL067308

Semmouri, I. (2022). *Temporal effects of chemical and physical stressors on marine zooplankton: a molecular approach* [PhD Thesis]. Ghent University.

Semmouri, I., De Schamphelaere, K. A. C., Mortelmans, J., Mees, J., Asselman, J., & Janssen, C. R. (2023). Decadal decline of dominant copepod species in the North Sea is associated with ocean warming: Importance of marine heatwaves. *Marine Pollution Bulletin*, *193*. https://doi.org/10.1016/j.marpolbul.2023.115159

Sherman, K., Belkin, I. M., Friedland, K. D., O'Reilly, J., & Hyde, K. (2009). Accelerated Warming and Emergent Trends in Fisheries Biomass Yields of the World's Large Marine Ecosystems. *AMBIO: A Journal of the Human Environment*, *38*(4), 215–224. https://doi.org/10.1579/0044-7447-38.4.215

Siegel, V., Gröger, J., Neudecker, T., Damm, U., & Jansen, S. (2005). Long-term variation in the abundance of the brown shrimp *Crangon crangon* (L.) population of the German Bight and possible causes for its interannual variability. *Fisheries Oceanography*, *14*(1), 1–16. https://doi.org/10.1111/j.1365-2419.2004.00301.x

Simpson, G. L. (2023). *gratia: Graceful ggplot-Based Graphics and Other Functions for GAMs Fitted using mgcv* (R package version 0.8.1). https://gavinsimpson.github.io/gratia

Smith, K. E., Burrows, M. T., Hobday, A. J., King, N. G., Moore, P. J., Gupta, A. Sen, Thomsen, M. S., Wernberg, T., & Smale, D. A. (2022). *Biological Impacts of Marine Heatwaves*. https://doi.org/10.1146/annurev-marine-032122

Sparnocchia, S., Schiano, M. E., Picco, P., Bozzano, R., & Cappelletti, A. (2006). The anomalous warming of summer 2003 in the surface layer of the Central Ligurian Sea (Western Mediterranean). *Annales Geophysicae*, *24*(2), 443–452. https://doi.org/10.5194/angeo-24-443-2006

Stenseth, N. Chr., Ottersen, G., Hurrell, J. W., Mysterud, A., Lima, M., Chan, K., Yoccoz, N. G., & Ådlandsvik, B. (2003). Review article. Studying climate effects on ecology through the use of climate indices: the North Atlantic Oscillation, El Niño Southern Oscillation and beyond. *Proceedings of the Royal Society of London. Series B: Biological Sciences*, *270*(1529), 2087–2096. https://doi.org/10.1098/rspb.2003.2415

Tan, H., & Cai, R. (2018). What caused the record-breaking warming in East China Seas during August 2016? *Atmospheric Science Letters*, *19*(10). https://doi.org/10.1002/asl.853

Temming, A., & Damm, U. (2002). Life cycle of *Crangon crangon* in the North Sea: a simulation of the timing of recruitment as a function of the seasonal temperature signal. *Fisheries Oceanography*, *11*(1), 45–58. https://doi.org/10.1046/j.1365-2419.2002.00184.x

Temming, A., & Hufnagl, M. (2015). Decreasing predation levels and increasing landings challenge the paradigm of non-management of North Sea brown shrimp (Crangon crangon). *ICES Journal of Marine Science*, *72*(3), 804–823. https://doi.org/10.1093/icesjms/fsu194

Tiews, K. (1970). *Synopsis of biological data on the common shrimp Crangon crangon (Linnaeus, 1758)* (Fisheries Report 57). https://www.fao.org/3/ac765t/AC765T02.htm

Trenberth, K. E., & Shea, D. J. (2006). Atlantic hurricanes and natural variability in 2005. *Geophysical Research Letters*, *33*(12). https://doi.org/10.1029/2006GL026894

Tripati, A. K., Roberts, C. D., & Eagle, R. A. (2009). Coupling of CO_2 and Ice Sheet Stability Over Major Climate Transitions of the Last 20 Million Years. *Science*, *326*(5958), 1394–1397. https://doi.org/10.1126/science.1178296

Tulp, I., Bolle, L., Meesters, E., & de Vries, P. (2012). Brown shrimp abundance in northwest European coastal waters from 1970 to 2010 and potential causes for contrasting trends. *Marine Ecology Progress Series*, *458*, 141–154. https://doi.org/10.3354/meps09743

Turan, H., Kaya, Y., & Erdem, M. E. (2011). Proximate Composition, Cholesterol, and Fatty Acid Content of Brown Shrimp (*Crangon crangon* L. 1758) from Sinop Region, Black Sea. *Journal of Aquatic Food Product Technology*, *20*(1), 100–107. https://doi.org/10.1080/10498850.2010.526753

van der Molen, J., & Pätsch, J. (2022). An overview of Atlantic forcing of the North Sea with focus on oceanography and biogeochemistry. *Journal of Sea Research*, *189*, 102281. https://doi.org/10.1016/j.seares.2022.102281

Verfaillie, E., Van Lancker, V., & Renard Centre of Marine Geology. (2015). *Bathymetric Position Index (zones) : large scale slopes, crests, flats and depressions on the Belgian continental shelf (UG_RCMG_BPI_z)*. VLIZ. https://www.vliz.be/en/imis?module=dataset&dasid=635

Verlé, K., Pecceu, E., & Van Hoey, G. (2023). *Analyses of fishing activities in the Belgian part of the North Sea, Flemish Banks and proposed management areas for seafloor integrity*.

Vermeersch, X. (2023). *From sea to land: challenges in the development of European brown shrimp (Crangon crangon) as an innovative niche product in the Belgian shrimp fishery*.

Vertongen, B. (2024). *Interview with (retired) fishermen (10/01/2024)*.

Vlaamse Milieu Maatschappij (VMM). (2023, September). *Hittegolven en andere temperatuurextremen (1892-2022/2023)*. https://www.vmm.be/klimaat/hittegolven-en-andere-temperatuurextremen

Walsh, J. E., Thoman, R. L., Bhatt, U. S., Bieniek, P. A., Brettschneider, B., Brubaker, M., Danielson, S., Lader, R., Fetterer, F., Holderied, K., Iken, K., Mahoney, A., McCammon, M., & Partain, J. (2018). The High Latitude Marine Heat Wave of 2016 and Its Impacts on Alaska. *Bulletin of the American Meteorological Society*, *99*(1), S39–S43. https://doi.org/10.1175/BAMS-D-17-0105.1

Wanner, H., Brönnimann, S., Casty, C., Gyalistras, D., Luterbacher, J., Schmutz, C., Stephenson, D. B., & Xoplaki, E. (2001). North Atlantic Oscillation-Concepts and studies. *Surveys in Geophysics*, *22*(4), 321–381. https://doi.org/10.1023/A:1014217317898

Wear, R. G. (1974). Incubation in British Decapod Crustacea, and the Effects of Temperature on the Rate and Success of Embryonic Development. *Journal of the Marine Biological Association of the United Kingdom*, *54*(3), 745–762. https://doi.org/10.1017/S0025315400022918

Weiss, A. (2001). Topographic position and landforms analysis (Conference Poster). In *ESRI International User Conference* (Vol. 200).

Welleman, H. C., & Daan, N. (2001). Is the Dutch shrimp fishery sustainable? *Senckenbergiana Maritima*, *31*(2), 321–328. https://doi.org/10.1007/BF03043040

Wickham, H. (2016). *ggplot2: Elegant Graphics for Data Analysis*. Springer-Verlag New York. https://ggplot2.tidyverse.org

Wickham, H., Averick, M., Bryan, J., Chang, W., McGowan, L., François, R., Grolemund, G., Hayes, A., Henry, L., Hester, J., Kuhn, M., Pedersen, T., Miller, E., Bache, S., Müller, K., Ooms, J., Robinson, D., Seidel, D., Spinu, V., … Yutani, H. (2019). Welcome to the Tidyverse. *Journal of Open Source Software*, *4*(43), 1686. https://doi.org/10.21105/joss.01686

Wickham, H., François, R., Henry, L., Müller, K., & Vaughan, D. (2023). *dplyr: A Grammar of Data Manipulation* (R package version 1.1.4). https://CRAN.R-project.org/package=dplyr

Wickham, H., Hester, J., Chang, W., & Bryan, J. (2022). *devtools: Tools to Make Developing R Packages Easier* (R package version 2.4.5). https://CRAN.R-project.org/package=devtools

Wickham, H., Vaughan, D., & Girlich, M. (2023). *tidyr: Tidy Messy Data* (R package version 1.3.0). https://CRAN.R-project.org/package=tidyr

Williams, R., Conway, D. V. P., & Hunt, H. G. (1994). The role of copepods in the planktonic ecosystems of mixed and stratified waters of the European shelf seas. *Hydrobiologia*, *292*(1), 521–530. https://doi.org/10.1007/BF00229980

Wood, S. (2023). *Mixed GAM Computation Vehicle with Automatic Smoothness Estimation* (1.9-1).

Wood, S. N. (2003). Thin-plate regression splines. *Journal of the Royal Statistical Society (B)*, *65*(1), 95–114.

Wood, S. N. (2004). Stable and efficient multiple smoothing parameter estimation for generalized additive models. *Journal of the American Statistical Association*, *99*(467), 673–686.

Wood, S. N. (2011a). Fast stable restricted maximum likelihood and marginal likelihood estimation of semiparametric generalized linear models. *Journal of the Royal Statistical Society (B)*, *73*(1), 3–36.

Wood, S. N. (2011b). Fast Stable Restricted Maximum Likelihood and Marginal Likelihood Estimation of Semiparametric Generalized Linear Models. *Journal of the Royal Statistical Society Series B: Statistical Methodology*, *73*(1), 3–36. https://doi.org/10.1111/j.1467-9868.2010.00749.x

Wood, S. N. (2017). *Generalized Additive Models: An Introduction with R (2nd edition)* (2nd ed.). Chapman and Hall/CRC.

Wood, S. N., Pya, N., & Saefken, B. (2016). Smoothing parameter and model selection for general smooth models (with discussion). *Journal of the American Statistical Association*, *111*, 1548–1575.

WoRMS. (n.d.). *Crangon crangon (Linnaeus, 1758)*. Retrieved July 9, 2024, from https://www.marinespecies.org/aphia.php?p=taxdetails&id=107552#sources

WoRMS. (2024). *Copepoda*. https://www.marinespecies.org/aphia.php?p=taxdetails&id=1080

Zhang, R. (2016, March). *Atlantic Multi-decadal Oscillation (AMO) and Atlantic Multidecadal Variability (AMV)*. NCAR Climate Guide. https://climatedataguide.ucar.edu/climate-data/atlantic-multi-decadal-oscillation-amo

Zuur, A. F., Ienon Elena N., Walker, N., Saveliev, A. A., & Smith, G. M. (2009). *Mixed effects models and extensions in ecology with R* (L. Gail, K. Krickeberg, J. M. Samet, A. Tsiatis, & W. Wong, Eds.; Vol. 36). Springer.

APPENDIX A: LITERATURE

$$\underbrace{\frac{\partial \overline{T}}{\partial t}}_{\text{Temperature tendency}} = \underbrace{-\ \overline{\mathrm{u}} \cdot \nabla \overline{T}}_{\text{Horizontal advection}} + \underbrace{\overline{\nabla \cdot (\kappa_{\mathrm{h}} \nabla T)}}_{\text{Horizontal mixing}} - \underbrace{\frac{1}{h} \kappa_{\mathrm{z}} \frac{\partial T}{\partial z}\Big|_{-h}}_{\text{Vertical mixing}}$$

$$\underbrace{- \left(\frac{\overline{T} - T_{-h}}{h} \right) \left(\underbrace{\frac{\partial h}{\partial t}}_{\text{MLD tendency}} + \underbrace{\mathrm{u}_{-h} \cdot \nabla h}_{\text{Lateral induction}} + \underbrace{w_{-h}}_{\text{Vertical advection}} \right)}_{\text{Entrainment}}$$

$$+ \underbrace{\frac{Q_{\mathrm{SW}} - Q_{\mathrm{SW}(-h)} + Q_{\mathrm{LW}} + Q_{\mathrm{sens}} + Q_{\mathrm{lat}}}{\rho c_{\mathrm{p}} h}}_{\text{Air–sea heat flux}},$$

Figure A- 1 *Equation which describes the rate of change of vertically averaged seawater temperature in the mixed layer, where T is temperature in the surface mixed layer, t is the time, u = (u,v) is the two-dimensional horizontal (x,y) velocity vector, w is vertical (z) velocity, ∇ is the horizontal gradient operator, QSW and QLW represent respectively the short and longwave radiative components, QSW(-h) represents the escaping fraction of shortwave radiation via the bottom of the surface layer, Qlat and Qsens are respectively the net latent and sensible turbulent heat fluxes into the ocean, ρ is the seawater density (Cronin et al., 2019), cp is the specific heat capacity of seawater, b is the mixed-layer depth, and Kh and Kz are the horizontal and vertical diffusivity coefficients.Moisan & Niiler (1998) piled by Moisan & Niiler (1998) and was extracted from Oliver et al. (2021).*

Table A- 1 *Summary of the amount of marine heatwaves (MHW) in the southern North Sea during the period of 1982-2021. An overall increase is witnessed over the four decades, with a low amount of MHW in the first decade (D1) and a high amount in decade 4 (D4). A distinction is made between winter- and summer marine heatwaves, with the winter MHW occurring during January, February and March, and the summer MHW during July, August and September. This table was derived from Mohamed et al. (2023).*

Decade	MHW frequency		
	Annual	Winter	Summer
D1 (1982-1991)	6	2	1
D2 (1992-2001)	11	2	5
D3 (2002-2011)	23	4	7
D4 (2012-2021)	31	8	10
Total	71	16	23

Table A- 2 *Correlation factors of the different climate modes (AMO, NAO) with the annual and seasonal MHW frequency and duration. Significant correlations are underlined. The table and results are extracted from Mohamed et al. (2023).*

Climate mode	MHW frequency			MHW duration (days)		
	Annual	Winter	Summer	Annual	Winter	Summer
AMO	0,45	0,30	0,43	0,41	0,33	0,39
NAO	0,12	0,39	0,10	0,10	0,19	-0,01

Table A- 3 Taxonomic overview of Crangon crangon according to World Register of Marine Species (WoRMS) (WoRMS, n.d.).

Crangon crangon (Linneaus, 1758)	
Kingdom	Animalia
Phylum	Arthropoda
Subphylum	Crustacea
Class	Malacostraca
Subclass	Eumalacostraca
Superopder	Eucarida
Order	Decapoda
Suborder	Pleocyemata
Infraorder	Caridea
Superfamily	Cragonoidea
Family	Cragonidae
Genus	*Crangon*
Species	*crangon*

Table A- 4 Summary of different relations between egg/larval development time in days (D) and water temperature (T) found in literature. An extensive summary is provided in Temming & Damm (2002), table was derived from Campos & Van Der Veer (2008).

Literature	Relation
Egg development	
Belgian waters (Redant, 1978)	$D = 1031.34 * T^{-1.354}$
U.K. waters (Wear, 1974)	$D = 20437 * (T + 3.6)^{-2.3}$
Dutch coastal waters, summer eggs (Boddeke, 1982)	$D = 1230.27 * T^{-1.43}$
Dutch coastal waters, winter eggs (Boddeke, 1982)	$D = 1548.82 * T^{-1.49}$
Larval development	
Wadden Sea area (Temming & Damm, 2002)	$D = 941.78 * T^{-1.347}$
Dutch coastal waters, summer larvae (Boddeke, 1982)	$D = 952.09 * T^{-1258}$
Dutch coastal waters, winter larvae (Boddeke, 1982)	$D = 1148.42 * T^{-1.405}$

APPENDIX B: METHODS

Table B- 1 *Coordinates of ILVO and LifeWatch stations. ILVO coordinates are extracted from the DATRAS Trawl Survey Database for the year 2021. LifeWatch coordinates are extracted from Mortelmans et al. (2019). These coordinates were used in Qgis to construct several maps.*

Station	Longitude	Latitude
LifeWatch		
120	2.702483	51.18608
130	2.90535	51.27055
215	2.61075	51.27487
230	2.85035	51.30868
330	2.809083	51.43412
700	3.221017	51.377
710	3.138283	51.44122
780	3.057283	51.47137
ZG02	2.500717	51.33515
ILVO		
1	3.2495	51.4447
2	3.2174	51.4607
3	3.1752	51.4391
4	3.1361	51.4246
5	3.0122	51.452
6	3.0018	51.4015
7	2.9916	51.3201
8	2.987	51.3648
9	2.961	51.3348
10	2.8382	51.2674
11	2.8665	51.3515
12	2.8426	51.3069
13	2.8079	51.2327
14	2.8613	51.3272
16	2.7911	51.1922
17	2.736	51.1823
18	2.8162	51.3183
19	2.6925	51.1852
20	2.7303	51.3256
21	2.6586	51.251
22	2.6136	51.1985
23	2.5882	51.1472
24	2.5973	51.1747
26	2.7759	51.2516
27	3.0796	51.3212
28	2.6628	51.3115
35	3.155	51.4477
37	3.1686	51.496
38	3.1284	51.4627

49	3.0112	51.285
91	2.6175	51.1613
92	3.0575	51.3358
93	3.236	51.3906

SmartShrimp Protocol

Before measurements, the camera is calibrated by taking 20 pictures of the illuminated surface containing a dotted square. In the first four pictures, the dotted square needs to be placed in the corners. In the other 16 pictures, the location of the dotted square can be random (**Figure B- 1-A**).After calibration, the software is ready for length measurements. First of all, the total weight of the haul is determined. Next, raw shrimp are cleaned and placed on the illuminated plate as shown in (**Figure B- 1-B**). Important hereby is that shrimp can't touch each other, otherwise errors will occur. To enhance the measurement, shrimp also need to lay on its side and as straight as possible. After the plate is completely covered with shrimp, a picture is taken. The Halcon® algorithm identifies the different shapes on the plate based on light contrast. Each shape is simplified in order to filter away the antenna of the shrimp. The length of the shrimp is thus defined as the length from head to tail. For each shape, the longest path is determined by built-in algorithm. Halcon® software determines the length of this path and visualizes this in the output of SmartShrimp, as can be seen in (**Figure B- 1-C**). Lengths of shrimp is stored in a general database. After length measurements, total weight of the haul is again determined, after which the shrimp are disposed.

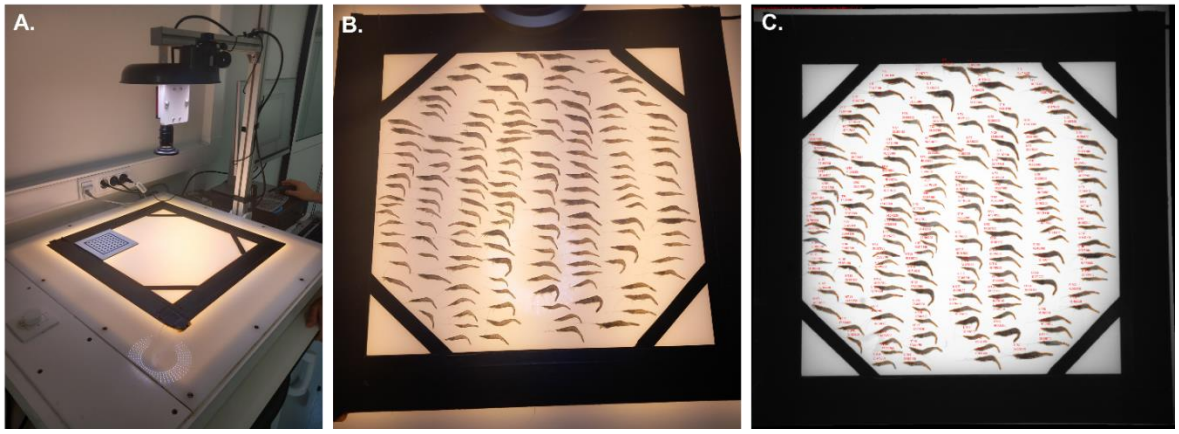

Figure B- 1 *Pictures of the length measurements with the SmartShrimp software. (A) Calibration of the camera by taking 20 pictures of the illuminated plate with a dotted square on top. (B) Shrimp placed on the illuminated plate, ready for length measurements. (C) Output of the SmartShrimp software. Each shrimp labelled with a unique identification number and a length measurement. Pictures taken on 12/09/2023.*

Table B- 2 Selected parameters from the available LifeWatch data series.

Parameter name	Parameter description	Unit
Station	Sampled station	-
Longitude	Longitude of the sampled station	°
Latitude	Latitude of the sampled station	°
Day	Day of sampling	-
Month	Month of sampling	-
Year	Year of sampling	-
Salinity	Salinity measured at the sampled station	ppt
Conductivity	Conductivity measured at the sampled station	$\mu S\ cm^{-1}$
Secchi Depth	Secchi depth measured at the sampled station	Cm
Beta carotene	Beta carotene concentrations at the sampled station	$\mu g\ L^{-1}$
Chlorophyll *a*	Chlorophyll *a* concentrations at the sampled station	$\mu g\ L^{-1}$
Chlorophyll *b*	Chlorophyll *b* concentrations at the sampled station	$\mu g\ L^{-1}$
Ammonium_NH4	Ammonium concentrations at the sampled station	$\mu mol.N\text{-}NH_4\ L^{-1}$
Nitrate_NO3	Nitrate concentrations at the sampled station	$\mu mol.N\text{-}NO_3\ L^{-1}$
Nitrite_NO2.	Nitrite concentrations at the sampled station	$\mu mol.N\text{-}NO_2\ L^{-1}$
Phosphate_PO4	Phosphate concentrations at the sampled station	$\mu mol.N\text{-}PO_4\ L^{-1}$

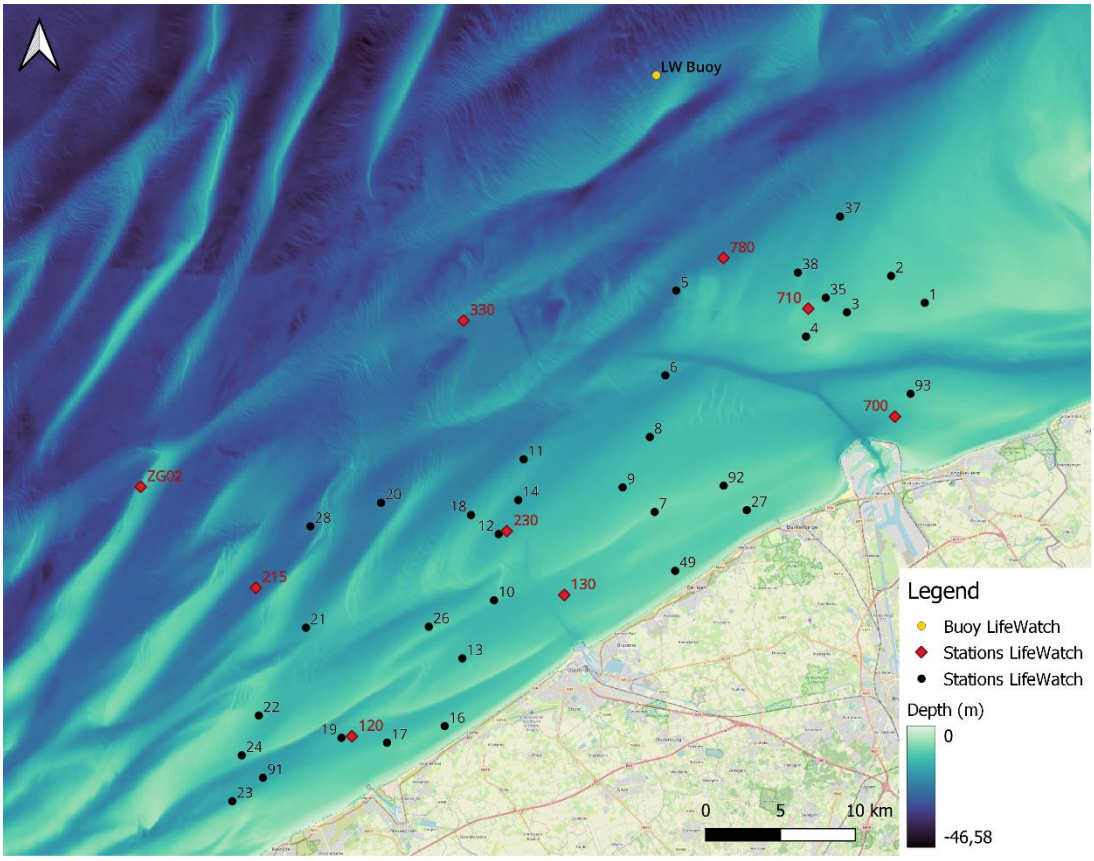

Figure B- 2 Bathymetric map of the BPNS. Locations of LifeWatch stations are indicated with red diamonds, ILVO stations are indicated with black dots and the location of the LifeWatch buoy is indicated in yellow. Bathymetric data was extracted from EMODNet *and was visualized in Qgis on 17/12/2023.*

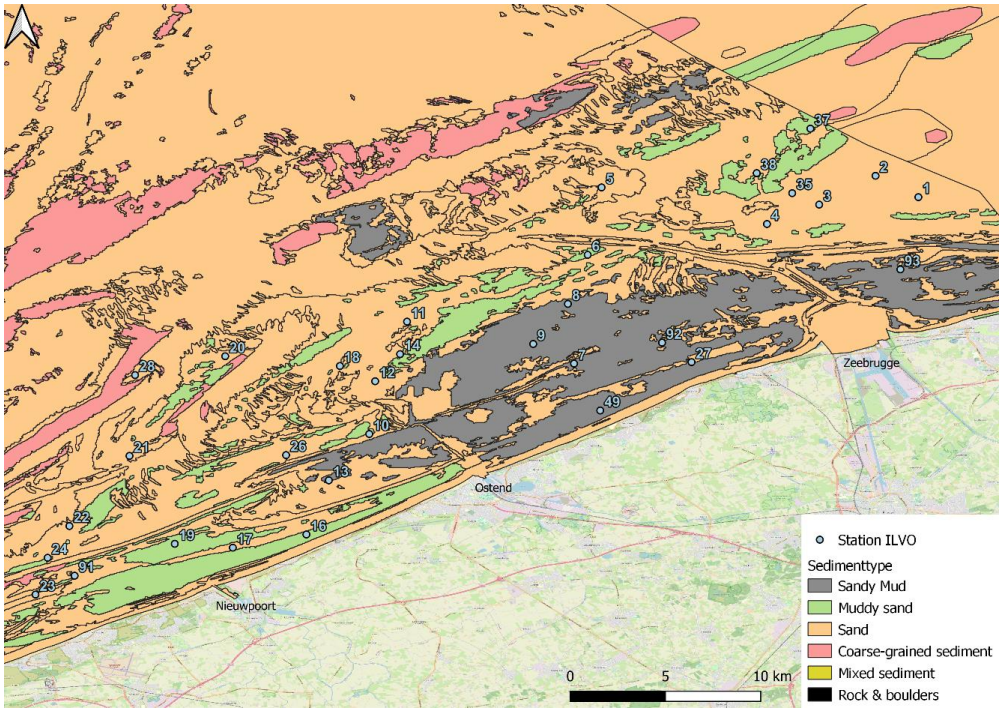

Figure B- 3 Map of the different substrate types present in the BPNS. ILVO stations are indicated with blue dots. Substrate data of the Multiscale-Folk7 dataset is extracted from EMODNet. *This dataset contains seven classification, of which six are shown in the legend. The "Mud" classification is not present and thus not shown in the legend. This substrate map was created in Qgis on 01/12/2023.*

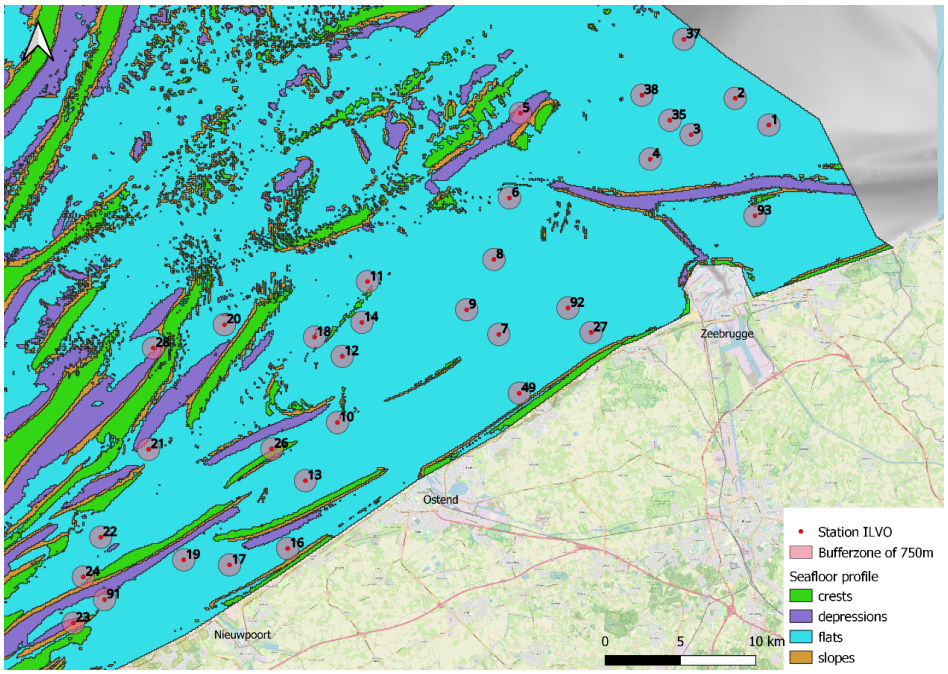

Figure B- 4 Overview of the profile of the seafloor of the BPNS with the focus on sandbanks. Crests of sandbanks are indicated with green, slopes with orange, depressions with purple and flat areas with blue. The ILVO stations are indicated with red dots. Around the ILVO stations, a buffer zone of 750m is present, indicated with pink. Data is extracted from EMODNet and was visualized on 17/12/2023.

Table B- 3 *Summary of the samples taken during the 2023 DYFS-campaign of ILVO (sample 1-20) and the offshore campaign in November (sample 21-24). Date of collection, approximated time of sampling, station number, coordinates of the station and haul duration are given. Samples 21-24 were taken at a LifeWatch station, other samples were taken at ILVO stations.*

Sample Number	Date	Time	Station	Coordinates		Haul duration (min)
				Latitude	Longitude	
1	13/09/2023	15h40	49	51.2817	3,0018	15
2	13/09/2023	16h40	27	51.3190	3.0748	15
3	13/09/2023	17h40	49	51.2817	3.0018	15
4	13/09/2023	08h30	10	51.2777	2.8607	15
5	14/09/2023	09u40	9	51.3418	2.9860	15
6	14/09/2023	11h10	4	51.4371	3.1537	15
7	14/09/2023	12h40	37	51.5043	3.1903	15
8	14/09/2023	13h50	38	51.4714	3.1467	15
9	14/09/2023	14h50	1	51.4375	3.2359	15
10	14/09/2023	15h40	3	51.4328	3.1709	15
11	18/09/2023	9h40	14	51.3237	2.8520	15
12	18/09/2023	10h40	20	51.3259	2.7309	15
13	18/09/2023	11h35	18	51.3133	2.8062	15
14	18/09/2023	12h50	11	51.3410	2.8440	15
15	18/09/2023	14h30	6	51.3932	2.9846	15
16	18/09/2023	16h00	8	51.3658	2.9898	15
17	19/09/2023	10h00	17	51.1891	2.7530	15
18	19/09/2023	10h35	17	51.1891	2.7530	30
19	19/09/2023	12h00	14	51.3170	2.8365	15
20	19/09/2023	13h05	14	51.3170	2.8365	30
21	16/11/2023	10h10	230	51.30868	2.85035	20
22	16/11/2023	14h00	230	51.30868	2.85035	20
23	17/11/2023	10h30	230	51.30868	2.85035	20
24	17/11/2023	14h10	230	51.30868	2.85035	10

APPENDIX C: RESULTS

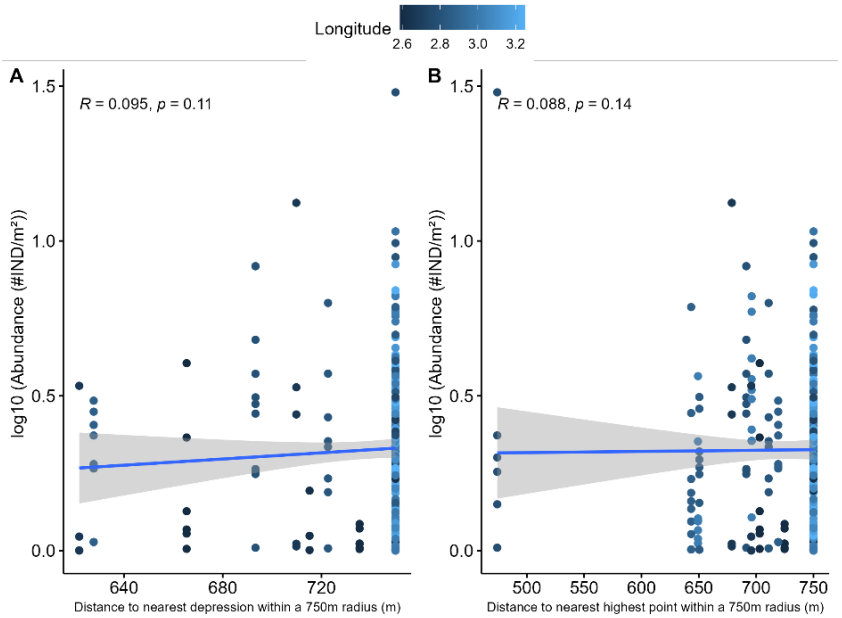

Figure C- 1 *Correlation between the log10-transformed C. crangon abundance (#IND m^{-2}) and the distance to the [A] nearest depression and [B] highest point within a radius of 750m around the sampled station. Spearman Rho- and p-values are shown in the scatterplots. The shaded area represents the 95% confidence interval. The longitude of the sampled station is indicated with the shown colour gradient.*

Table C- 1 *Number of days above 20 °C or 22°C for each year from 2014-2023. The threshold values of 20°Cand 22°C was arbitrarily defined. The table is based on the ICOS-buoy temperature measurements at a depth of 3m in the water column. Due to technical issues, data of 2014, 2016,2017 is lacking.*

Year	Days above 20°C	Days above 22°C
2015	0	0
2018	52	7
2019	21	0
2020	17	0
2021	0	0
2022	62	1
2023	15	0

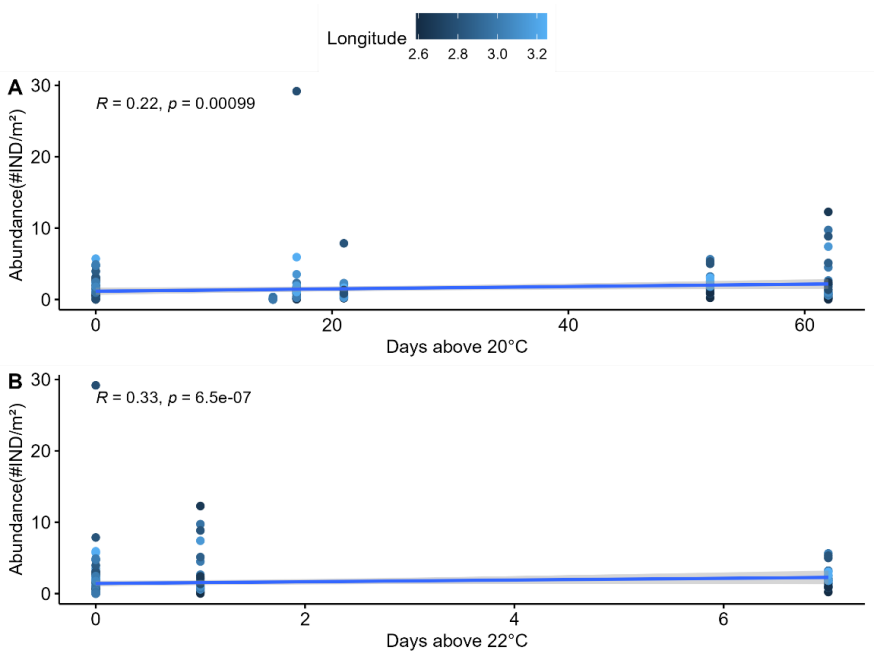

Figure C- 2 *Scatter plot of the number of days with water temperatures above [A] 20°C and [B] 22°C in relation to the abundance of C. crangon in the BPNS. Correlations were determined based on the Spearman's rank correlation coefficient method, and Spearman rho values and p-values are shown. Shadings show the 95% confidence interval. The colour gradient indicates the location of the measured Crangon abundance, expressed by the longitude.*

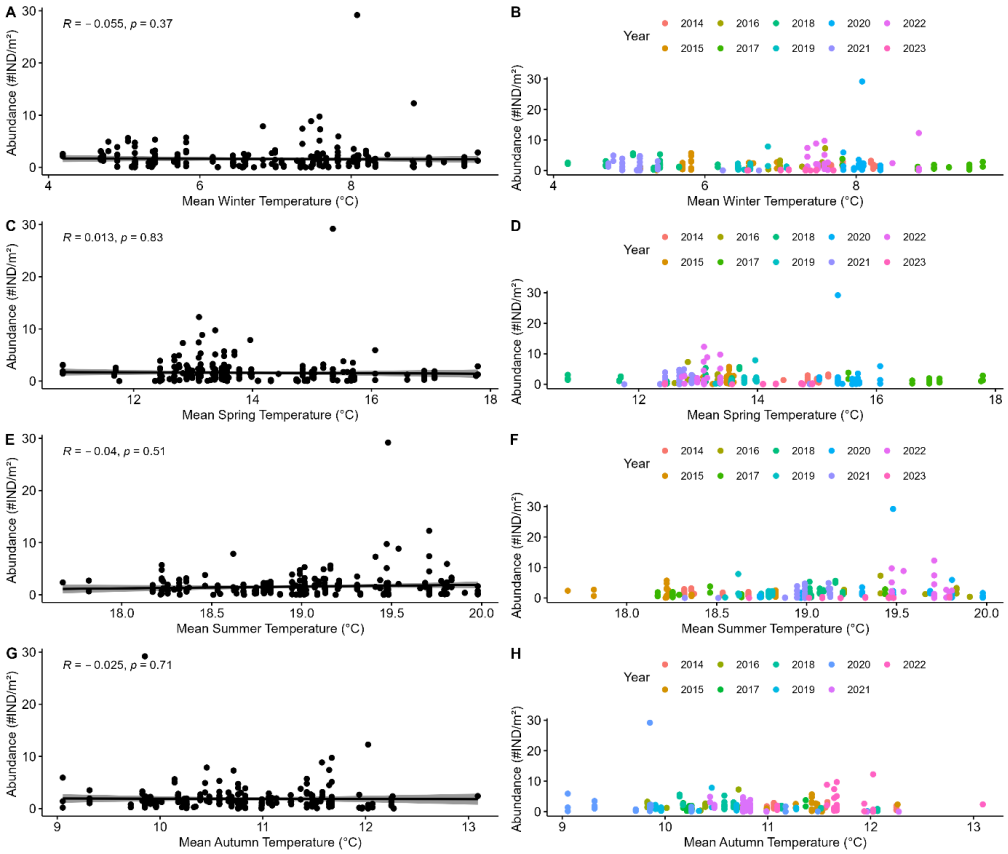

Figure C- 3 *Scatter plots of the mean water temperatures (°C) on a three-month scale in relation to the abundance of C. crangon in September (#IND m^{-2}) in the BPNS. Scatter plots [A], [C], [E] and [G] show the Spearman correlation, with the Spearman Rho value and p-value shown in the graph.*

Shaded areas represent the 95% confidence interval. Scatter plots [B], [D], [F] and [H] illustrate the same scatterplots as in [A], [C], [E] and [G] respectively, but show a colour distinction based on the year of measurement. Winter months are January, February and March; Spring months are April, May and June; Summer months are July, August and September; Winter months are October, November and December.

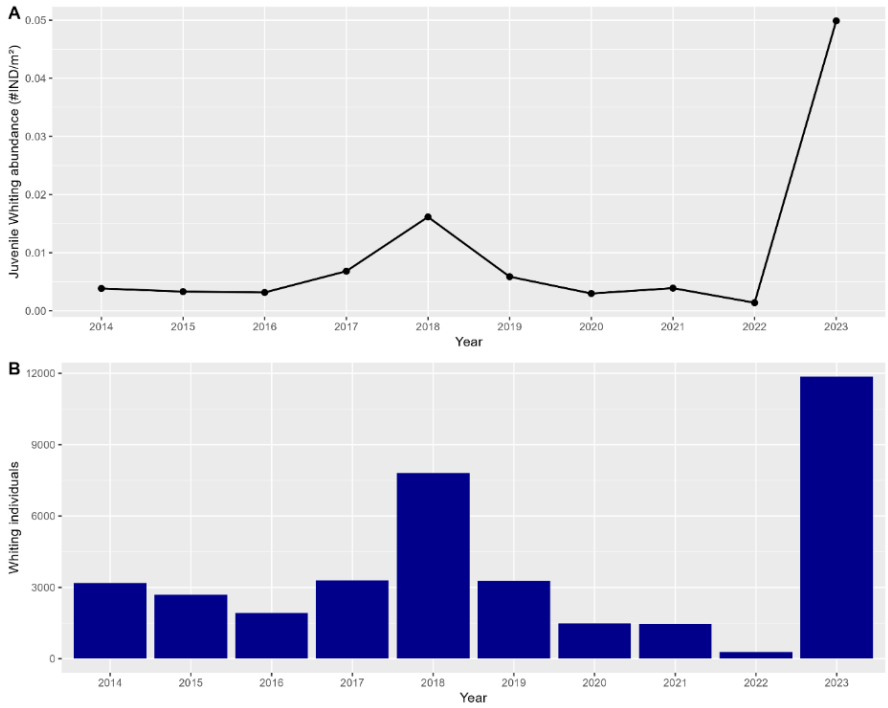

Figure C- 4 *[A] Relative abundance of juvenile whiting (#individuals m^{-2}) in the BPNS in September during the observed period (2014-2023). [B] Number of sampled whiting individuals in September per year. Samples were taken at the ILVO stations.*

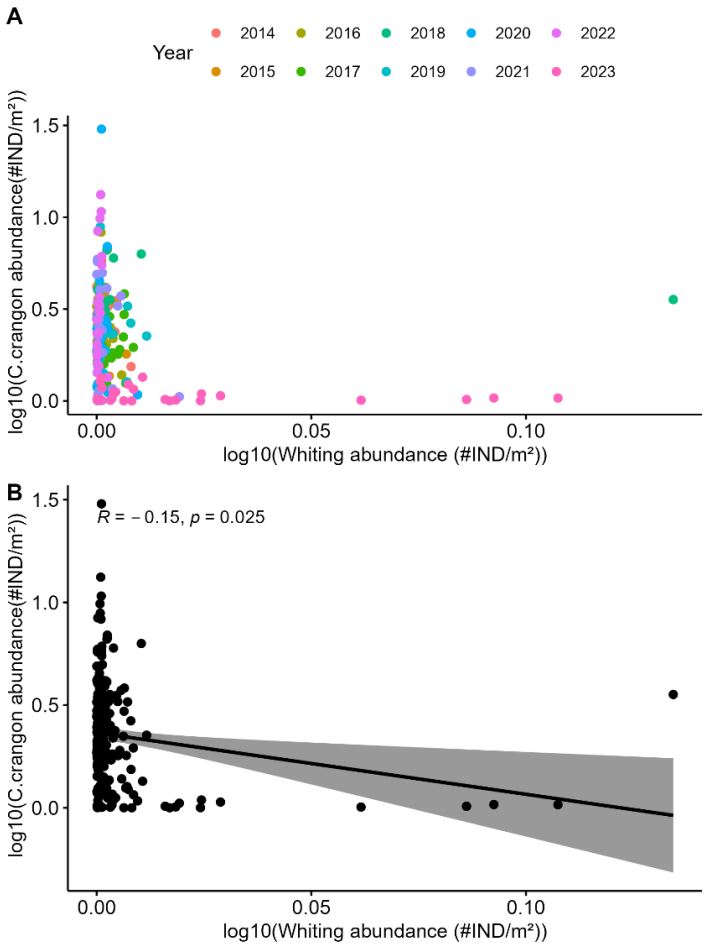

Figure C- 5 *Relation between the log10-transformed whiting abundance (#IND m^{-2}) and the log10-transformed C. crangon abundance (#IND m^{-2}), both in September. [A] Distinction is made based on year of sampling. [B] Scatterplot of the datapoints. The Spearman Rho and p-value is shown in the plot. The shaded area represents the 95% confidence interval. For both plots, pseudo count (all datapoints + 1) was implemented in order to account for zero-values (log10(1) = 0) .*

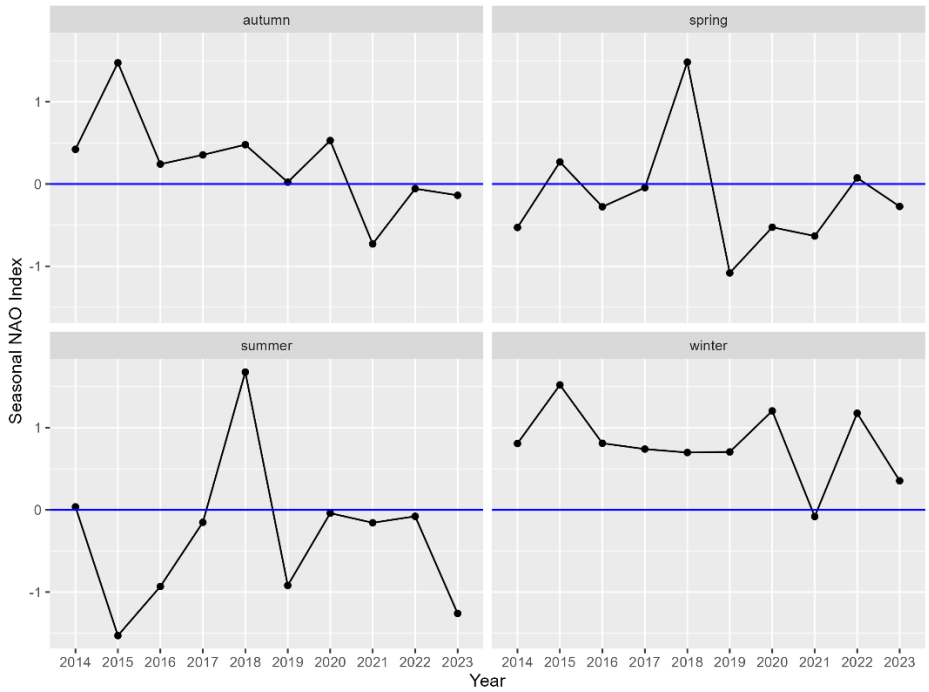

Figure C- 6 Trends of the seasonal North Atlantic Oscillation (NAO)-indices for the period 2014-2023. NAO indices are calculated on a 3-month scale.

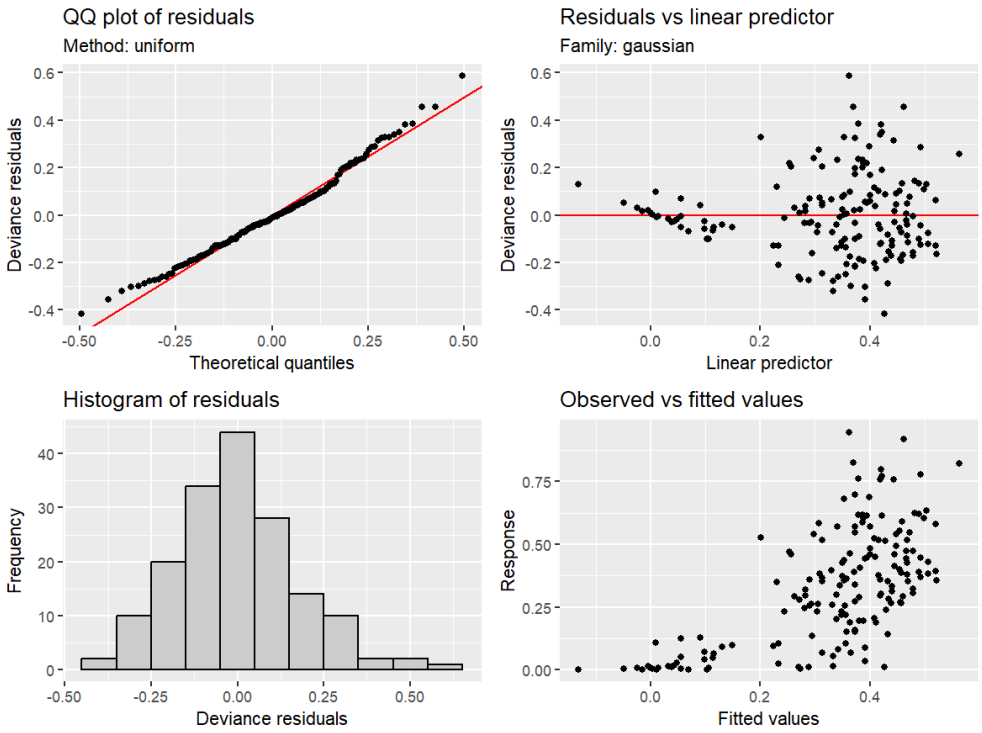

Figure C- 7 Diagnostic plot of Generalized model 1. The QQ-plot and the histogram of the residuals are used to verify normality. The plot of standardized residuals against fitted values assesses homogeneity.

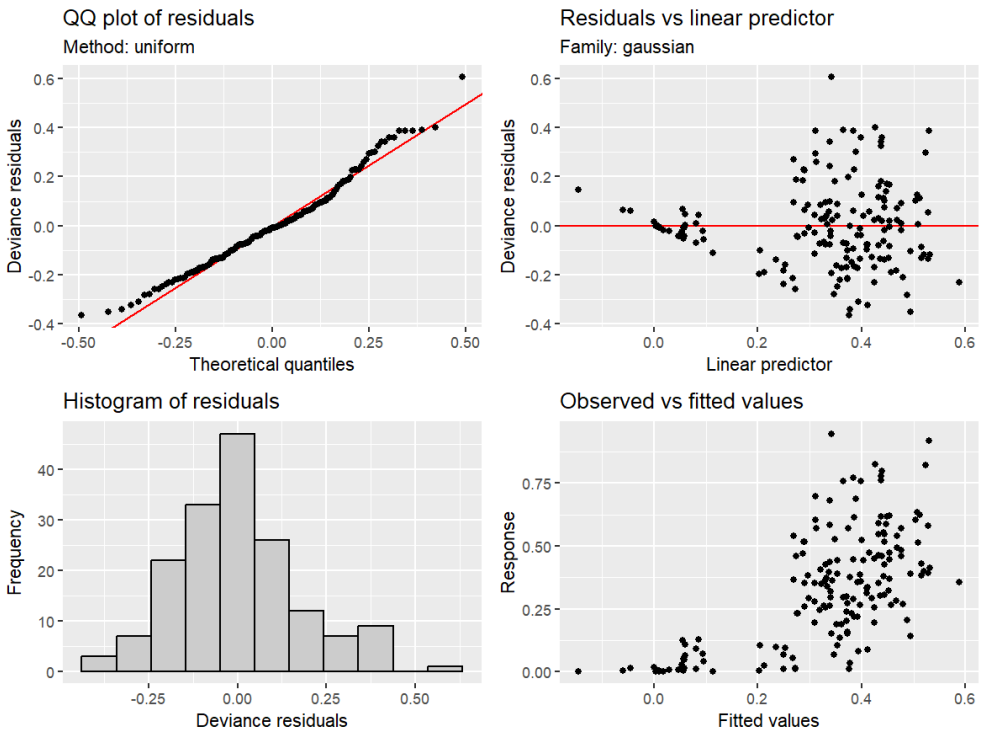

Figure C- 8 *Diagnostic plot of Generalized model 2. The QQ-plot and the histogram of the residuals are used to verify normality. The plot of standardized residuals against fitted values assesses homogeneity.*

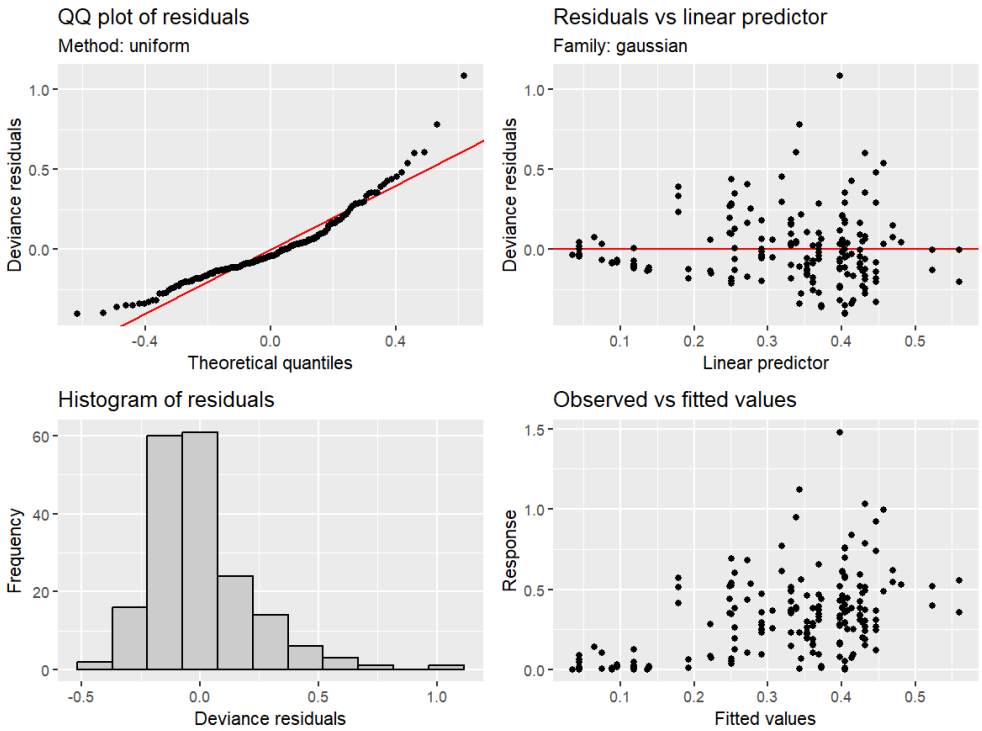

Figure C- 9 *Diagnostic plot of Generalized model 3. The QQ-plot and the histogram of the residuals are used to verify normality. The plot of standardized residuals against fitted values assesses homogeneity.*

Table C- 2 Results of the different protein and lipid extraction. Station 3 to 93 are ILVO stations and were sampled in September. Station 230 is a LifeWatch station and was sampled in November. From each ILVO station, five subsamples were analysed. From the LifeWatch station, six subsamples were analysed.

Station	Sample	Protein content (mg protein /mg shrimp tissue)	Lipid content (mg lipid /mg shrimp tissue)
3	1	0.0294	0.01249
	2	0.1086	0.01428
	3	0.2858	0.01087
	4	0.2130	0.00862
	5	0.1855	0.01185
6	1	0.2623	0.00388
	2	0.1063	0.00443
	3	0.0494	0.01464
	4	0.2105	0.00966
	5	0.1157	0.01029
9	1	0.2876	0.01016
	2	0.2594	0.00560
	3	0.3636	0.00596
	4	0.3609	0.00377
	5	0.2261	0.00534
13	1	0.3106	0.01816
	2	0.2195	0.03268
	3	0.0783	0.01851
	4	0.0786	0.01732
	5	0.0927	0.01405
20	1	0.0906	0.00212
	2	0.0545	0.00218
	3	0.1205	0.01505
	4	0.1048	0.01428
	5	0.1394	0.01451
49	1	0.1328	0.02501
	2	0.4523	0.01144
	3	0.2288	0.03081
	4	0.3926	0.02716
	5	0.4247	0.01980
93	1	0.1330	0.02763
	2	0.4046	0.01218
	3	0.0799	0.03334
	4	0.2029	0.02604
	5	0.7070	0.01884
230	1	0.1732	0.01283
	2	0.1458	0.01089
	3	0.1739	0.01267
	4	0.1801	0.0169
	5	0.1298	0.0167
	6	0.2506	0.0174

Table C- 3 R^2-value and equations of the three Bradford and Bligh and Dyer (B&D) extractions that were performed. In the equation, X stands for the present protein concentration (mg/ml) and Y stands for the measured absorbance.

Extraction	R^2-value	Equation
Bradford 1	0.9952	Y = 1.1738X + 0.4846
Bradford 2	0.9996	Y = 1.2658X + 0.4883
Bradford 3	0.9996	Y = 1.2927X + 0.4978
Bradford 4	0.9843	Y = 2.3239X + 0.0333
B&D1	0.9987	Y = 0.841X – 0.0532
B&D2	0.9998	Y = 3.9906X - 0.021
B&D3	0.9996	Y = 3.3509 – 0.0282
B&D4	0.9991	Y = 3.3766X – 0.0452

APPENDIX D: DISCUSSION

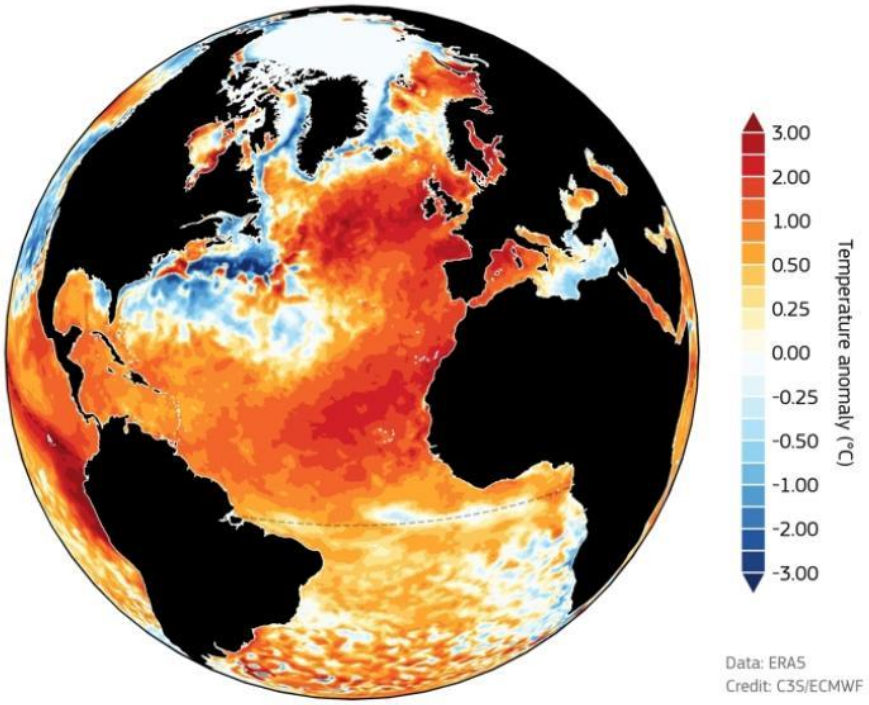

Figure D- 1 *The difference in water temperature in June in the north Atlantic region, compared to the climatological mean of the period 1991-2020. Figure derived from Copernicus (2023).*

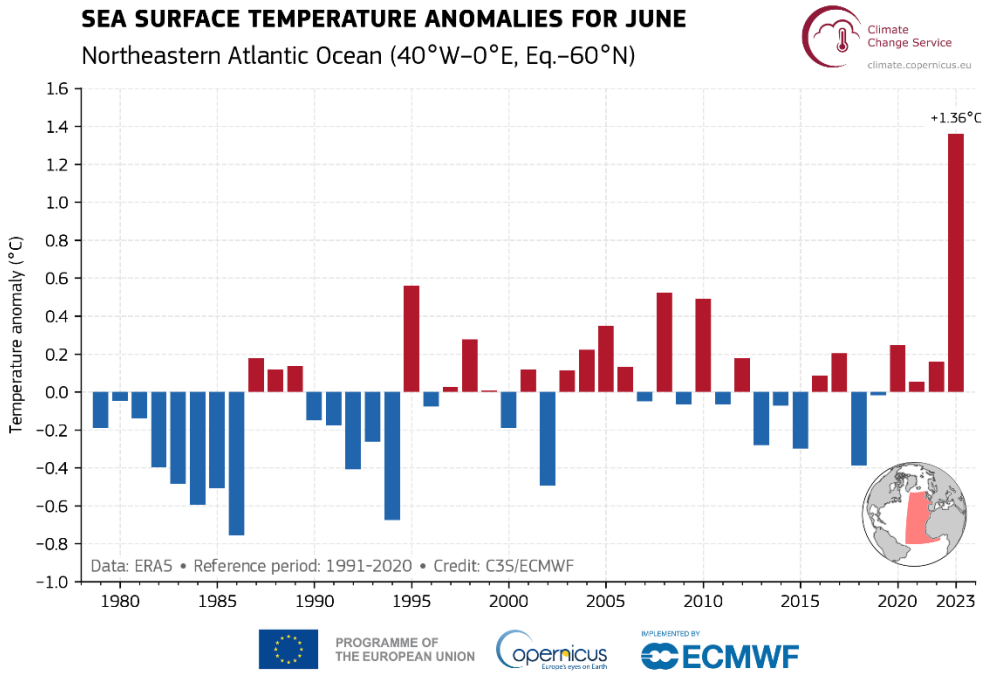

Figure D- 2 *Water temperature anomalies in the northeaster Atlantic region in June compared to the climatological mean over the period of 1979-2023. Figure derived from Copernicus (2023).*